



**Institute for Water
and Energy Sciences
(incl. Climate Change)**



**PAN-AFRICAN UNIVERSITY
INSTITUTE FOR WATER AND ENERGY SCIENCES
(including CLIMATE CHANGE)**

Master Dissertation

Submitted in partial fulfillment of the requirements for the Master degree in
CLIMATE CHANGE ENGINEERING

Presented by

RICHARD POSITE VITHUNDWA

**CLIMATE CHANGE IMPACTS ON SNOW COVER DYNAMICS IN THE
RWENZORI MOUNTAINS, EAST AFRICA**

To be defended on .../04/2024 Before the Following Committee:

Chair

Supervisor	Mohamed Saber	Prof	Kyoto University, Japan
Co-supervisor	Abdelbaki Cherifa	Prof	University of Tlemcen, Algeria
External Examiner			
Internal Examiner			

PAN-AFRICAN UNIVERSITY
INSTITUTE OF WATER AND ENERGY SCIENCES
(including CLIMATE CHANGE)

**CLIMATE CHANGE IMPACTS ON SNOW COVER DYNAMICS IN THE
RWENZORI MOUNTAINS, EAST AFRICA**

A thesis submitted to the Pan African University Institute of Water and Energy Sciences (including Climate Change) in partial fulfilment of the requirements for the degree of Master of Science in Climate Change (Engineering option).

By

Richard Posite Vithundwa
PAUWES/2022/MCC15

Supervisor: Prof. Mohamed Saber
Co-supervisor: Prof. Abdelbaki Cherifa

March 2024

Tlemcen, Algeria

THESIS APPROVAL

Submitted by

Richard Posite Vithundwa



22th March 2024

Student

Signature

Date

Approved by Examining Board

Examiner

Signature

Date

Thesis/ Dissertation Advisors

Prof. Mohamed Saber



29th March 2024

Name of Advisor

Signature

Date

Prof. Abdelbaki Cherifa

Name of Co-Advisor

Signature

Date

Institute Dean

Name of the Dean

Signature

Date

Pan African University

Name of Rector

Signature

Date

DEDICATION

To my beloved mother, Kavugho Mivughire Jeannine, and Dad, Kasereka Malisaba Gaston, as well as to all those passionate about climate and cryospheric modeling.

STATEMENT OF THE AUTHOR

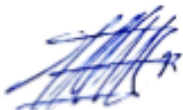
By my signature below, I declare that this thesis/dissertation is my work. I have followed all ethical principles of scholarship in the preparation, data collection, data analysis, and completion of this thesis or dissertation. I have given all scholarly matter recognition through accurate citations and references. I affirm that I have cited and referenced all sources used in this document. I have made every effort to avoid plagiarism. I submit this document in partial fulfillment of the requirements for a MSc degree from the Pan African University. This document is available from the PAU Library to borrowers under the rules of the library. I declare that I have not submitted this document to any other institution for the award of an academic degree, diploma or certificate. Scholars may use brief quotations from this thesis or dissertation without special permission if they make an accurate and complete acknowledgment of the source. The dean of the academic unit may grant permission for extended quotations or reproduction of this document. In all other instances, however, the author must grant permission.

Name: Richard Posite Vithundwa

Academic unit: Climate Change Engineering

PAU Institute: PAUWES

Signature:



Date: March 22th 2024

BIOGRAPHICAL SKETCH

Richard Posite Vithundwa is a distinguished Master of Science candidate in Climate Change Engineering at the Pan African University of Water and Energy Sciences (PAUWES) located in Tlemcen, Algeria. With an Engineering degree specializing in Water and Forest from the Official University of Semuliki in the Democratic Republic of Congo, Richard has established a formidable academic and professional foundation. As a Senior Lecturer and Researcher at his alma mater, the Official University of Semuliki, Richard Posite Vithundwa has significantly contributed to the academic community. He possesses experience in areas such as farming operations, forestry stewardship, and specialized knowledge in Statistics and Geographic Information Systems (GIS) analysis. His expertise extends into planning, organising, and coordinating both administrative and operational procedures, underscored by a robust capability in project management. This diverse skill set is complemented by his participation in start-up building training sessions while at PAUWES, showcasing his continuous drive for personal and professional development. Driven by a self-motivated and versatile disposition, he excels in communication, multitasking, fostering interpersonal relationships, and adaptability. His interest lies in the nexus of climate, hydrological, and forest modeling and is currently researching on the impacts of climate change on snow cover dynamics within the challenging terrain of the Rwenzori mountains in Eastern Africa.

ACKNOWLEDGEMENT

I would like to express my heartfelt gratitude to the Pan African University and the African Union Commission for their belief in me and for awarding me a full scholarship to pursue the Master of Science in Climate Change program at PAUWES, in addition to providing funding for this research. My sincere thanks also go to the government and people of Algeria for their warm welcome and hospitality during my two-year stay in Algeria. I am deeply grateful to my supervisor, Prof. Mohamed Saber, whose guidance and insightful contributions were instrumental in the successful completion of this thesis. My gratitude also extends to Prof. Abdelbaki Cherifa, the co-supervisor of this work, for his remarkable guidance. I would also like to thank Professor Richard Taylor from University College London in the United Kingdom, who guided me during the topic design, and Professor Awoke Guadie from Arba Minch University in Ethiopia, as he motivated me. May Mr. Eric, Conservator of the Virunga National Park in the Mutsora station, DR Congo, receive recognition for his invaluable inputs, constant guidance, and motivation throughout the research process. My profound gratitude goes to my brother Kakule Posite Pochelin and to everyone in Congo as well as in Uganda who provided immense help during my field survey. Special thanks to my brothers, sisters, and friends for their comfort and support in times of need. Finally, my heartfelt appreciation goes to the entire PAUWES community, including the administration, staff, all lecturers, and my fellow students of the 8th cohort, especially those in the Climate change track.

To all of you, I extend my deepest gratitude.

ACRONYMS, ABBREVIATIONS, AND SYMBOLS

°	Degrees
°C	Degrees Celsius
ASON	August-September-October-November season
A _x	Maximum
B _a	Baker
CCD	Cold Cloud Duration
CHIRPS	Climate Hazards Group InfraRed Precipitation with Stations
CHIRTS	Climate Hazards Group InfraRed Temperature with Stations
CL	Control Limit
CM _{hyd}	Climate Model for Hydrological Downscaling
CMIP6	Coupled Model Intercomparison Project Phase 6
CZ	Central Zone
DEM	Digital Elevation Model
DJF	December-January-February season
DM	Distribution Mapping
DRC	Democratic Republic of the Congo
E	East
ELAs	Equilibrium Line Altitudes
ENSO	El Niño-Southern Oscillation
ERA5	ECMWF Reanalysis version 5
FEWS NET	Famine Early Warning Systems Network
FF	Far Future
GCMs	General Circulation Models
Ge	Gessi
GHCN	Global Historical Climatology Network
GIS	Geographic Information System
GSOD	Global Summary of the Day
HRUs	Hydrologic Response Units
ICCN	Institut Congolais de Conservation de la Nature
In	Minimum
ISRIC	International Soil Reference and Information Centre

J2000	Jena 2000 model
JAMS	Java-based Modeling System
JJ	June-July season
Km ²	Square Kilometers
LCL	Lower Control Limit
LGM	Last Glacial Maximum
MAE	Mean Absolute Error
MAM	March-April-May season
MODIS	Moderate Resolution Imaging Spectroradiometer
MRI-ESM2-0	Meteorological Research Institute Earth System Model version 2.0
N	North
NASA	National Aeronautics and Space Administration
NDSI	Normalized Difference Snow Index
NDSI	Normalized Difference Snow Index
NF	Near Future
NOAA	National Oceanic and Atmospheric Administration
NSE	Nash-Sutcliffe Efficiency
Obs	Observed
p	P Value
Pbias	Percent Bias
pH	Potential of Hydrogen
r	Correlation Coefficient
r1i1p1f1	1st realization, 1st initialization, 1st physics, and 1st forcing
R ²	Coefficient of Determination
Ra	Rainfall
RCP	Representative Concentration Pathway
RFE2	Rainfall Estimate version 2
RS	Remote Sensing
S	South
Sc	Snow Cover
ScenarioMIP	Scenario Model Intercomparison Project
SD	Standard Deviation
Sim	Simulated

Sp	Speke
SRTM	Shuttle Radar Topography Mission
SSP1-1.9	Shared Socioeconomic Pathways 1 - 1.9 W/m ²
SSP1-2.6	Shared Socioeconomic Pathways 1 - 2.6 W/m ²
SSP2-4.5	Shared Socioeconomic Pathways 2.4.5 W/m ²
SSP3-7.0	Shared Socioeconomic Pathways 3 - 7.0 W/m ²
SSP4-3.4	Shared Socioeconomic Pathways 4 - 3.4 W/m ²
SSP4-6.0	Shared Socioeconomic Pathways 4 - 6.0 W/m ²
SSP5-3.4-OS	Shared Socioeconomic Pathways 5 - 3.4 W/m ² - Overshoot
SSP5-8.5	Shared Socioeconomic Pathways 5.8.5 W/m ²
St	Stanley
TAMSAT	Tropical Applications of Meteorology using Satellite data and ground-based data
TARCAT	TAMSAT African Rainfall Climatology And Time series
TIR	Thermal Infrared
Tmax	Maximum Temperature
Tmin	Minimum Temperature
UCL	Upper Control Limit
US	United States
ITCZ	Intertropical Convergence Zone
UTM	Universal Transverse Mercator
W	West
WGS	World Geodetic System
WM	Whole Mountain
X	Mean
γ	Sen's Slope Estimator
$\mu\text{S/cm}$	Microsiemens per centimeter
ω	Mann-Kendall Tau

TABLE OF CONTENTS

THESIS APPROVAL.....	i
DEDICATION	ii
STATEMENT OF THE AUTHOR	iii
BIOGRAPHICAL SKETCH	iv
ACKNOWLEDGEMENT	v
ACRONYMS, ABBREVIATIONS, AND SYMBOLS.....	vi
TABLE OF CONTENTS	ix
LIST OF FIGURES	xii
LIST OF TABLES IN THE APPENDICES	xiv
ABSTRACT.....	xv
1. INTRODUCTION	1
1.1. Background, Problem statement, and Research gaps.....	1
1.2. Research Objectives	4
1.3. Research questions	4
1.4. Research hypothesis	5
1.5. Significance of the study	5
1.6. Scope and limitations of the study	6
2. LITERATURE REVIEW.....	7
2.1. Climate characteristics of mountainous regions.....	7
2.2. Climate modeling and projections.....	8
2.2.1. ScenarioMIP's contributions to climate projections and CMIP6 advancements.....	8
2.2.2. Climate uncertainty through the role of shared socioeconomic pathways	9
2.3. Critical intersection of snow cover, climate change, and environmental impact.....	12
2.3.1. Significance of snow cover in environmental systems.....	12
2.3.2. Climate change and snow dynamics.....	13
2.4. MODIS data accuracy and J2000 model insights for snow cover forecasting.....	15
2.4.1. Challenges and limitations in assessing snow cover extent in mountainous regions .	15
2.4.2. Potential of MODIS for snow cover analysis.....	15

2.4.3. J2000 model's effectiveness in snow dynamics simulation.....	16
2.5. Eco-geological dynamics and climatic paradoxes of the Rwenzori mountains	17
2.5.1. Topographical and geological characteristics of the Rwenzori mountains	17
2.5.2. Rwenzori climatic features and glaciation.....	18
2.5.3. Biodiversity and hydrology of the Rwenzori mountains.....	19
3. STUDY AREA AND METHODS	22
3.1. Study area.....	22
3.2. Data collection.....	23
3.2.1. Reanalysis climate data and Global Climate Models (GCMs).....	23
3.2.2. Snow cover data.....	24
3.2.3. Geospatial data	25
3.3. Processing and analysis	25
3.3.1. Distribution mapping for climate variable downscaling in Rwenzori mountains	25
3.3.2. GCM performance in simulating climate variables over the Rwenzori mountains ..	26
3.3.3. Temporal and spatial trends analysis in Rwenzori mountains climate	27
3.3.4. JAMS/J2000 model and set up	28
3.3. 5. Snow cover assessment	30
4. RESULTS AND DISCUSSION.....	31
4.1. Results	31
4.1.1. Climate change assessment	31
4.1.1.1. Historical climate on Rwenzori mountains	31
4.1.1.2. Projected climate on Rwenzori mountains	38
4.1.2. Snow cover dynamics on Rwenzori mountains.....	42
4.1.2.1. Historical snow cover dynamics.....	42
4.1.2.2. Model accuracy and performance in simulating observed snow cover dynamics ..	49
4.1.2.3. Projected snow cover dynamics	50
4.2. Discussion	55
4.2.1. Climate dynamics and future trends in the Rwenzori mountains.....	55

4.2.1.1. Climate dynamics in the Rwenzori mountains: Insights from historical temperature and rainfall.....	55
4.2.1.2. Future climate trends and implications for the Rwenzori mountains.....	56
4.2.2. Snow cover dynamics in the Rwenzori mountains.....	57
4.2.2.1. Complexities of Snow cover dynamics in the Rwenzori Mountains: Insights from historical analysis	57
4.2.2.2. Projected snow cover dynamics in the Rwenzori mountains: Insights into climate change impacts and modeling approach.....	59
5. CONCLUSIONS AND RECOMMENDATIONS.....	61
5.1. Conclusions	61
5.2. Recommendations	61
6. REFERENCES	63
APPENDICES	82

LIST OF FIGURES

Figure 1. Scenario Matrix for Climate Model Experimentation Informing the Sixth Coupled Model Intercomparison Project (CMIP6).	12
Figure 2.(a) Democratic Republic of the Congo (1) and Republic of Uganda (2) location in Africa; (b) Rwenzori Mountains in the Eastern african rift valley; (c) Rwenzori mountains aspect map; (d) Topographic lines in the central zone of the Rwenzori mountains	23
Figure 3.Topographical attributes of the Rwenzori mountains.....	29
Figure 4.Soil texture, water holding capacity, root depth, and leaf area index of the Rwenzori mountains.....	29
Figure 5.Flow chart of climate change assessment on snow dynamics in the Rwenzori mountains	30
Figure 6.Inter-annual temperature (A_x) maximum, (I_n) minimum, and (R_a) rainfall over the 1991-2020 period	32
Figure 7.Monthly spatial distribution of maximum temperature (T_{max}), minimum temperature (T_{min}), and rainfall on Rwenzori mountains over the 1991-2020 period.	32
Figure 8. Decadal spatial distribution of maximum temperature (T_{max}) and minimum temperature (T_{min}) on Rwenzori mountains over the 1991-2020 period.	33
Figure 9. Decadal spatial distribution of rainfall on Rwenzori mountains over the 1991-2020 periods.....	33
Figure 10.Monthly temperature (T_{max}) maximum, (T_{min}) minimum, and rainfall over the 1991-2020 period	34
Figure 11.Seasonal temperature (a) maximum, (b) minimum, and (c) rainfall over the 1991-2020 period	35
Figure 12.Seasonal spatial distribution of maximum temperature (T_{max}) and minimum temperature (T_{min}) on Rwenzori mountains over the 1991-2020 period	36
Figure 13.Seasonal spatial distribution of rainfall on Rwenzori mountains over the 1991-2020 period	37
Figure 14.Scatter plot matrix of interactions between maximum temperature (T_{max}), minimum temperature (T_{min}), and rainfall over the 1991-2020 period	38
Figure 15.Spatial difference of climate between Past (1991-2020), near future (2021-2060) and far future (2061-2100) time periods under ssp245 scenario.	39
Figure 16.Spatial difference of climate between Past (1991-2020), near future (2021-2060) and far future (2061-2100) time periods under ssp585 scenario	40
Figure 17.Interannual variations in snow cover dynamics across different mountain peaks	43

Figure 18. Seasonal snow cover dynamics across Rwenzori mounts during 2000-2022 period..	44
Figure 19. Monthly snow cover dynamic on (a) Baker, (b) Gessi, (c) Speke, (d) Stanley, and (e) Overall scales	45
Figure 20. Overall snow cover dynamics scatter plot matrix analysis and climate-snow cover relationships over the 2000-2022 period.....	46
Figure 21. June month-specific scatter plot matrix analysis of snowpack variation across Baker and Stanley peaks and climate-snow cover relationships over the 2000-2022 period	47
Figure 22. February month-specific snow cover dynamics scatter plot matrix analysis of Mount Stanley and climate-snow cover relationships over the 2000-2022 period	48
Figure 23. Model agreement with MODIS snow cover data	49
Figure 24. Projected annual snow cover dynamic on (a) Baker, (b) Gessi, (c) Speke, (d) Stanley, and (e) Overall scales.....	51
Figure 25. Differences in snow cover area between projected and observed (Obs) data.	52
Figure 26. Projected monthly snow cover under different period and scenarios.....	54

LIST OF TABLES IN THE APPENDICES

Appendix 1.Mann-Kendall test and Sen’s slope estimator for temperatures and rainfall over the 1991-2020 period.....	82
Appendix 2.Mann-Kendall test and Sen’s slope estimator for temperatures and rainfall in near future (2021-2060 period).....	83
Appendix 3.Mann-Kendall test and Sen’s slope estimator for temperatures and rainfall in far future (2061-2100 period).....	85
Appendix 4.Mann-Kendall test and Sen’s slope estimator for historical snow cover data (2000-2022period).....	87
Appendix 5.Mann-Kendall test and Sen’s slope estimator for projected snow cover dynamics.	88
Appendix 6.Variance analysis on historical snow cover dataset.....	91

ABSTRACT

This study conducts a comprehensive assessment of climate change impacts on snow cover dynamics within the Rwenzori Mountains, employing an extensive dataset to delve into historical trends and future projections. Focused on evaluating climate patterns from 1991 to 2020 and forecasting future scenarios under SSP245 and SSP585, the research analyzes snow cover changes from 2000 to 2022 and projects forthcoming snow dynamics. Using reanalysis climate data from CHIRPS and CHIRTS for rainfall and temperature, respectively, alongside MODIS snow cover observations, the study methodically investigates past climate and snow cover trends. The J2000 hydrological model, calibrated and validated with actual snow cover data, is used to simulate future snow dynamics amidst evolving climate conditions. The intricate analysis of interannual, seasonal, and monthly variations in both climate and snow cover data, was supported by advanced statistics for trend analysis and model assessment. Historical data underscore significant climatic shifts over recent decades, with rising temperatures and variable rainfall patterns significantly influencing snow cover dynamics. Notably, the analysis reveals a clear warming trend, alongside marked interannual rainfall variability. These climatic changes are expected to persist in future projections. These climatic changes are closely linked to variations in snow cover dynamics, underscoring the sensitivity of the Rwenzori Mountains' snow cover to climate fluctuations. Forecasts from the J2000 model suggest significant decreases in future snow cover across various scenarios, although a modest rise is anticipated on Mount Baker in the near term (2030-2065). The observed trends in climate and snow cover dynamics highlight the acute susceptibility of the Rwenzori Mountains to current and imminent climate change impacts. By offering crucial insights into the effects of climate change on alpine snow cover, this study lays a solid foundation for subsequent research and informs policy development in climate adaptation and hydrological management.

Key words: Snow cover dynamics, Rwenzori mountains, Climate modeling, CMIP6 scenarios, Cryospheric modeling, MRI-ESM2-0 model, JAMS/J2000 model

1. INTRODUCTION

1.1. Background, Problem statement, and Research gaps

Climate change's impact on snow dynamics is a pressing concern within hydrology and water resources management. Human-induced greenhouse gas emissions exacerbate global warming, leading to shifts in climate patterns, including alterations in seasonal cycles, long-term trends, and broader climate systems (Grimmond, 2007). Snow, a crucial component of the climate system and hydrological cycle, interacts with various environmental factors such as surface thermal energy, atmospheric dynamics, and soil thermal conditions (Landwehr et al., 2021; Frei et al., 2012). A significant consequence of global warming is the modification of snowmelt runoff, both in terms of quantity and timing (Irannezhad et al., 2015; He et al., 2021). Increasing temperatures accelerate glacial retreat and advance snowmelt onset. Beyond impacting vegetation growth and sustaining river flow, riparian plants, and aquatic ecosystems through enhanced water availability (Rood et al., 2012; Mankin et al., 2015), snowmelt can trigger floods and erosion.

Since the 1950s, the global climate system has undergone significant transformations due to global warming, leading to heightened vulnerability to natural disasters like floods and droughts, consequently impacting agricultural economies (Masson-Delmotte et al., 2021; Parmesan et al., 2022). The exacerbation of natural disaster impacts by climate change and its implications for mitigation and adaptation strategies have received considerable attention (Banholzer et al., 2014). Accurate regional-level predictions of future climate changes are vital for effectively addressing and adapting to the challenges posed by climate change (Kumar et al., 2021). To achieve this, the study of recent climate variations and the projection of future changes are imperative (Schär et al., 2004; Loukas et al., 2007). Such insights are essential for devising adaptation strategies tailored to the specific needs of each region (Javadinejad et al., 2021).

Hence, having precise and reliable climate data observed directly from the ground is crucial for any region. Unfortunately, in numerous areas worldwide, obtaining accurate and consistent climate data is challenging due to inadequate and uneven distribution of climate gauge stations. This is evident in the Rwenzori mountains region, where in-situ data are scarce for both the DRC and Ugandan sides (Taylor et al., 2009; Nakulopa et al., 2022). Thankfully, advancements in remote sensing technologies, such as satellite-based climate estimates, now offer viable alternatives to bridge this gap more effectively.

Satellite-based products play a pivotal role in addressing the challenge of limited data and enhancing its quality, particularly in regions with sparse ground-based hydro-meteorological data,

notably in developing countries. Several researchers have underscored the importance of satellite-derived climate data for various purposes, including drought and environmental monitoring, early warning systems, and snowmelt and flood forecasting (Paredes Trejo et al., 2016; Funk et al., 2015; Wang & Russell, 2016; Sheffield et al., 2018; Maggioni & Massari, 2018; Levizzani & Cattani, 2019). Reanalysis climate data from the CHIRPS (Climate Hazards Group InfraRed Precipitation with Stations) database for precipitation (Funk et al., 2015) and from CHIRTS (Climate Hazards Group InfraRed Temperature with Stations) for temperature (Verdin et al., 2020) provide freely available daily climate data with high gridded spatial resolution (Funk et al., 2015; Verdin et al., 2020). These databases (CHIRPS and CHIRTS) undergo a multi-stage synthesis process incorporating satellite records and in-situ station data, ensuring their reliability and versatility for scientific investigations (Funk et al., 2015; Verdin et al., 2020). Previous studies have examined rainfall distribution over lower altitude zones using satellite-based products. Nakulopa et al. (2022) found that rainfall in the complex terrain of the Rwenzori mountains exhibits high spatial and temporal variability. However, these studies have often disregarded the influence of topography on rainfall patterns. Additionally, there is a lack of comprehensive analysis of the climate in the region, as other climatic factors such as temperature have not been adequately considered.

Following IPCC guidelines, assessing the impacts of climate change necessitates relevant climate projections at various scales (Getachew & Manjunatha, 2022; Isinkaralar, 2023). However, challenges persist in selecting appropriate General Circulation Models due to uncertainties (Ahmadalipour et al., 2017; Huang et al., 2021). Advancements in climate modeling, exemplified by CMIP6, offer solutions (Alaminie et al., 2021). CMIP6 models feature higher resolutions, enhanced parameters, and additional components (Hofer et al., 2020; Kamruzzaman et al., 2021). Notably, CMIP6's utilization of socioeconomic pathways (SSPs) instead of radiative forcing values offers more realistic future scenarios. Moreover, CMIP6 emphasizes model intercomparison to address biases and processes (Song et al., 2021; Wyser et al., 2020).

Accurately assessing snow cover extent in mountainous regions poses challenges due to harsh weather conditions, complex accessibility, and limited communication infrastructure. However, advancements in Remote Sensing (RS) and Geographic Information System (GIS) technologies have opened unprecedented opportunities for their application in mountain climates. These technologies have proven effective in various areas, including snow cover analysis, terrain analysis, mountain hazard planning, and watershed management (Kongoli et al., 2012; Yang et al., 2016; Reddy and Sarkar, 2012; Rai et al., 2014; Rautela et al., 2022). Dhari et al. (2011) highlight the significant benefits brought about by these resources. Satellite imagery, coupled

with advanced computer analysis techniques, has enabled the development of reliable, accurate, and consistent datasets for hydrological investigations. Unlike traditional methods, these technologies allow for the amalgamation of multi-spectral spatial information, which can be effectively presented in a comprehensible format such as maps. Therefore, remote sensing emerges as the primary tool for measuring the extent and properties of snow cover (Yang et al., 2016).

Fresh snow exhibits high reflectivity in the visible wavelength region, which gradually decreases as the snow ages (Singh et al., 2010). The reflectivity of snow depends on various characteristics, including shape, size, debris content, depth, and surface roughness (Singh et al., 2010). Visible, near-infrared, and thermal infrared data from satellites like MODIS, IRS, and Landsat are used to collect information about the snowpack's surface and aerial conditions. These wavelengths are selected because they have limited penetration through the snowpack. However, the accuracy of the data is affected by cloud cover and shadows, emphasizing the importance of using cloud-free images for better accuracy.

On the scale of the Rwenzori mountains, Taylor et al. (2006) used Landsat imagery from 1987, 1995, and 2003 to analyze glacier/snow dynamics by calculating the Normalized Difference Snow Index (NDSI). They projected a significant reduction in snow cover, even predicting its definitive disappearance within the next two decades from 2004 based on the extrapolation of trends in glacial recession since 1906 studied by Kaser and Osmaston (2002). However, this approach may introduce inconsistencies due to variations in sensor characteristics, atmospheric conditions, missing or incomplete data for certain days of the year, and image processing techniques (Zhang et al., 2022b). Furthermore, a significant gap in these analyses is the lack of a thorough examination of seasonal and monthly variations in snow/glacier cover, which could offer more detailed insights into the dynamics of these critical environmental features. Additionally, extrapolating trends in glacial recession to project the definitive disappearance of snow/glacier cover may oversimplify the complex dynamics of snow cover change on the Rwenzori Mountains. This approach may not adequately account for factors such as local climatic variability, topographic influences, and potential changes in precipitation patterns, leading to uncertainties in the projected outcomes. Therefore, the use of daily MODIS products spanning several years may be more suitable to overcome these challenges. The Moderate Resolution Imaging Spectroradiometer (MODIS) snow products encompass a long temporal coverage ranging from 2000 to the present, ensuring continuity and consistency in the data and facilitating the development of long-term scenarios. They are widely acknowledged for their robustness and extensive usage worldwide, including in mountainous regions (Muhammad and Thapa, 2021).

Additionally, the use of modeling approaches that consider both climatic and geospatial factors may reduce uncertainties in projected snow cover dynamics (Kis & Pongrác, 2023).

In light of the scarcity of ground-based climate and snow data, the current study employs CHIRPS and CHIRTS climate data, alongside MODIS snow data, to conduct a comprehensive assessment of climate change impacts on snow cover dynamics in the Rwenzori mountains. Emphasizing the interplay between climate change effects and snow cover dynamics within the region, the study aims to fill the gap in real-world data by using satellite-based products and modeling techniques.

1.2. Research Objectives

The study's goal is to comprehensively assess the impact of climate change on Rwenzori mountains snow cover dynamics, providing a comprehensive understanding of both the impact of climate change in the Rwenzori mountains and how this, in turn, affects snow cover dynamics within the region.

Specifically, the study aims:

- ✓ Analyze 1991-2020 climate on Rwenzori Mountains, focusing on interannual, seasonal, and monthly variations.
- ✓ Contrast projected climate conditions under SSP245 and SSP585, for near and far future.
- ✓ Assess 2000-2022 snow cover dynamics on Rwenzori, including interannual, seasonal, and monthly variations and climatic influences.
- ✓ Validate the J2000 model's accuracy and performance with MODIS snow cover data and project future snow dynamics for the Rwenzori Mountains under SSP245 and SSP585 scenarios.

1.3. Research questions

In light of the research objectives, the following questions guided our investigation:

- How have interannual, seasonal, and monthly climate patterns in the Rwenzori Mountains evolved between 1991 and 2020?
- What are the contrasting projected climate conditions under SSP245 and SSP585 scenarios for the near and far future periods, and how do these scenarios differ from historical data in terms of temperature and precipitation?
- How do snow cover dynamics vary across different seasons and years in the Rwenzori Mountains from 2000 to 2022, and what climatic factors influence these variations?
- How accurately does the J2000 model simulate snow cover dynamics in the Rwenzori Mountains when compared to MODIS snow cover data, and what are the projected

changes in snow cover extent and duration under SSP245 and SSP585 scenarios for the future periods?

1.4. Research hypothesis

Given the research questions, the following predicted responses directed our exploration:

- Variations in interannual, seasonal, and monthly climate patterns observed in the Rwenzori Mountains between 1991 and 2020 are indicative of climate change impacts, with potential shifts in temperature and precipitation regimes over the study period.
- Projected climate conditions under SSP245 and SSP585 scenarios for both near and far future periods will demonstrate divergent trends compared to historical data, reflecting the influence of different emission scenarios on future climate dynamics in the Rwenzori Mountains.
- The analysis of snow cover dynamics from 2000 to 2022 will reveal significant temporal variations and spatial distributions, with climatic influences playing a key role in shaping snow cover patterns across different seasons and years in the Rwenzori Mountains.
- Validation of the J2000 model's accuracy and performance using MODIS snow cover data will confirm the reliability of the model in simulating snow dynamics in the study area. Additionally, projections of future snow cover dynamics under SSP245 and SSP585 scenarios will provide insights into potential changes in snow extent and duration, contributing to our understanding of the impacts of climate change on snow cover dynamics in the Rwenzori Mountains.

1.5. Significance of the study

The significance of this study is multifaceted. By examining climate data from 1991 to 2020, the research provides nuanced insights into the evolving climate patterns of the Rwenzori Mountains, crucial for informing adaptation strategies and mitigating risks posed by climate change. Moreover, the contrasting projections of future climate conditions under different emission scenarios offer foresight into potential climatic trajectories, guiding decision-making processes related to infrastructure planning and disaster management. Additionally, the assessment of snow cover dynamics from 2000 to 2022, alongside an analysis of climatic influences, enhances our understanding of hydrological implications and snow-related hazards, essential for effective water resource management and risk mitigation. Finally, the validation of the J2000 model's accuracy and its projections of future snow dynamics contribute to refining modeling techniques, aiding policymakers, researchers, and stakeholders in devising targeted strategies to safeguard vulnerable communities and ecosystems in the Rwenzori mountains region and beyond.

1.6. Scope and limitations of the study

This thesis undertakes a comprehensive analysis of the impacts of climate change on snow cover dynamics in the Rwenzori Mountains, employing a novel approach that integrates satellite data (MODIS data), climate reanalyses (CHIRPS and CHIRTS), and hydrological modeling (J2000 model) to overcome the challenge of limited ground-based meteorological observations in the region. Covering the period from 1991 to 2022, it explores interannual, seasonal, and monthly variations in climate and snow cover, alongside future projections under SSP245 and SSP585 scenarios, thereby providing a detailed overview of past trends and future potential changes in the Rwenzori Mountains' snow cover. However, this study is constrained by its reliance on remote sensing data and modeling outputs due to the scarcity of in-situ observations. Such dependence introduces inherent uncertainties related to the resolution and accuracy of satellite data and the assumptions embedded in climate models and reanalyses. These factors limit the precision of our findings, highlighting the balance between innovative methodological approaches and the inherent constraints of data and model-dependent research in remote, data-sparse environments.

2. LITERATURE REVIEW

2.1. Climate characteristics of mountainous regions

Mountainous regions, with their intricate topography characterized by high elevations, steep slopes, and diverse landforms, exert a profound influence on global climate patterns (Viloria & Tricio, 2023). As underscored by Wypych et al. (2023), these unique climate characteristics necessitate a comprehensive understanding to anticipate and address the repercussions of climate change on these ecologically sensitive areas. The temperature dynamics in mountainous climates exhibit altitude-dependent patterns, resulting in the establishment of temperature inversion layers as elevation increases (Pepin et al., 2022). This phenomenon, as elucidated by Bell et al. (2022), holds considerable implications for species distribution and biodiversity, as well as influencing weather patterns, precipitation, and cloud formation.

The precipitation patterns in mountainous regions are intricately tied to orographic effects, where moist air ascends over mountain barriers, inducing enhanced rainfall on windward slopes and creating rain shadows on the leeward side. The empirical investigation conducted by Lee et al. (2023), using the Weather Research and Forecasting (WRF) model, has provided insights into the elevation-dependent intensification of rainfall. This orographic precipitation, as articulated by Forte and Rossi (2023), significantly contributes to downstream water resources. The critical role of snow cover and glaciers in mountainous climates cannot be overstated, with Li et al. (2023) emphasizing their impact on climate regulation through albedo. Snow cover enhances the Earth's surface reflectivity, cooling the climate by reflecting more sunlight into space. Conversely, diminishing snow cover contributes to warming as darker surfaces absorb more sunlight. Glaciers, acting as reservoirs, regulate climate by storing water as ice and releasing it gradually, influencing streamflow during dry periods (Knight & Harrison, 2023). Ongoing research efforts by Huss et al. (2017) seek to comprehend the response of mountain glaciers to climate change, with implications for water resource management and sea-level rise.

Extreme weather events, such as avalanches, landslides, and flash floods, are inherent to mountainous climates due to steep terrain and rapid weather fluctuations (Lutz et al., 2020). An understanding of the frequency and intensity of these events is imperative for effective hazard mitigation and disaster preparedness in mountainous regions.

The impact of climate change on mountainous regions is a focal point of concern. Studies by Beniston et al. (2018) and Li et al. (2021) highlight discernible shifts in temperature, precipitation patterns, and the reduction of glaciers, all of which have cascading effects on ecosystems, water resources, and communities reliant on mountain environments. This growing body of literature

underscores the urgency of continued research to comprehend, anticipate, and mitigate the multifaceted impacts of climate change on mountainous regions.

The interconnection of mountainous climate systems extends beyond local impacts, influencing global atmospheric circulation patterns. Mountains, as highlighted by Kad et al. (2023), serve as barriers to air masses, shaping broader weather systems. Changes in mountainous climate dynamics can instigate cascading effects on regional and global climates.

2.2. Climate modeling and projections

2.2.1. ScenarioMIP's contributions to climate projections and CMIP6 advancements

The field of climate modeling and projections has seen considerable advancements, underscored by a collaborative effort within the scientific community to enhance our understanding of climate dynamics and their implications for society. The Scenario Model Intercomparison Project (ScenarioMIP) for CMIP6, as described by O'Neill et al. (2016), plays a pivotal role in this endeavor by offering multi-model climate projections based on varied future scenarios. This initiative facilitates a wide range of integrated studies, proving instrumental for the Intergovernmental Panel on Climate Change (IPCC) assessments and addressing critical science and policy questions related to climate forcings and warming limits.

Building on the foundation laid by ScenarioMIP, McBride et al. (2021) conducted a comparative analysis of CMIP6 historical climate simulations against an empirical model, highlighting the complexities of projected warming rates and the significant role of aerosol radiative forcing and methane emissions in climate sensitivity and achieving Paris Agreement targets. This comparative approach not only reveals the intricacies within climate modeling efforts but also emphasizes the variability in climate feedback mechanisms over time, a crucial aspect of climate projections. In a similar vein, Tokarska et al. (2020) sought to reconcile the stronger warming projections of CMIP6 models with empirical evidence, providing an observationally constrained perspective that offers a more optimistic outlook for achieving the Paris Agreement targets under ambitious mitigation scenarios. This approach underscores the importance of empirical grounding in future projections, emphasizing the utility of past and present climate data in refining future climate models.

Further exploring the impacts of climate change, Dutta et al. (2022) investigated global solar energy potential under changing climate conditions, unveiling region-specific variations that highlight the interplay between climate change and renewable energy resources. Such insights are crucial for developing adaptive strategies in energy planning, underscoring the need for an

integrated approach to climate and energy policy. Extending the discussion to climate extremes, Deepa et al. (2024) highlighted the increased frequency and severity of extreme events, emphasizing the substantial risks posed to human health, agriculture, and water resources. This review elucidates the critical need for robust adaptation and mitigation strategies to address the challenges posed by extreme climate phenomena.

Addressing the broader implications of climate modeling and scenario development, Gütschow et al. (2021) and Pielke Jr & Ritchie (2021) critique the current practices of scenario development and misuse in climate policy analysis and research. They advocate for more transparent and scientifically coherent scenario development practices to enhance the policy relevance and credibility of climate research, highlighting the importance of aligning scientific inquiry with real-world policy and adaptation needs. Regional analyses by Kumar et al. (2022), Das et al. (2022), Almazroui et al. (2020), and Bouramdane (2022) further contribute to our understanding of the differential impacts of climate change, particularly emphasizing temperature and precipitation changes in regions like Africa. These studies underscore the urgent need to address climate vulnerabilities in less economically developed regions, highlighting the global nature of climate change and the localized nuances of its impacts.

2.2.2. Climate uncertainty through the role of shared socioeconomic pathways

The Shared Socioeconomic Pathways (SSPs) encompass a suite of divergent yet interconnected narratives, each meticulously crafted to illuminate the multifaceted challenges and opportunities that could shape our global future. These narratives, rooted in an intricate mesh of greenhouse gas emissions, land use dynamics, aerosol concentrations, and socioeconomic trajectories, provide a robust scaffold for the Scenario Model Intercomparison Project (ScenarioMIP) within the broader Coupled Model Intercomparison Project Phase 6 (CMIP6). The essence of ScenarioMIP lies in its strategic employment of these SSP-based scenarios to forge forward-looking climate projections. This endeavor not only anchors a critical segment of CMIP6 but also lays the groundwork for an integrated exploration of potential climate impacts, adaptive capacities, and mitigation trajectories (O'Neill et al. 2016; Riahi et al. 2017).

Central to the ethos of ScenarioMIP is a dual-fold objective: to dissect the climate system's responsiveness to an array of forcing scenarios and to navigate the murky waters of uncertainty that future climate change heralds, especially as it pertains to land use changes, emissions pathways, and socio-economic evolution. The meticulous selection of scenarios under ScenarioMIP's umbrella ranging from the continuity of RCP narratives to the introduction of novel "gap scenarios" is emblematic of a concerted effort to straddle a wide spectrum of scientific

inquiries and policy dialogues (Van Vuuren et al. 2012; Van Vuuren et al. 2014). This selection process is underpinned by a stringent criterion of feasibility within integrated assessment models (IAMs), ensuring each scenario's relevance to contemporary societal concerns and the ambitious benchmarks set by international accords like the Paris Agreement (Riahi et al. 2017; Elmar et al. 2017; Smith et al. 2023).

The suite of SSP scenarios delineated for ScenarioMIP encapsulates a rich tableau of possible futures, each painting a distinct picture of the world's navigational strategies through the climate crisis. At one end of the spectrum lies SSP5-8.5, a portrayal of a world racing along the fast lane of economic growth, heavily reliant on fossil fuels, thereby catapulting to high greenhouse gas emissions. This narrative starkly contrasts with SSP1-2.6, where the global community coalesces around sustainability, embarking on a concerted push towards renewable energy, resulting in a significant curtailment of emissions. The selection of these scenarios, each underpinned by its own unique set of assumptions and implications, mirrors the diversity of pathways humanity might take. This diversity is instrumental in probing a myriad of research questions and policy considerations, ranging from the impact of land-use dynamics on climate to the exploration of climate outcomes under various mitigation efforts (O'Neill et al. 2016; Riahi et al. 2017). Delving deeper, ScenarioMIP serves as a crucible for addressing some of the most pressing scientific questions of our time. It interrogates the climate system's sensitivity to divergent socio-economic pathways, scrutinizes the ramifications of overshoot scenarios, and explores the viability of emergent constraints as a means to refine climate projections (Van Vuuren et al. 2012; Van Vuuren et al. 2014; O'Neill et al. 2016; Riahi et al. 2017).

Within the landscape of future global developments, the Shared Socioeconomic Pathways (SSPs) (Figure 1) provide a comprehensive spectrum of scenarios, each articulating distinct narratives about how societal choices influence climate outcomes (O'Neill et al. 2016; Riahi et al. 2017). SSP5-8.5, often referred to as "Taking the highway," envisions a trajectory of unfettered economic growth and urbanization, heavily reliant on fossil fuels, which propels high energy demand and significant greenhouse gas emissions. This scenario anticipates technological advancements and a global population that peaks mid-century, yet it does so at the expense of environmental integrity, without any dedicated efforts towards climate mitigation, serving as a benchmark for high-emission futures (O'Neill et al. 2016; Riahi et al. 2017; Elmar et al. 2017). Contrastingly, SSP3-7.0, or "A rocky road," portrays a world fragmented by regional rivalries, where economic growth is sluggish, and environmental concerns are sidelined. High population growth, security-focused regional policies, and a dependence on coal characterize this pathway, leading to medium-high emissions and scant global cooperation on climate initiatives. This scenario

underscores the challenges posed by a lack of unified global action against climate change (O'Neill et al. 2016; Oliver et al. 2017). SSP4-6.0 and its counterpart, SSP4-3.4, delve into a world marked by growing inequalities. The former, "A road divided," reflects a divergence where advanced economies enjoy the fruits of sustainable practices and technological innovations, while others fall behind, culminating in medium-level emissions driven by disparate mitigation efforts. The latter scenario intensifies the quest for lower radiative forcing through more vigorous global emission reduction efforts, showcasing the potential of widespread adoption of clean technologies and enhanced international collaboration (Riahi et al. 2017; Malte et al. 2019).

In the middle of the spectrum, SSP2-4.5 encapsulates a "business as usual" scenario where current trends persist without significant shifts, leading to moderate mitigation and adaptation challenges. This pathway benefits from gradual technological and social advancements, coupled with steady economic and demographic growth, aiming for a balanced approach to climate change (Riahi et al. 2017; Magnus et al. 2022). The SSP5-3.4-OS scenario presents a narrative of "Overshoot and mitigation," where initial high emissions set the stage for rapid decarbonization efforts. This pathway acknowledges the potential for temporary overshooting of climate targets before a determined push towards cleaner energy sources and carbon dioxide removal technologies facilitates stabilization at lower warming levels (O'Neill et al. 2016; Melnikova, et al. 2021).

At the more optimistic end of the spectrum, SSP1-2.6, dubbed "Taking the green road," champions a future committed to sustainability and renewable energy, bolstered by global cooperation. This scenario forecasts rapid technological progress, a declining population trend, and substantial environmental conservation efforts, all geared towards ambitious climate policies that seek to cap warming well below 2°C. Building on this vision, SSP1-1.9 aims to venture "Towards a better world," with aspirations to curtail emissions further to keep warming around 1.5°C. Achieving net-zero emissions by mid-century and leveraging significant carbon dioxide removal technologies underscore this pathway's commitment to surpassing the Paris Agreement's more stringent targets, emphasizing equity and environmental preservation (O'Neill et al. 2016; Riahi et al. 2017).

Through this multifaceted inquiry, ScenarioMIP significantly enriches our understanding of how human endeavors could shape the Earth's climate system, highlighting the profound uncertainties that lace our socioeconomic fabric and environmental stewardship efforts. In doing so, ScenarioMIP not only contributes to the scientific discourse on climate change but also informs the strategic contours of global policy and action, aiming for a sustainable and resilient future.

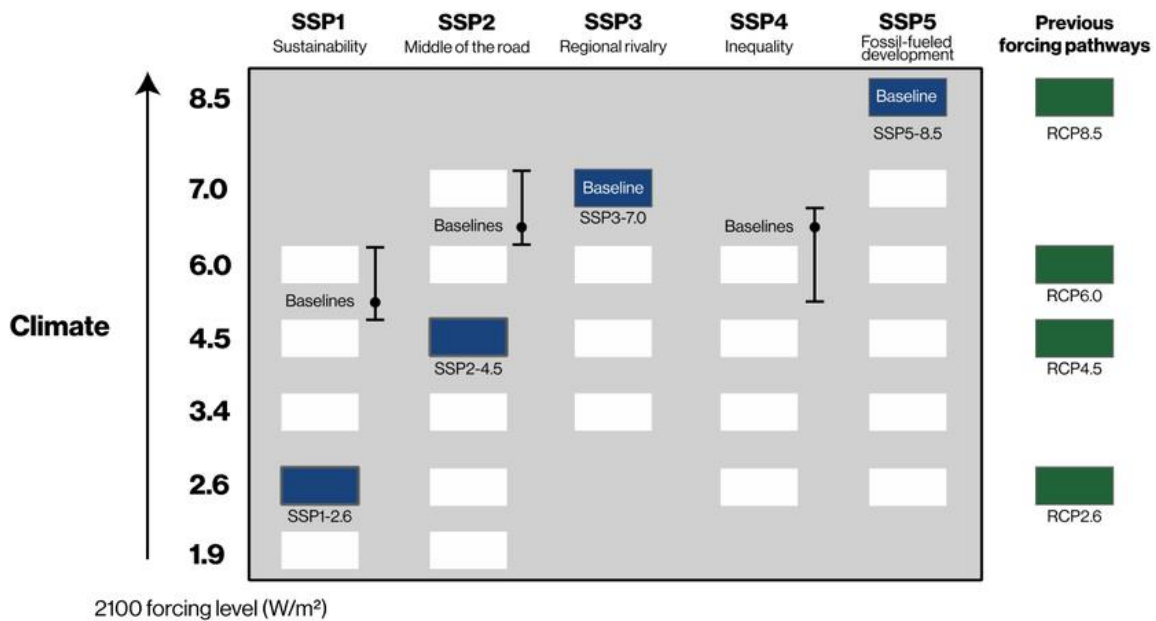


Figure 1. Scenario matrix for climate model experimentation informing the sixth coupled model intercomparison project (CMIP6) (O'Neill et al. 2016 and Benveniste et al. 2020). Baseline ranges for SSP 1, 2, and 4 scenarios are illustrated with black lines. Blue rectangles highlight the primary (Tier 1) scenarios designated for focused examination in climate model experiments.

2.3. Critical intersection of snow cover, climate change, and environmental impact

2.3.1. Significance of snow cover in environmental systems

Snow cover holds profound implications beyond its aesthetic contribution to landscapes, playing a crucial role in hydrology, climate regulation, ecology, water resource management, and understanding climate change dynamics. Snow cover is integral to the hydrological cycle, acting as a natural reservoir that significantly contributes to river flow through gradual melting. This process is vital for replenishing freshwater sources, affecting water availability for both ecosystems and human consumption, and is essential for predicting changes in river discharge (Yoo et al., 2020; Chu et al., 2023; Michel et al., 2023; Cervera & Durán, 2023).

Snow also serves as an insulating layer that influences soil temperature and protects vegetation from extreme cold, contributing to climate regulation through the albedo effect, where it reflects sunlight to help regulate regional and global climates. Changes in snow cover patterns can thus have significant effects on temperature regimes, impacting ecosystems and biodiversity (Liu et al., 2023; Miska et al., 2023; Long and Zhang, 2023; Guo et al., 2022). Moreover, snow cover provides habitat and protection for various organisms, influencing their life cycles and leading to ecosystem shifts, highlighting the need for effective water resource management in regions dependent on snowmelt (Chu et al., 2023; Michel et al., 2023; Zhang et al., 2023).

The intricate relationship between snow cover and climate change is evident, with global temperature increases leading to observable alterations in snow extent, duration, and depth. This transformation highlights the importance of snow cover in the Earth's hydrological cycle, where it acts as a critical component of the cryosphere, interacting with ice, glaciers, and permafrost, and contributes to our understanding of climate change impacts (Barnett et al., 2005; Derksen and Brown, 2012; Daloz et al., 2022). Altered snowmelt regimes due to climate change can substantially influence water resources, necessitating a comprehensive understanding of snow cover dynamics for anticipating future changes and mitigating impacts on ecosystems, human activities, and socio-economic sectors dependent on predictable snow patterns (Molotch et al., 2010; Barnett et al., 2008; Parmesan, 2007; Post et al., 2009; Scott et al., 2012; Steiger et al., 2017). The study of snow cover in the context of climate change thus transcends disciplinary boundaries, encompassing ecological, hydrological, and socio-economic dimensions critical to global environmental change.

2.3.2. Climate change and snow dynamics

Understanding the impacts of climate change on snow dynamics requires a comprehensive synthesis of findings from multiple studies that explore the intricate relationships between temperature, precipitation, and snowpack changes across various geographic and climatic zones. Insights from seminal works by Kapnick and Hall (2012), Easterling et al. (2017), Stewart (2009), Hayhoe et al. (2007, 2010), Siirila-Woodburn et al. (2021), and additional contributions from DeBeer et al. (2016), Oleksy and Richardson (2021), Salathe et al. (2008), and Bibi et al. (2018), among others, provide a nuanced understanding of how climate change is reshaping snow dynamics globally and regionally.

Stewart (2009) broadens the perspective by examining global climatic impacts on mountain snowpack and snowmelt runoff, highlighting the role of geographic location, elevation, and latitude in determining the nature of these impacts. This global view reveals that while some regions experience decreased snowpack and earlier melt due to warmer temperatures, others may see increases in snowpack attributed to heightened precipitation, illustrating the complex and varied nature of snow dynamics responses to climate change.

The regional analyses provided by Hayhoe et al. (2007, 2010) for the US Northeast and Great Lakes underscore the localized effects of climate change on snow dynamics and hydrological cycles. They forecast warmer temperatures, decreased snow depth, extended growing seasons, and earlier bloom dates, emphasizing the importance of region-specific adaptation and mitigation strategies to address the challenges posed by these changes. Siirila-Woodburn et al. (2021) project

a stark future for the western United States, with significant declines in snowpack and shifts towards low-to-no snow conditions within a few decades if greenhouse gas emissions continue unabated. This anticipated change threatens water resources, ecosystem services, and economic activities dependent on seasonal snow, highlighting the urgency of implementing comprehensive climate change mitigation and adaptation strategies. Kapnick and Hall (2012) provide a foundational understanding of the mechanisms by which regional-scale warming influences the temporal and geographical structure of snowpack changes in western North America. They demonstrate that warming significantly affects snowpack during the mid to late snow season (March through May), leading to decreased snow accumulation and increased melt rates. This period of sensitivity to temperature coincides with the greatest observed losses in snowpack across the region, underlining the direct impact of rising temperatures on snow dynamics. Easterling et al. (2017) expand on the variability in precipitation and its effects on snow dynamics within the United States, noting a national trend towards increased heavy precipitation events and regional differences in annual precipitation changes. These shifts, coupled with warming temperatures, contribute to reduced snow water equivalent and snow cover extent, particularly in the western United States. Their projections of continued declines in snowpack and alterations in precipitation patterns underscore the need for adaptive water management strategies in response to changing snow dynamics.

Adding to this body of knowledge, DeBeer et al. (2016) review climatic, cryospheric, and hydrological changes in western Canada, emphasizing the widespread warming and associated declines in snow cover. They call for improved understanding and predictive capabilities to manage the impacts of climate change on regional water resources. Oleksy and Richardson (2021) discuss the differential warming of lake surface and deep waters, suggesting that increasing stratification may influence lake ecology and biogeochemistry in ways that could have broader implications for water resource management in temperate regions. Salathe Jr et al. (2008) highlight the importance of mesoscale feedbacks in the Pacific Northwest, indicating that regional climate models can offer valuable insights into local responses to climate change, including alterations in snow dynamics. Lastly, Bibi et al. (2018) review the climatic and associated changes on the Tibetan Plateau, noting significant warming trends and their impact on the cryosphere, which serves as a crucial water source for millions of people.

From these insights, it is clear that climate change is profoundly altering snow dynamics across a wide range of geographic and climatic regions. The collective findings emphasize the critical role of temperature and precipitation changes in driving these dynamics, with significant implications for water resources management, ecosystem services, and regional economies. The variability in

responses across different regions underscores the necessity for localized studies and adaptive management strategies that consider the unique climatic, geographical, and ecological characteristics of each area. Further research, improved climate models, and sustained observational efforts are essential for enhancing our understanding of these complex systems and developing effective responses to the challenges posed by climate change.

2.4. MODIS data accuracy and J2000 model insights for snow cover forecasting

2.4.1. Challenges and limitations in assessing snow cover extent in mountainous regions

The endeavor to gauge snow cover extent in mountainous terrains is fraught with considerable obstacles. These include severe meteorological conditions, inadequate communication networks, and the constraints inherent in traditional measurement methodologies. The complex and varied topography of mountain regions exacerbates these challenges, often leading to measurement inaccuracies. Severe weather conditions frequently obstruct the evaluation of snow cover extent. Moreover, the scarcity of communication infrastructure in secluded mountain areas further complicates this evaluation process.

Franz et al. (2013) highlight the scarcity of ground-based observation stations and the logistical challenges associated with maintaining and accessing these stations in rugged terrains. This scarcity impedes the corroboration of satellite-derived measurements, underscoring the necessity for the development of self-sufficient, robust observation systems capable of consistent data transmission from even the most remote locations. Conventional snow cover assessment techniques, such as in-field surveys and aerial imagery, are beset by several limitations. Huang et al. (2011) note that these traditional methods are labor-intensive, time-consuming, and offer only limited spatial coverage, rendering them unsuitable for comprehensive assessments. Additionally, the reliability of these approaches is often compromised by subjective interpretations and the inaccessibility of specific sites.

On the contrary, the employment of Landsat imagery may introduce discrepancies in more detailed analyses due to variations in sensor specifications, atmospheric conditions, incomplete data for certain periods, and differences in image processing approaches (Zhang et al., 2022). Consequently, leveraging satellite-based measurements, such as MODIS data, may provide valuable insights, although these too are not without their limitations.

2.4.2. Potential of MODIS for snow cover analysis

The validation of snow cover models is pivotal in enhancing our understanding of hydrological processes, water resource management, and climate change impacts. With the advent of the

Moderate Resolution Imaging Spectroradiometer (MODIS), researchers have gained an invaluable tool for monitoring snow cover over vast and inaccessible regions. Among the various studies dedicated to this endeavor, the work by Parajka and Blöschl (2006) stands out for its comprehensive evaluation of MODIS snow cover products over Austria, revealing an impressive classification accuracy of 95% on cloud-free days despite the recurrent challenge of cloud cover obscuring 63% of the landscape on average.

The reliability of MODIS snow cover data has been corroborated by studies across different geographical settings. Klein and Barnett (2003) validated MODIS snow cover maps against in-situ measurements and other satellite products over the Upper Rio Grande River Basin, highlighting the high agreement of MODIS data with ground observations. Similarly, Maurer et al. (2003) evaluated MODIS products against snow-covered area data products, underscoring the potential of MODIS in capturing snow dynamics even in cloud-prone regions.

The utility of MODIS data extends beyond mere validation exercises. Simic et al. (2004) and Tekeli et al. (2005) have demonstrated the application of MODIS snow cover maps in modeling snowmelt runoff processes, affirming the data's accuracy and utility in hydrological modeling. These studies underscore the potential of integrating MODIS snow cover data into water resource management and flood forecasting models, thereby enhancing our ability to predict and manage water resources more effectively.

However, the validation and application of MODIS data are not without challenges. Cloud cover significantly impacts the usability of MODIS snow cover products, a limitation noted across various studies (Parajka and Blöschl, 2006; Klein and Barnett, 2003; Maurer et al., 2003). Additionally, the accuracy of MODIS data can vary with land cover types and topographical features, indicating the need for continuous refinement of classification algorithms and cloud masking techniques (Riggs et al., 2006; Romanov et al., 2003).

Despite these challenges, the consensus among researchers is clear: MODIS snow cover products represent a critical resource for the validation of snow cover models and the advancement of hydrological science. The integration of MODIS data with ground observations and other satellite products can provide a more accurate and comprehensive understanding of snow cover dynamics, ultimately contributing to better water management practices and climate change mitigation efforts (Bitner et al., 2002; Zhou et al., 2005; Hall et al., 2002).

2.4.3. J2000 model's effectiveness in snow dynamics simulation

The efficacy of the J2000 model in simulating snow dynamics and its responsiveness to climate change is highlighted through its application across varied hydrological settings. This is

evidenced by research conducted by Gao et al. (2012) in the central Tibetan Plateau and Nepal et al. (2021) in the Western Himalaya, demonstrating the model's robust performance in these distinct and challenging environments. Gao et al. (2012) demonstrated the model's ability to capture the hydrological processes of a glacierized catchment with limited data, highlighting a significant increase in runoff in response to a rise in air temperature. Similarly, Nepal et al. (2021) applied the model to predict future snow cover dynamics, revealing expected reductions in snow cover area across various climate scenarios.

The combined insights from these validations present the J2000 model as a versatile tool for hydrological forecasting in snow-dependent regions, capable of accurately projecting the impacts of climate variability on water resources. The model's demonstrated sensitivity to meteorological changes, particularly temperature and precipitation, enables effective simulation and future projection of snow cover dynamics. This capability is vital for sustainable water resources management and planning in mountainous and glacierized landscapes. The J2000 model, through these studies, emerges as an essential asset in the hydrological science community, offering robust predictions that can guide adaptive strategies in the face of climatic uncertainties (Gao et al. 2012; Nepal et al. 2021).

2.5. Eco-geological dynamics and climatic paradoxes of the Rwenzori mountains

2.5.1. Topographical and geological characteristics of the Rwenzori mountains

The Rwenzori Mountains, an imposing range of Precambrian crystalline rocks, stand as a monumental horst uplifted amidst the African continent. This geological marvel, framed by the grabens of Lakes Albert and Edward to its north and south, underwent a significant tilt from ESE to WNW in the Late Pliocene, as identified by Taylor and Howard (1998). This tilt has sculpted the landscape, creating deeply incised valleys with eastern catchments larger than their western counterparts due to the horst's orientation. The region's rugged alpine landscape, delineated by Gummert et al. (2016), is further marked by its steep slopes, abundant rainfall, and active fault lines which predispose it to frequent landslides (Jacobs et al., 2016a). The mountains' geological fabric is woven from Archaean Gneisses and Palaeoproterozoic units, with Koehn et al. (2017) noting a complex nappe structure that narrates a tale of profound geological evolution.

These mountains, often referred to as the "Mountains of the Moon," present a terrain that vividly reflects the forces of geomorphology, from fluvial erosion and hillslope diffusion to the impacts of glaciation and tectonic uplift a dynamism noted by Kaufmann et al. (2016) with a rock uplift rate of 1-2 mm/year. This dynamic interplay between geological processes and tectonic activity

has endowed the Rwenzori Mountains with their unique topographical and geological identity within the East African Rift system.

Tracing the origins and geological timeline of the Rwenzoris, one finds a landscape deeply influenced by tectonic and volcanic activities. The age of these mountains, as determined through the study of the metamorphic rocks gneiss, schist, amphibolite, and quartzite reveals an onset of rock uplift and exhumation dating back to the Oligocene, with possible roots reaching into the Eocene, according to Osmaston (1989). This rich geological tapestry is further accentuated by signs of past climatic shifts, including glaciation markers like cirques and moraines, highlighting the ongoing evolution driven by natural forces such as erosion and weathering (Garellick et al., 2022).

2.5.2. Rwenzori climatic features and glaciation

The Rwenzori Mountains, a captivating climatic and glacial paradox, exhibit a fascinating gradient of environmental conditions from their lush foothills to their glaciated peaks. At the core of their climatic complexity is the significant role of altitude, which orchestrates a decrease in temperature by approximately 0.6°C for every 100 meters ascended, transitioning from steamy rainforests with average temperatures of 24°C and annual rainfall exceeding 2,000mm, to the afro-alpine zone where temperatures plummet to an average of 8°C , with precipitation surpassing 3,000mm annually (Kervyn et al., 2007; Specht et al., 2014; Osmaston, 1966). This vertical climatic zonation creates a distinctive ecological staircase, each level harboring unique ecosystems.

Adding to this climatic intricacy is the influence of the Intertropical Convergence Zone (ITCZ), a dynamic factor contributing to the Rwenzori's bimodal rainfall pattern. During the wet season, as the ITCZ hovers near the Rwenzoris, the mountains experience heavy rainfall, essential for sustaining the glaciers and the diverse montane ecosystems (Taylor et al., 2020; Kizonde, 2012). However, the shifting patterns of the ITCZ during the dry season result in significantly less precipitation, highlighting the seasonal rhythm that influences the Rwenzori's climate and hydrology (Kizonde, 2012). Also, given its geographic situation in Eastern African zone, the interannual variability of rainfall over the Rwenzori mountains may be subject to the influence of teleconnections such as the El Niño-Southern Oscillation (ENSO) and the Indian Ocean Dipole (IOD) (Nicholson, 2019; Mbigi et al., 2022). These teleconnections exert significant impacts on the timing and intensity of rainfall, with ENSO particularly influential across all seasons (Vaidya, 2005; Preethi et al., 2015).

Yet, the Rwenzori Mountains are facing the undeniable impact of climate change, with studies indicating a worrying trend of rising temperatures, particularly at higher elevations, and changes in rainfall patterns, including increased variability and intensity of storms. These climatic shifts are contributing to accelerated glacial retreat, with some glaciers losing over 1 meter in ice thickness annually, posing threats to the region's biodiversity and water resources (Taylor et al., 2020; Kizonde, 2012).

The paleoclimatic history of the Rwenzoris, particularly during the Last Glacial Maximum (LGM) approximately 19-26.5 thousand years ago, reveals a past characterized by a steeper lapse rate and more pronounced glacial advance. The glacial retreat during the last glacial termination underscores the region's long-standing sensitivity to climatic fluctuations, as evidenced by moraine sequences that provide insights into past equilibrium line altitudes (ELAs) and climatic conditions (Doughty et al., 2023; Garelick et al., 2022; Osmaston, 1989; Doughty et al., 2021). These historical climatic shifts, juxtaposed with contemporary changes, underscore the Rwenzori Mountains' critical role in understanding regional and global climatic dynamics, emphasizing the urgent need for comprehensive studies to mitigate the impacts of current and future climatic changes on this unique mountainous ecosystem.

2.5.3. Biodiversity and hydrology of the Rwenzori mountains

The Rwenzori Mountains, cradled within the Albertine Rift, stand as a testament to the remarkable biodiversity endemic to this area, featuring a rich tapestry of flora and fauna that is unparalleled in the region. The Albertine Rift's diverse forest ecosystems, transitioning from lowland rainforests to alpine montane forests, present a compelling study of biodiversity's altitude correlation. Notably, Poulsen et al. (2005) elucidate this relationship, revealing that species richness peaks at mid-elevations rather than following a linear increase with altitude, suggesting a complex matrix of historical and contemporary environmental factors that shape species distributions. Further insights from Lehmann et al. (2008), Plumptre et al. (2007), and Bruhl et al. (1997) enhance our understanding, indicating that altitude and climatic conditions intricately mold biodiversity patterns across the Rwenzori Mountains. For instance, the endemic plants and amphibians, thriving in these unique ecosystems, highlight the region's ecological significance. However, this biodiversity is under considerable threat from deforestation, climate change, and habitat fragmentation. It is estimated that significant portions of the Rwenzori's habitats have been lost or degraded in recent decades, making the conservation of these ecosystems more critical than ever (Bruhl et al., 1997).

The environmental factors underpinning the biodiversity in the Rwenzori Mountains, such as soil properties, precipitation, and altitude, showcase a detailed interrelation with the region's species composition and richness. Poulsen et al. (2005) notably illustrate that species diversity is not merely a function of altitude but also profoundly influenced by soil pH and cation concentration, shedding light on the intricate dependency of floral diversity on soil conditions. This complex interplay underscores the Rwenzori Mountains as a biodiversity hotspot, governed by intricate environmental interactions, and highlights the urgency for continued, focused research efforts to delve deeper into these patterns.

On the hydrological front, the Rwenzori Mountains exhibit a unique ecological and hydrogeological framework, primarily driven by the region's distinctive precipitation patterns and geothermal characteristics. The geothermal systems, particularly in areas such as Katwe-Kikorongo, Buranga, and Kibiro, are chiefly recharged by meteoric waters. Bahati et al. (2005) report subsurface temperatures suggesting a vast geothermal potential, with estimates indicating temperatures as high as 200°C in some regions, thereby pointing to a significant, yet untapped, geothermal resource awaiting sustainable exploration. The glaciers of the Rwenzori Mountains, crucial to the region's hydrology, face a paradox as Taylor et al. (2009) unveil that glacier melt contributes minimally to alpine river flows. This revelation, pivotal for water resource management, challenges existing paradigms and advocates for a reevaluation of strategies in the face of retreating glaciers.

Furthermore, the limnological attributes of the Rwenzori's alpine lakes and pools, detailed by Eggermont et al. (2007), provide a foundational understanding against which future environmental and biological shifts can be gauged. These ecosystems, predominantly located above 3,500 m elevation, feature specific conductance values ranging from 5 to 52 $\mu\text{S}/\text{cm}$ at 25°C, categorizing them as dilute systems with significant in- and outflow dynamics. This precise limnological data underscores the lakes' oligotrophic to mesotrophic status, emphasizing their phosphorus-limited nature. Additionally, the sensitivity of these lakes to climate warming, as investigated by Eggermont et al. (2010), through chironomid-based reconstructions of mean annual air temperature, exhibits a warming trend, with temperature changes oscillating between a cooling of -2.03°C and a warming of $+3.22^\circ\text{C}$. This variance highlights the ecological vulnerability of the Rwenzori lakes and underscores their value as early-warning systems in the face of global warming.

This integration of biodiversity and hydrological insights paints a comprehensive picture of the Rwenzori Mountains as a region of significant ecological importance and complex hydrological systems. Governed by a myriad of environmental interactions and facing the looming threats of

climate change and anthropogenic pressures, the Rwenzori Mountains necessitate continued research and sustainable management practices to ensure the preservation and protection of this unique mountain range and its invaluable ecosystems.

3. STUDY AREA AND METHODS

3.1. Study area

The Rwenzori Mountains, spanning approximately 110 kilometers in length and 50 kilometers in width, traverse the border between the Democratic Republic of Congo and Uganda (Figures 2a and 2b). Situated within the Eastern African Rift Valley (Taylor et al., 2009), these mountains are specifically situated within the Beni territory in the Democratic Republic of Congo, as well as in the Kasese, Kabarole, and Bundibugyo districts in the Republic of Uganda (Figure 2b).

Physiographically, the mountains exhibit three distinct sectors: north, central, and south. The north sector is traversed by the Ruimi-Wasa fault and the Bwamba Border fault. In contrast, the central sector, distinguished by its highest elevations reaching 5109 meters (Figure 2d) and broadest width, is intersected by the Lamy fault. The south sector experiences a pronounced decrease in elevation. These geological characteristics significantly influence the geomorphic attributes of the Rwenzori Mountains (Nyakecho and Hagemann, 2014; Katumwehe et al., 2015). According to Taylor et al. (2009), the drainage basins of the Rwenzori Mountains discharge through various outlets, including the Mubuku River, Semuliki River, Lake George, Lake Edward, and alpine lakes.

The lithological composition of the Rwenzori Mountains consists mainly of metamorphic rocks dating back to the Archean-Paleoproterozoic period. Gneisses and migmatites dominate the northern and southern parts of the mountains, while Paleoproterozoic amphibolite schists form an east-west belt, known as the Buganda-Toro belt, in the central region. The amphibolite schists are believed to originate from mafic volcanic rocks, and their metamorphic grade decreases from south to north. The Precambrian bedrock formations in the Rwenzori Mountains exhibit high resistance to erosion, leading to low erosion rates in the area (Bauer et al., 2011; Roller et al., 2012).

The precipitation patterns in the Rwenzori Mountains are influenced by the movement of the Inter Tropical Convergence Zone (ITCZ) and the orographic effect caused by the mountain's height. The ITCZ movement results in seasonal variations in precipitation, with two rainy seasons occurring from March to May and August to November. The orographic effect is responsible for an increase in mean annual precipitation from the foot of the mountains to higher altitudes (~3000 m). Limited data exist on precipitation at elevations above ~1370 m, but available measurements indicate a significant rise in mean annual precipitation with increasing elevation. Glacial activity has also played a role in shaping the landscape of the Rwenzori Mountains. Mount Stanley, the highest peak, currently retains a small permanent snow cover. However, glacial events in the

middle Pleistocene, including the Katarua, Rwimi Basin, and Mahoma Lake glaciers, have left their mark on the topography, characterized by U-shaped valleys, terminal moraines, and lateral moraines (Osmaston, 1989; Kaser and Noggler, 1991; Kaser and Osmaston, 2002; Taylor et al., 2009; Kaufmann and Romanov, 2012).

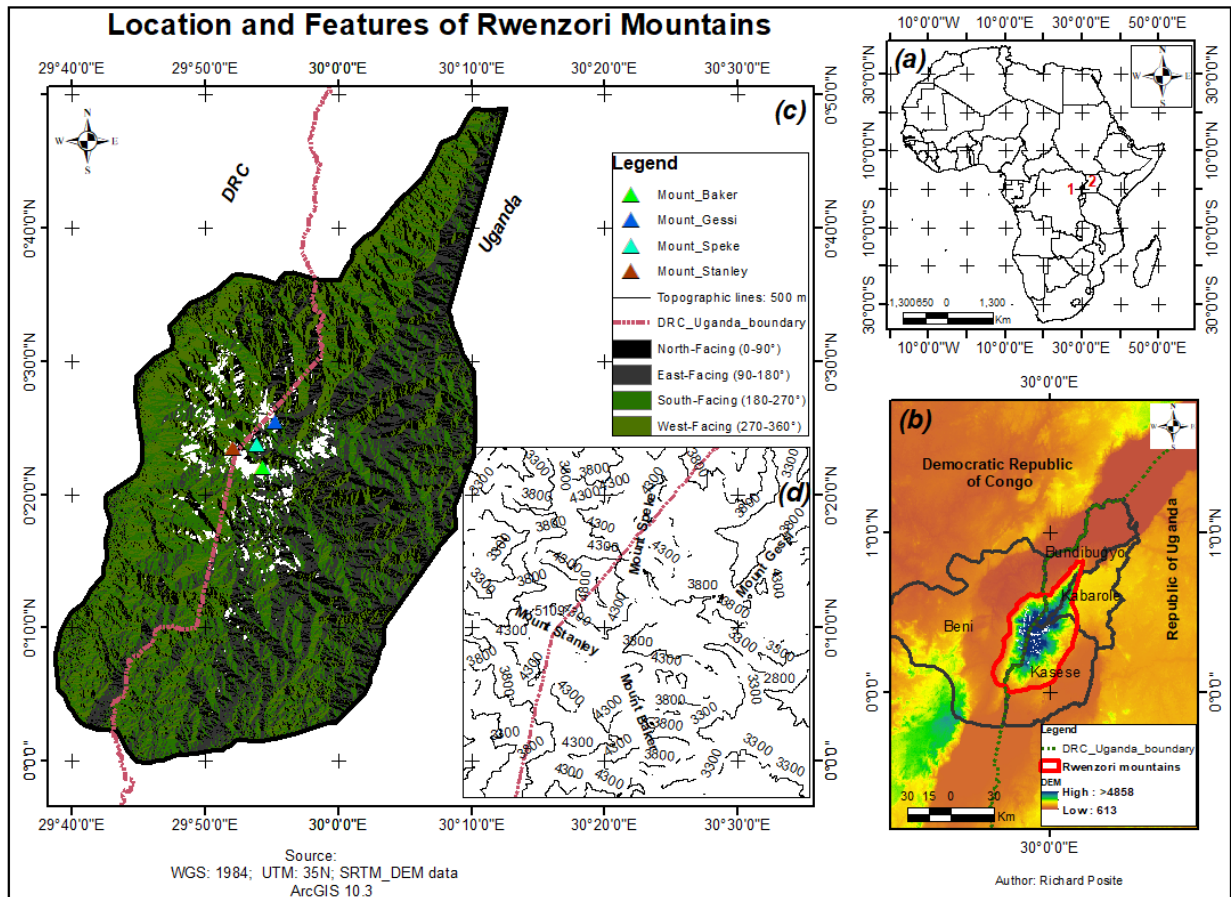


Figure 2.(a) Democratic Republic of the Congo (1) and Republic of Uganda (2) location in Africa; (b) Rwenzori Mountains in the Eastern african rift valley; (c) Rwenzori mountains aspect map; (d) Topographic lines in the central zone of the Rwenzori mountains. The Shuttle Radar Topography Mission (SRTM), Digital Elevation Model (DEM), and Democratic Republic of the Congo (DRC).

3.2. Data collection

3.2.1. Reanalysis climate data and Global Climate Models (GCMs)

Daily reanalysis climate data for the study area were sourced from the CHIRPS (Climate Hazards Group InfraRed Precipitation with Stations) database for precipitation (Funk et al., 2015), and from CHIRTS (Climate Hazards Group InfraRed Temperature with Stations) for temperature (Verdin et al., 2020) (Figure 5). The CHIRPS database offers freely available daily climate data with a gridded spatial resolution of 0.05° , covering a quasi-global extent (50°S – 50°N , 180°E –

180°W) (Funk et al., 2015). Developed to support the United States Agency for International Development Famine Early Warning Systems Network (FEWS NET), CHIRPS integrates methodologies from successful Thermal Infrared (TIR) precipitation products, such as NOAA's Rainfall Estimate (RFE2) and African Rainfall Climatology (Novella et al.2013), alongside the University of Reading's TAMSAT African Rainfall Climatology And Time series (TARCAT). Leveraging the Tropical Rainfall Measuring Mission Multi-satellite Precipitation Analysis version 7 (TMPA 3B42 v7), CHIRPS calibrates global Cold Cloud Duration (CCD) rainfall estimates, enhancing its accuracy (Funk et al., 2015). Similarly, the CHIRTS dataset offers a high-resolution ($0.05^\circ \times 0.05^\circ$) daily maximum and minimum temperature data series spanning 60°S–70°N, crucial for various scientific endeavors. Developed from the CHIRTSmax dataset, CHIRTS-daily disaggregates monthly mean maximum 2-meter air temperatures using daily temperature fields from the ERA5 reanalysis dataset, ensuring accuracy through validation against daily climate station observations from Global Historical Climatology Network (GHCN) and Global Summary of the Day (GSOD) (Verdin et al., 2020). Both CHIRPS and CHIRTS undergo a multi-stage synthesis process incorporating satellite records and in-situ station data, ensuring their reliability and versatility for scientific investigations, including climate studies, hydrological modeling, and agricultural assessments. The datasets used in this study span from 1983 to 2016, providing a robust foundation for analyzing climate and weather dynamics at detailed spatial and temporal scales.

For climate projection, one GCM, MRI-ESM2-0 model, from the Coupled Model Intercomparison Project Phase 6 (CMIP6) were selected based on its accuracy statistical measures (Figure 5). This model, is crucial for simulating future climate scenarios for the study area. The chosen Shared Socioeconomic Pathways (SSPs) encompass SSP2-4.5 and SSP5-8.5, which respectively depict medium and high-forcing scenarios reflecting diverse socioeconomic trajectories (Meinshausen et al., 2020). These selections align with the "middle-of-the-road" and "fossil-fueled" development scenarios, respectively. Rainfall, maximum and minimum temperature data for these models were accessed from the CMIP6 web data portal (<https://pcmdi.llnl.gov/CMIP6>), ensuring uniformity by exclusively using the 'r1i1p1f1' variant denoting the 1st realization, 1st initialization, 1st physics, and 1st forcing.

3.2.2. Snow cover data

The snow cover data used in the current study on the Rwenzori mountains is derived from the Moderate Resolution Imaging Spectroradiometer (MODIS) snow products. These products offer two significant advantages crucial for this research. Firstly, they encompass a long temporal

coverage ranging from 2000 to the present, facilitating the development of long-term scenarios. Secondly, MODIS snow products are widely acknowledged for their robustness and extensive usage worldwide, including in mountainous regions (Muhammad and Thapa, 2021), enabling comparisons with other studies. Snow cover is delineated using the Normalized Difference Snow Index (NDSI) alongside a series of screening techniques designed to mitigate errors and flag uncertain snow cover detections. In fact, the Normalized Difference Snow Index (NDSI) is effective in distinguishing snow from various surface features under a range of illumination conditions. This discrimination relies on the distinct reflectance and emittance properties of snow/ice and clouds. Typically, clouds exhibit high reflectance in the visible and near-infrared wavelengths, in contrast to snow, whose reflectance diminishes in the short-wave infrared wavelengths (Wang et al. 2022). The MODIS datasets used in the current study, possess a spatial resolution of 500 meters and are acquired from NASA's National Snow and Ice Data Center Distributed Active Archive Center, ensuring data reliability and quality. Various datasets corresponding to different principal peaks of the Rwenzori Mountains, namely Baker, Gessi, Speke, and Stanley, have been incorporated into the analysis. The MODIS snow products have previously been employed in hydrological modeling (Di Marco et al., 2021; Tong et al., 2021; Bhatta et al., 2020) and studies focusing on snowline shifting (Tang et al., 2021; Deng et al., 2021; Khadka et al., 2020; Nepal et al., 2021).

3.2.3. Geospatial data

Digital Elevation Model (DEM), land cover, and soil properties data were gathered for the study. The 90-meter resolution Digital Elevation Model (DEM) (Braun & Fotopoulos, 2007; Hasan, 2019) was obtained from the Shuttle Radar Topography Mission (SRTM) website. Land cover data were sourced from GlobCover (Pérez-Hoyos et al., 2017; Grekousis et al., 2015; Nepal et al., 2021) (Figure 5). Soil properties data were acquired from the ISRIC-World Soil Information website (Ribeiro et al., 2015). Additionally, a field survey was conducted to collect the geographical coordinates necessary for the validation of remotely obtained information.

3.3. Processing and analysis

3.3.1. Distribution mapping for climate variable downscaling in Rwenzori mountains

The downscaling process in this study was conducted using the Distribution Mapping (DM) approach (Figure 5), facilitated by the Climate Model for Hydrological Downscaling (CMhyd). This approach ensured spatial refinement and granularity necessary for localized climate impact assessments.

In the DM method, the distribution function of the simulated General Circulation Model (GCM) data is corrected with that of the observed data. This adjustment involves modifying the mean, standard deviation, and quantiles while retaining extreme data values. It operates under the assumption that observed data and model-simulated raw data follow the same distribution function, thereby minimizing unnecessary biases (Thiemeßl et al., 2012).

For precipitation, the gamma distribution function with shape parameter α and scale parameter β was utilized. This distribution function has been verified to be effective and is expressed in distribution 1, where x represents the observed variable, $\Gamma(\cdot)$ is Gamma function, α is form parameter, and β is scale parameter.

$$f_{\gamma}(x|\alpha, \beta) = x^{\alpha-1} \times \frac{1}{\beta^{\alpha} \Gamma(\alpha)} \times e^{-\frac{x}{\beta}}; x \geq 0, \alpha, \beta > 0 \quad (1)$$

The bias correction for precipitation is performed using distribution 2, known as the LOCI-corrected precipitation data, where $F_{\gamma}()$ and $F_{\gamma}^{-1}()$ are the gamma CDF (cumulative distribution function) and its inverse; $\alpha_{LOCI,m}$ and $\beta_{LOCI,m}$ are the fitted gamma parameters for the LOCI-corrected precipitation in a given month m ; and $\alpha_{obs,m}$ and $\beta_{obs,m}$ are the fitted gamma parameters for observed data (Ghimire et al., 2019).

$$P_{cor,m,d} = F_{\gamma}^{-1}(F_{\gamma}(P_{LOCI,m,d}|\alpha_{LOCI,m}, \beta_{LOCI,m})|\alpha_{obs,m}, \beta_{obs,m}) \quad (2)$$

For temperature, the Gaussian cumulative distribution function shown in (Wood et al. 2004, Londhe et al. 2023), or normal distribution with mean μ and standard deviation σ , is assumed to fit temperature best (Teutschbein & Seibert 2010, Londhe et al. 2023) (Distribution 3).

$$f_N(x|\varphi, \sigma) = \frac{1}{\sigma \sqrt{2\pi}} \times e^{-\frac{(x-\varphi)^2}{2\sigma^2}}; x \in R \quad (3)$$

Similarly, corrected temperature values are estimated using distribution 4, where $F_N()$ and $F_N^{-1}()$ are the Gaussian CDF and its inverse; $\varphi_{raw,m}$ and $\varphi_{obs,m}$ are fitted and observed means for the raw and observed temperature data at a given month, m ; and $\sigma_{raw,m}$ and $\sigma_{obs,m}$ are fitted and observed standard variation for the raw and observed temperature time series at a given month, m (Wood et al., 2004; Teutschbein & Seibert, 2010).

$$T_{cor,m,d} = F_N^{-1}(F_N(P_{raw,m,d}|\varphi_{raw,m}, \sigma_{raw,m})|\varphi_{obs,m}, \sigma_{obs,m}) \quad (4)$$

3.3.2. GCM performance in simulating climate variables over the Rwenzori mountains

Accurate simulation of climate variables in mountainous regions is critical for understanding regional climate dynamics, and thus, the performance of the MRI-ESM2-0 model in simulating CHIRTS and CHIRPS data over the Rwenzori Mountains was comprehensively assessed. For maximum temperatures (Tmax), the model demonstrated relatively low discrepancies with

observed values, indicated by a Mean Absolute Error (MAE) of 0.3035 and a Root Mean Squared Error (RMSE) of 0.1455. The positive correlation ($r= 0.538$) and R^2 of 0.29, have been observed. Although a negligible Percent Bias (Pbias) of 0.06 was observed, indicating minimal overestimation tendencies, the Nash-Sutcliffe Efficiency (NSE) value of 0.6963 signified a satisfactory fit to observed data. In simulating minimum temperatures (Tmin), the MRI-ESM2-0 model showed promising results, with a MAE of 0.2879 and a RMSE of 0.1229, suggesting relatively small discrepancies. The r of 0.583 and R^2 of 0.34, have been calculated. A negligible Pbias of -0.0024 indicated minimal underestimation tendencies. The model captured approximately 72% of Tmin variability (NSE = 0.7211), demonstrating its potential for simulating Tmin in mountainous regions.

Furthermore, the model's performance in simulating precipitation using CHIRPS data yielded high accuracy, with a MAE of 0.0811 and a RMSE of 0.0110. A negligible Pbias of 0.015 indicated minimal systematic deviation, while a strong positive correlation ($r= 0.947$) and high coefficient of determination ($R^2 = 0.8983$) highlighted the model's effectiveness in replicating observed rainfall patterns. The Nash-Sutcliffe Efficiency (NSE) of 0.8956 further emphasized the model's reliability in capturing rainfall variability. Therefore, based on its ability to accurately simulate climate dynamics in the Rwenzori Mountains, the MRI-ESM2-0 model has been chosen over other GCM for use in the current study.

3.3.3. Temporal and spatial trends analysis in Rwenzori mountains climate

The examination of temperature and rainfall data spanned three distinct periods: a 30-year baseline (historical) period from 1991 to 2020, and two 40-year intervals representing the near future (2021–2060) and far future (2061–2100) (Figure 5). Using Rstudio, Originlab, and ArcGIS 10.3 softwares, analyses were conducted both across the entire mountainous region and specifically within the central zone, where snow and glacier coverage are observed. A comprehensive investigation into historical and projected temperature and rainfall trends was undertaken using robust statistical methods, including the Mann-Kendall test and Sen's Slope analysis. Implemented through the R "trend" package, this methodical assessment has been previously endorsed by researchers (Zakeri *et al.*, 2019, Nyikadzino 2020, Joshi and Makhasana 2020, Salarian *et al.* 2022, Bharath and Venkatesh 2022) for trend detection in climate phenomena. The Mann-Kendall Test, a non-parametric technique, evaluates correlations between time and variables, with detection of statistically significant trends relying on the Z-value. A significance level of 0.05 was employed, yielding p-values for each analyzed time series. Additionally, the magnitude of trends was assessed using the Sen estimator, which computes

slopes across the dataset and derives Sen's slope through pairwise slopes' medians. The Kriging Algorithm was used to enhance the resolution of spatial distribution maps depicting climate variables. Isotherms and isohyets, representing equidistant values for temperatures and rainfall respectively, were used to enhance understanding of intricate spatial climate distribution over the region. Furthermore, the Linear Regression Algorithm was employed to analyze the relationships between different climate variables across the mountainous terrain.

3.3.4. JAMS/J2000 model and set up

Snow cover dynamics were evaluated using the JAMS/J2000 hydrological model, renowned for its efficacy in simulating cryospheric processes (Shen et al., 2018; Shrestha and Nepal, 2019). Implemented as part of the JAMS Modelling System, this model has demonstrated reliability across various mountainous regions, offering robust assessments of snow cover dynamics at multiple spatial scales (Shen et al., 2018; Eeckman et al., 2019; Shrestha and Nepal, 2019; Nepal et al., 2021). The J2000 snow module, a core component of the model, facilitates the simulation of snow accumulation, metamorphosis, and melt processes for individual spatial entities. Key variables such as snow cover extent, snow storage, and snowmelt are derived from the model outputs. Detailed information on the J2000 snow module is available on the official JAMS Modelling System website (<http://jams.uni-jena.de/ilmswiki>).

The J2000 hydrological model employs hydrological response units (HRUs) as spatial modelling entities, which were derived through an integrated workflow using various datasets. These HRUs were delineated based on the SRTM digital elevation model, land cover data, and soil properties. From the DEM, it has been mapped essential topographical attributes (Figure 3) such as slope, aspect, and curvature, while land cover data included parameters like root depth and leaf area index (Figure 3 and Figure 5). Soil data incorporated properties (Figure 4 and Figure 5) like water holding capacity, influencing processes such as infiltration, percolation, evapotranspiration, and soil moisture flow. Following the integration of these datasets, the HRU delineation workflow yielded a total of 2757 HRUs.

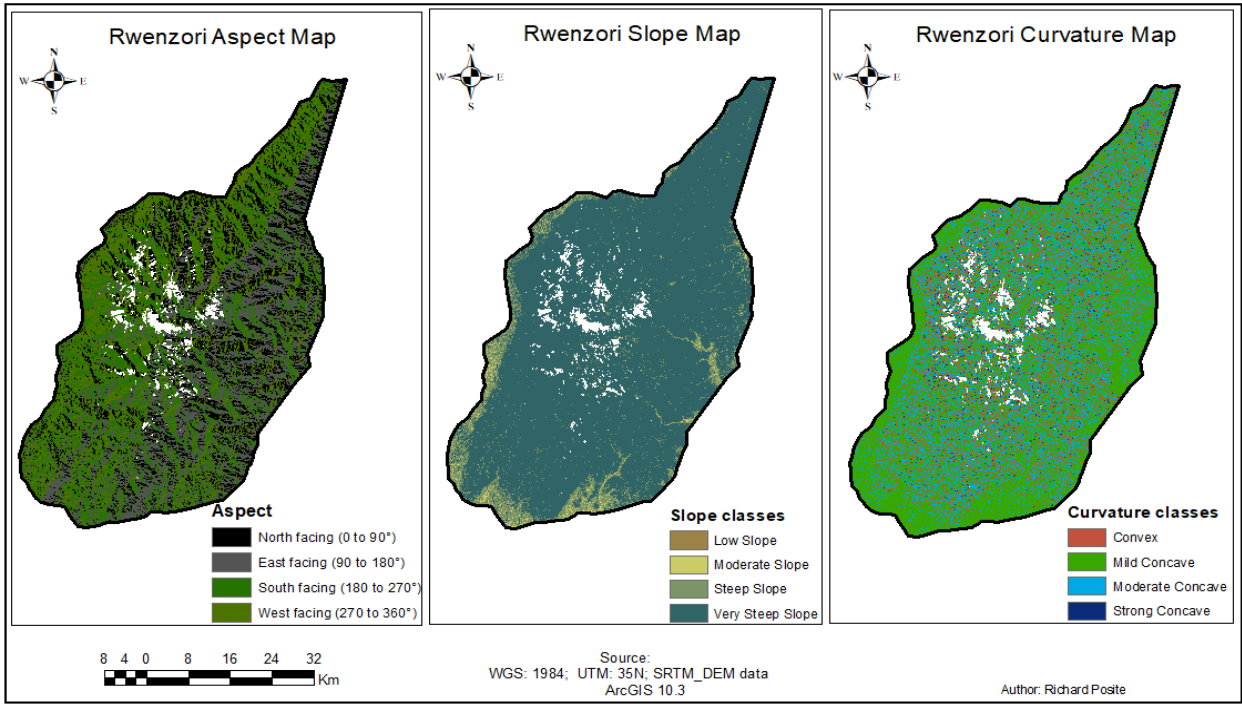


Figure 3. Topographical attributes of the Rwenzori mountains

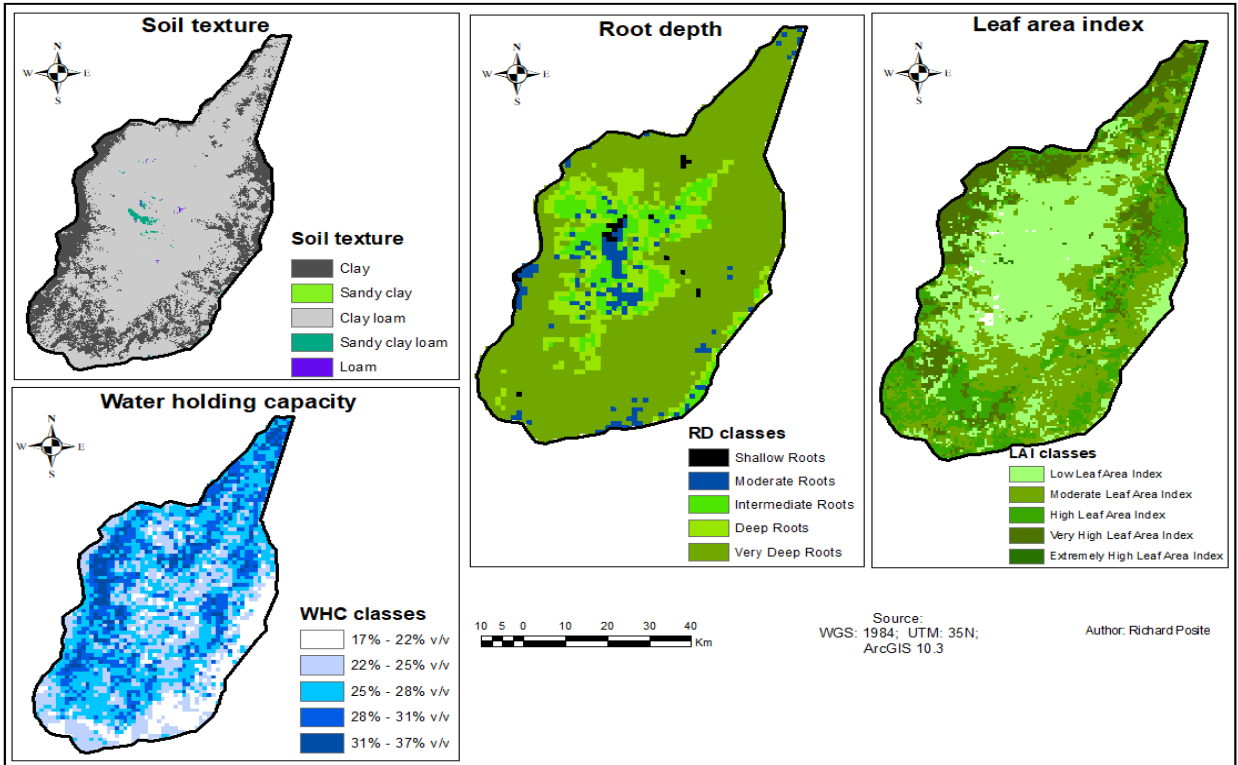


Figure 4. Soil texture, water holding capacity, root depth, and leaf area index of the Rwenzori mountains

3.3. 5. Snow cover assessment

Snow cover assessment involved the comparison of MODIS-derived snow cover data with model outputs for calibration (2000-2014) and validation (2015-2022) periods (Figure 23), with the snow cover area data serving as the model output for analyzing climate change impacts on snow dynamics. Two 35-year intervals representing near-future (2030–2065) and far-future (2066–2100) projections were considered, based on climate data from the MRI-ESM2-0 model and selected Shared Socioeconomic Pathways (SSPs) SSP2-4.5 and SSP5-8.5 (section 3.2.1) (Figure 5). Trend analysis for both historical and projected snow cover was conducted using the Mann-Kendall test and Sen’s method as outlined in section 3.3.3, while differences in snow cover dynamics across different mounts and timescales were assessed using ANOVA tests.

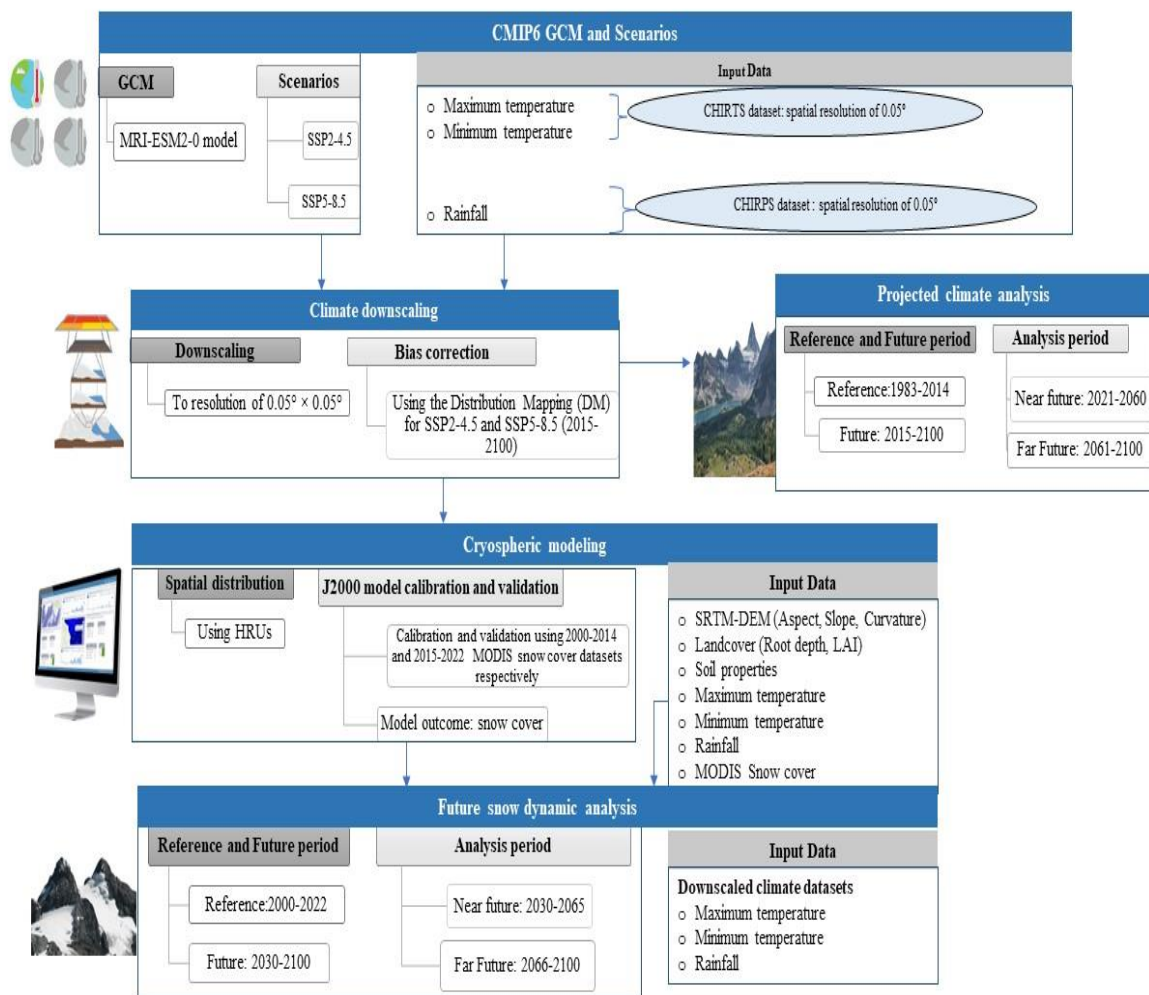


Figure 5. Flow chart of climate change assessment on snow dynamics in the Rwenzori mountains

4. RESULTS AND DISCUSSION

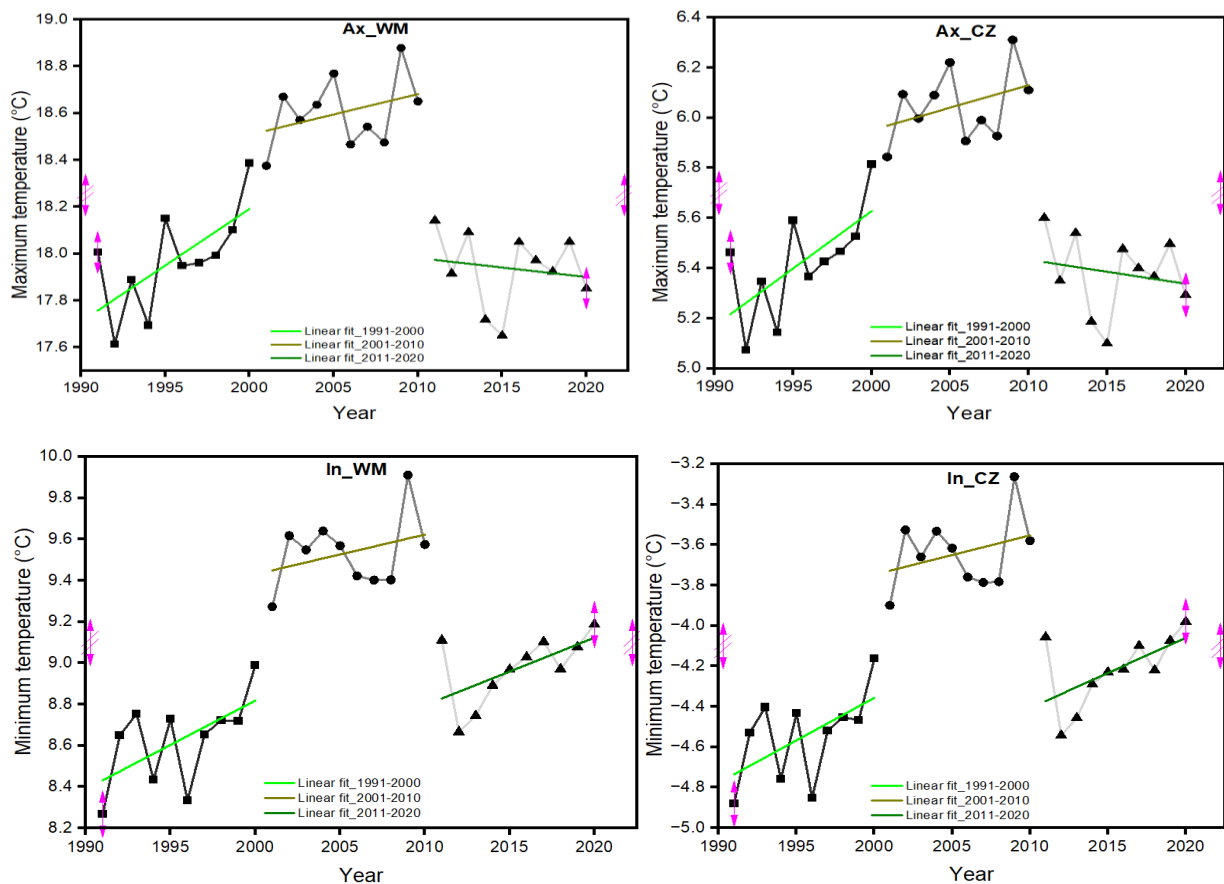
4.1. Results

4.1.1. Climate change assessment

4.1.1.1. Historical climate on Rwenzori mountains

4.1.1.1a. Interannual and decadal distribution of temperatures and rainfall on Rwenzori mountains

The CHIRTS dataset reveals fluctuations in temperature over the years. Across the entire mountain, mean values of temperatures ranged from 8.2 to 9.9 °C (Figure 8In_WM) for Tmin and 17.6 to 18.8 °C (Figure 6Ax_WM) for Tmax, respectively. Focusing solely on the central zone of the mountain, values ranged from -4.88°C to -3.26°C (Figure 6In_CZ) for Tmin and 5.07 to 6.31 °C (Figure 6Ax_CZ) for Tmax. Mann-Kendall and Sen's slope analysis indicate a significant positive trend in Tmin data over time across the entire mountain; whereas, focusing solely on the central zone of the mountain, this trend is observed for both Tmax and Tmin (Appendix 1). Regarding rainfall, the CHIRPS dataset illustrates fluctuations over time. Mean rainfall ranged from 1649.2 to 2202.8 mm (Figure 6Ra_WM) across the entire mountain range. Focusing solely on the central zone, mean values ranged from 2468 to 3129.91 mm (Figure 6Ra_CZ).



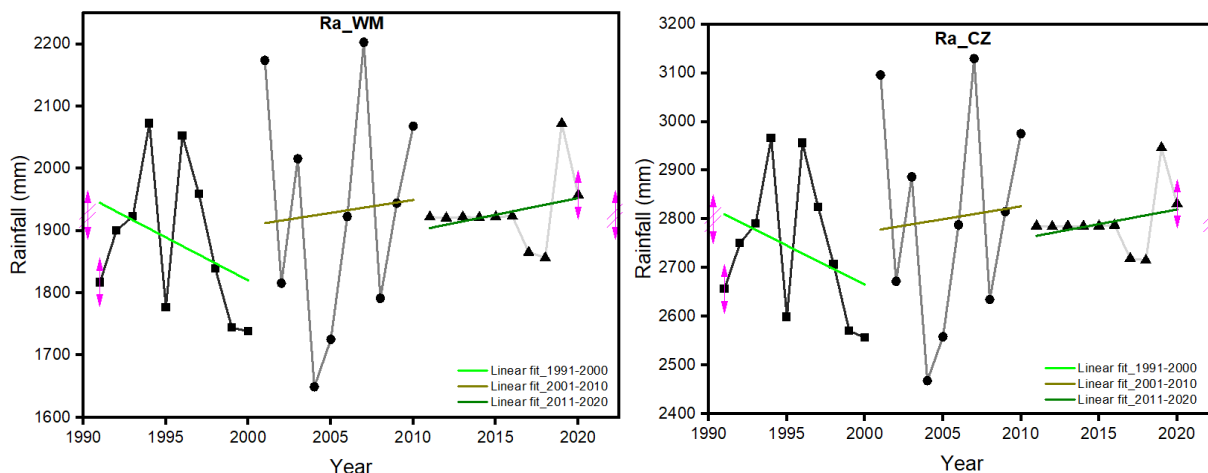


Figure 6. Inter-annual temperature (Ax) maximum, (In) minimum, and (Ra) rainfall over the 1991-2020 period. Whole mountain (WM), Central zone (CZ).

Spatially (Figure 7), on Rwenzori mountains, Tmax ranges from 5.15 to 28.42°C, while Tmin varies from -4.86 to 16.2°C. It is evident that temperature increases with decreasing altitude. Mean rainfall varies monthly from 107.03 to 237.26 mm, corresponding annually to 1284.36 to 2847.12 mm, with a trend indicating that rainfall increases with altitude. The configuration of isotherms and isohyets suggests that the central zone of the mountain, with its main peaks, receives lower temperatures and higher precipitation compared to surrounding areas.

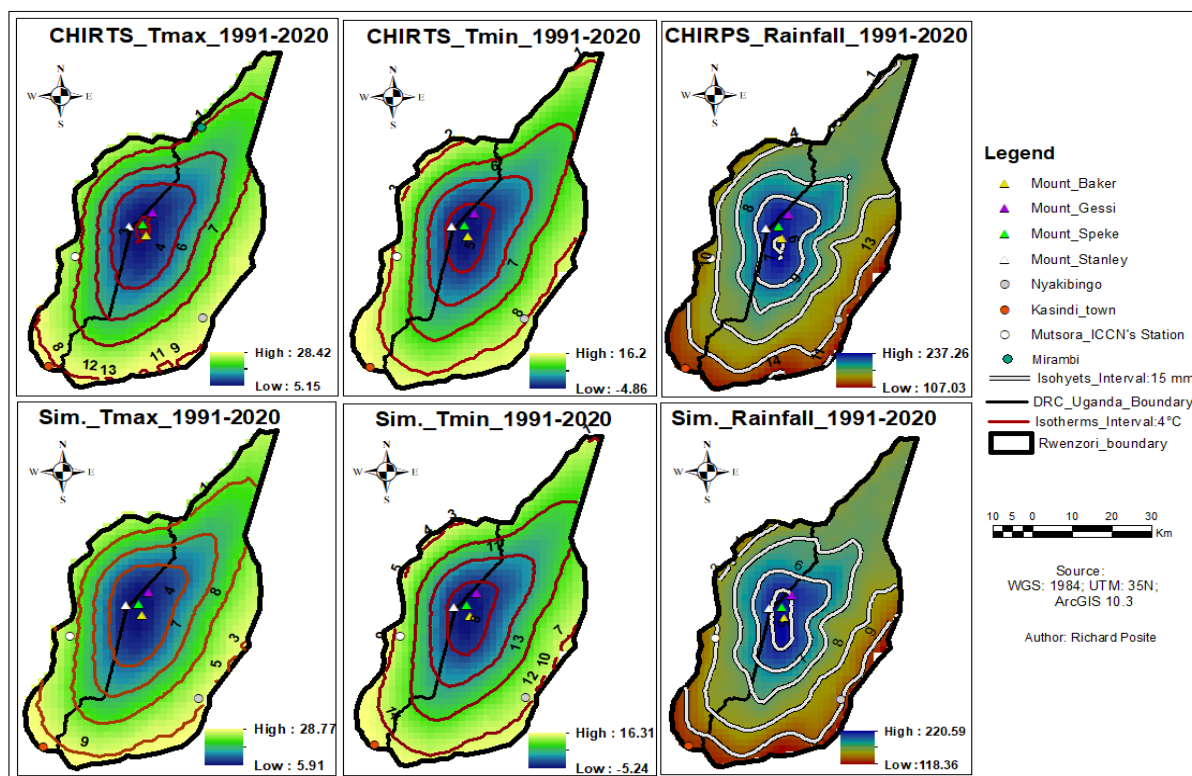


Figure 7. Monthly spatial distribution of maximum temperature (Tmax), minimum temperature (Tmin), and rainfall on Rwenzori mountains over the 1991-2020 period. Observed (Obs.), Simulated (Sim).

Spatially comparing decades, both daytime and nighttime temperatures were slightly warmer during the 2001-2010 period compared to other decades (Figure 8). Throughout all decades, temperature remained consistently lower in the central zone containing the peaks, contrasting with peripheral areas such as Kasindi (in DRC), Mutsora ICCN's station (in DRC), and the Nyakibingo region (in Uganda), as indicated by isotherm distribution. Regarding rainfall, spatial distribution remained relatively consistent during the first two decades (1991-2010 period) (Figure 9), while some redistribution occurred in the central zone during the last decade (2011-2020 period). During this decade, based on isohyet analysis, certain areas of Mount Stanley and Gessi experienced a decrease of 15 mm in rainfall compared to other parts of the central zone.

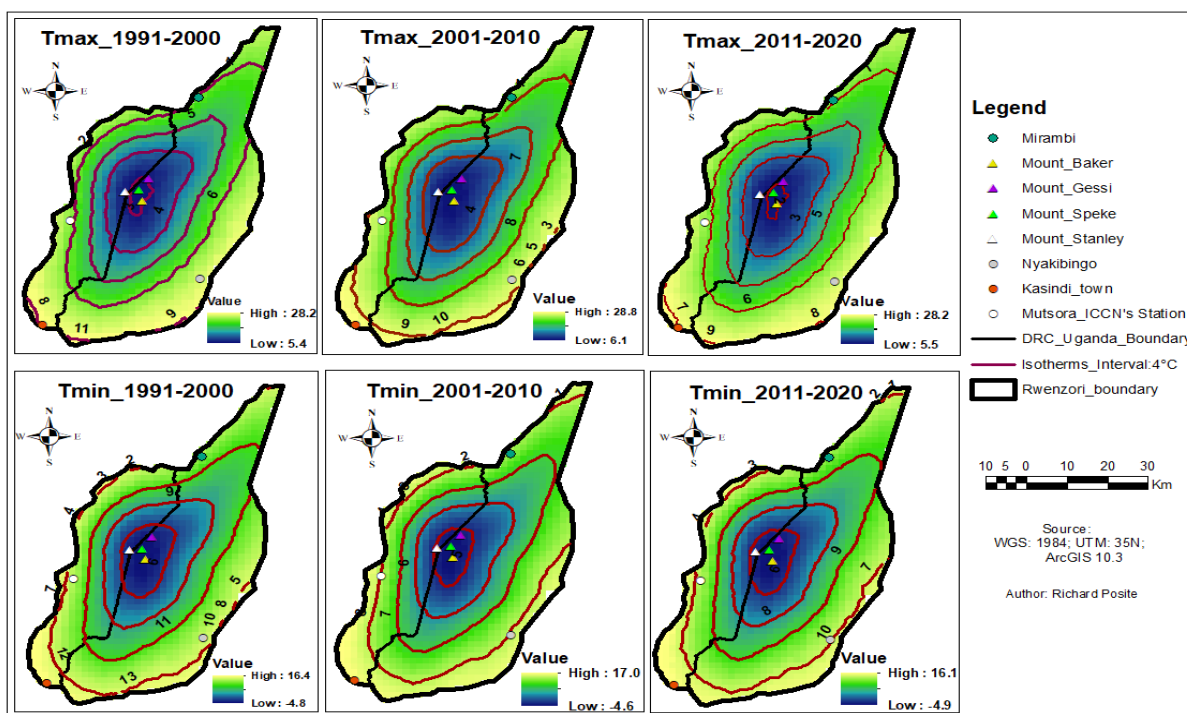


Figure 8. Decadal spatial distribution of maximum temperature (Tmax) and minimum temperature (Tmin) on Rwenzori mountains over the 1991-2020 period.

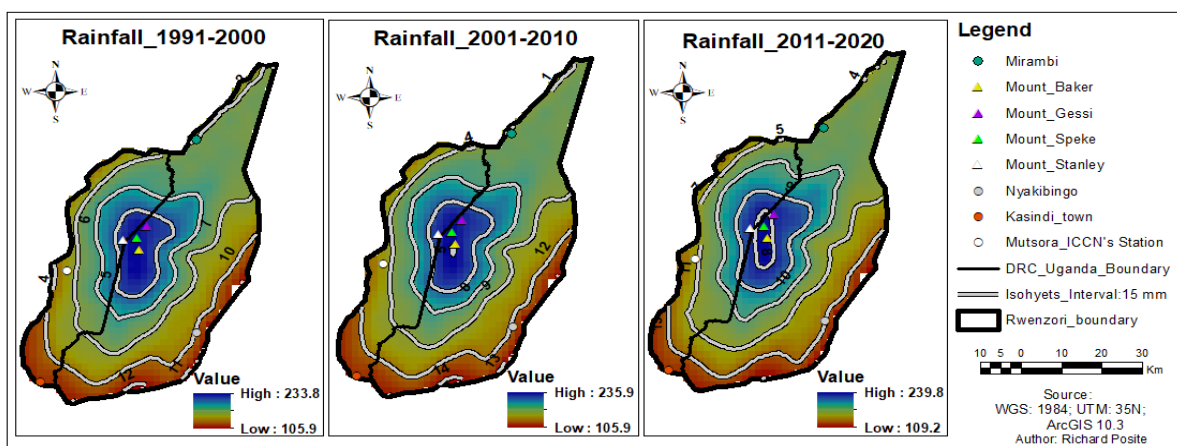


Figure 9. Decadal spatial distribution of rainfall on Rwenzori mountains over 1991-2020 period

4.1.1.1b. Monthly and seasonal distribution of temperatures and rainfall on Rwenzori mountains

Monthly trends of Tmax, Tmin, and rainfall exhibit variability across the entire Rwenzori Mountain range and when considering only its central zone (Figure 10). Generally, temperatures and rainfall are lowest in July and June. Mann-Kendall and Sen's slope tests (Appendix 1) reveal a significant positive trend in Tmax for the month of June and in Tmin during January, July, September, October, and December, when considering the entire mountain range. However, when focusing solely on the central zone of the mountain, divergent trends are observed. Here, significant positive trends in Tmax are observed in April, May, and July, while for Tmin, February exhibits a significant negative trend and May shows a positive trend. Concerning rainfall, the central zone experiences significant decreases in precipitation during March, while increases are recorded in July.

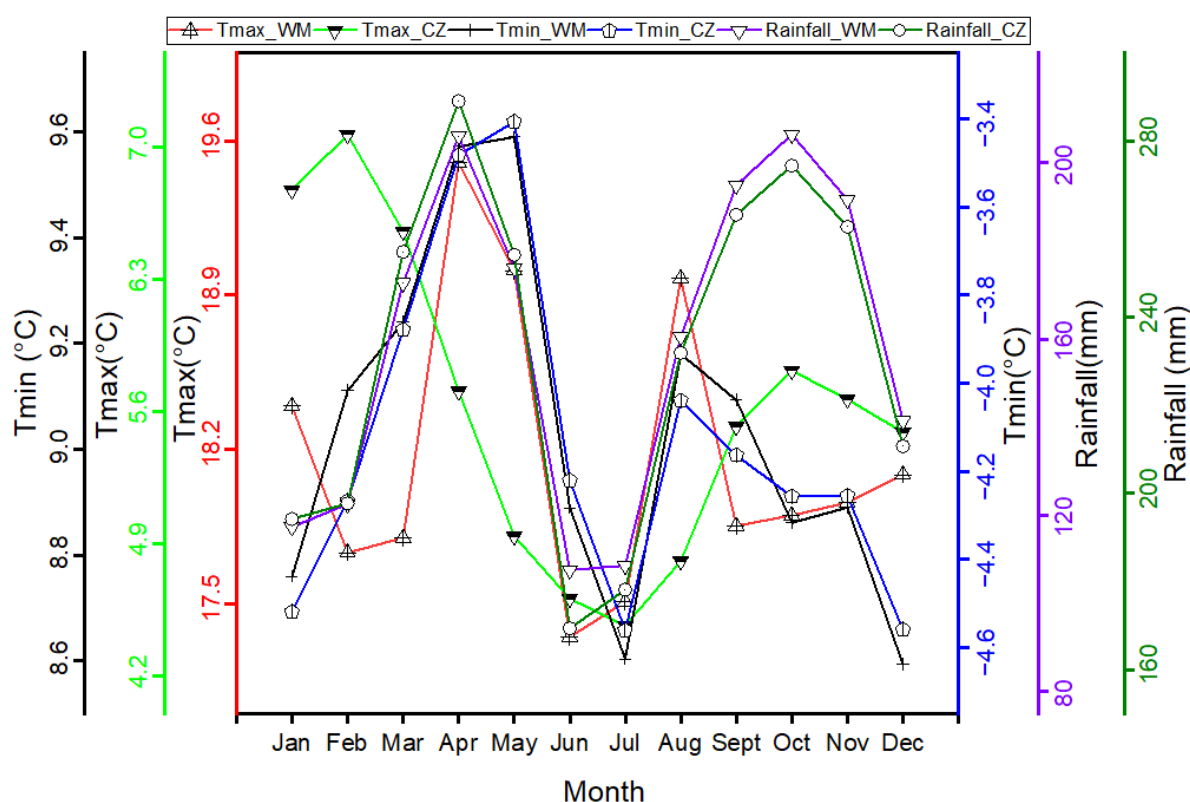


Figure 10. Monthly temperature (Tmax) maximum, (Tmin) minimum, and rainfall over the 1991-2020 period. Whole mountain (WM), Central zone (CZ).

Seasonally, across the entire Rwenzori mountains range, the highest mean Tmax value occurs during the DJF season (18.77°C), contrasting with the lowest in the JJ season (18.77°C) (Figure 11a). Similarly, for Tmin, the peak value (9.4677°C) is observed in MAM, while the lower (8.74°C) is recorded in JJ (Figure 11b). When focusing solely on the central zone of the mountain,

Tmax fluctuates between extremes of 4.53°C and 6.44°C, with the former in JJ and the latter in DJF (Figure 11a). Tmin displays a more limited range, reaching means of -4.39°C in JJ and -3.58°C in MAM (Figure 11b). Rainfall patterns reveal JJ as the driest period (216.1 mm) and ASON as the wettest (753.4 mm) across the entire range. Conversely, within the central zone, JJ exhibits the lowest rainfall (347.3 mm), while ASON records the highest (1029.9 mm) (Figure 11c). Analyzing trends using Mann-Kendall and Sen's slope tests, a notable increase in Tmin is observed during DJF, JJ, and ASON across the entire mountain range. However, focusing on the central zone, a positive trend in Tmax emerges during MAM and JJ (Appendix 1).

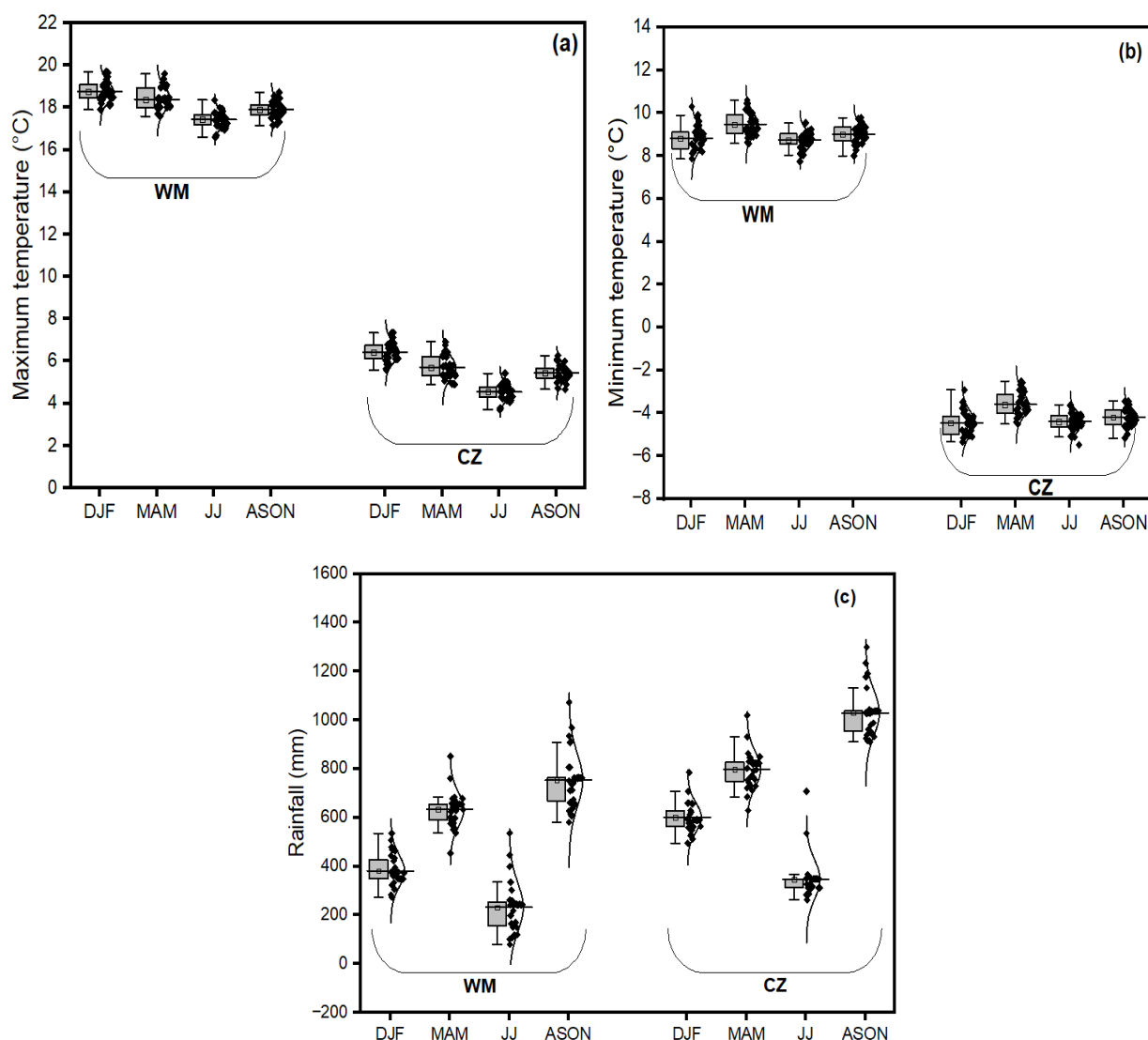


Figure 11. Seasonal temperature (a) maximum, (b) minimum, and (c) rainfall over the 1991-2020 period. Whole mountain (WM), Central zone (CZ), December-January-February (DJF), March-April-May (MAM), June-July (JJ), August-September-October-November (ASON)

Seasonal spatial distribution of temperature demonstrates significant variability (Figure 13), particularly evident in the central region where Tmax exhibits uneven distribution between seasons. During MAM and ASON seasons, Tmax distribution appears relatively uniform, however with slight temperature elevations observed in certain areas of Mounts Stanley and Gessi compared to the central zones. Conversely, during the DJF season, localized decreases in Tmax are observed in specific regions of Mount Speke relative to other central areas. Moreover, despite seasonal variations, Tmin displays subtle spatial differences marked by isotherm configurations. Concerning rainfall patterns, distinct differences in distribution are evident across seasons (Figure 13). During MAM and DJF, rainfall tends to be more concentrated in the central zone of the mountain compared to peripheral areas. In the JJ season, rainfall levels are elevated in the central zone, extending towards the western and northwestern regions of the mountain. Conversely, during the ASON season, heavy rainfall predominantly occurs in the central zone, with some extension into the northeastern part of the mountain.

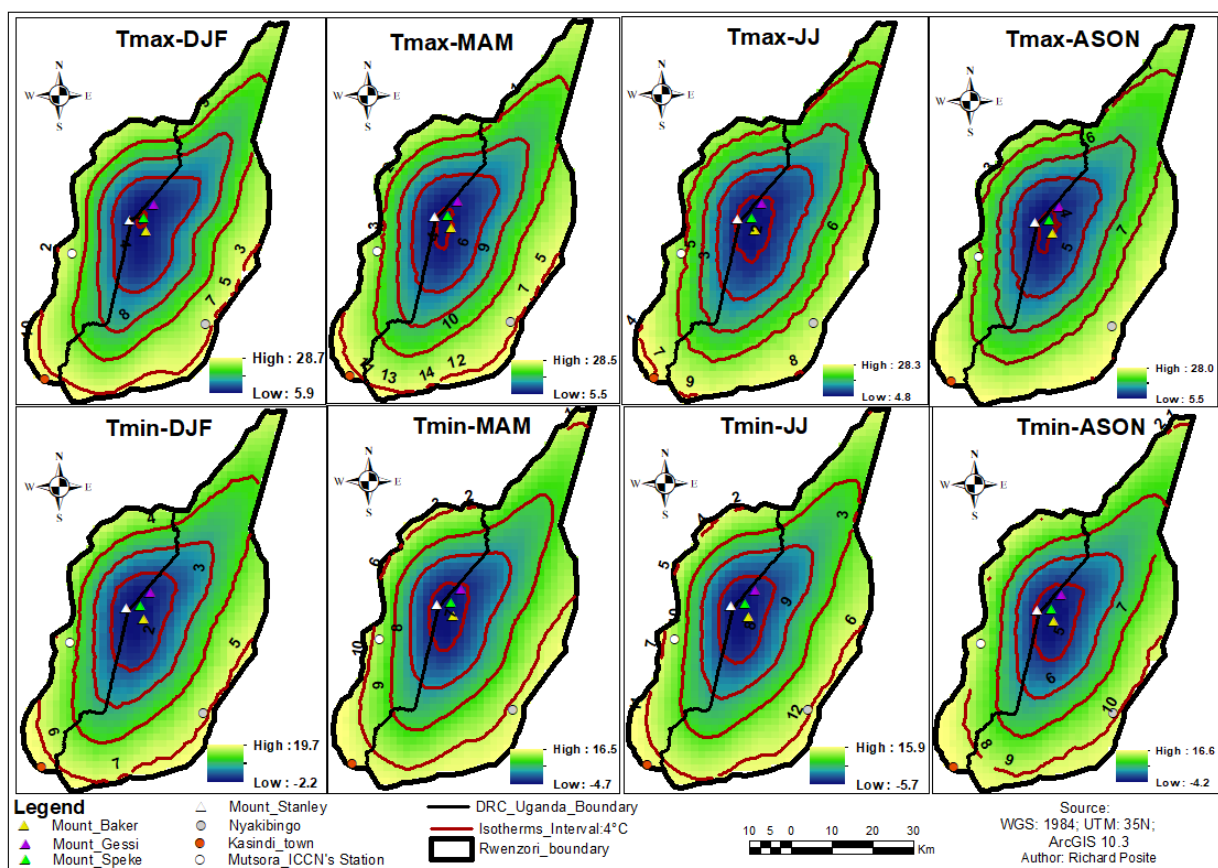


Figure 12. Seasonal spatial distribution of maximum temperature (Tmax) and minimum temperature (Tmin) on Rwenzori mountains over the 1991-2020 period. December-January-February (DJF), March-April-May (MAM), June-July (JJ), August-September-October-November (ASON)

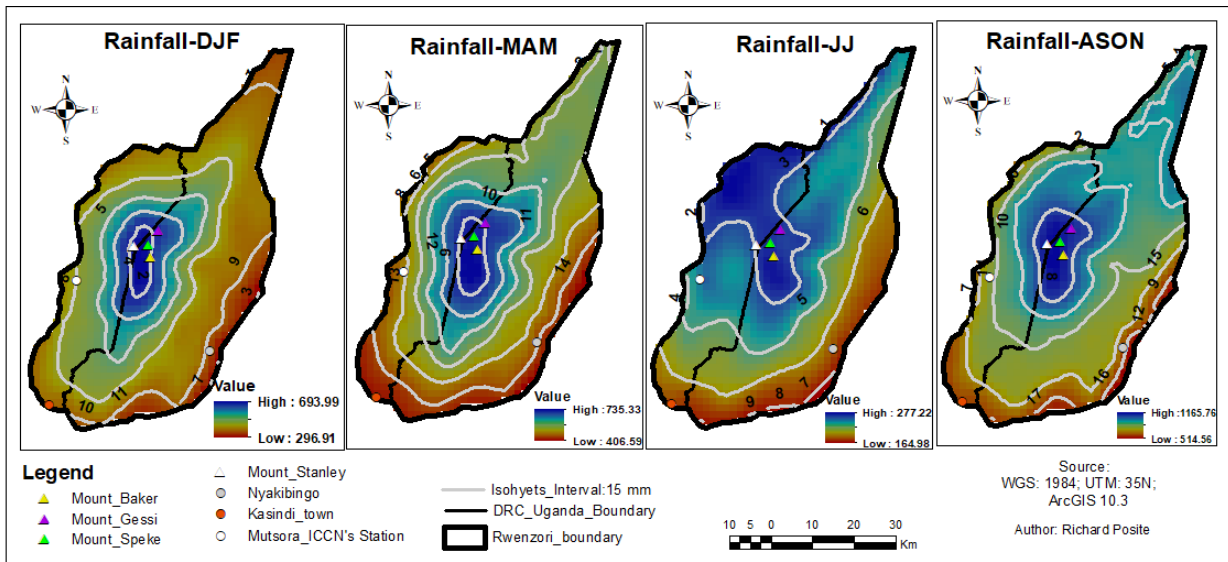


Figure 13. Seasonal spatial distribution of rainfall on Rwenzori mountains over the 1991-2020 period. December-January-February (DJF), March-April-May (MAM), June-July (JJ), August-September-October-November (ASON)

4.1.1.1c. Relationship between climate variables on the Rwenzori mountains

Strong relationships between Tmax and Tmin are observed across both the entire mountain range and the central region (Figure 14). As Tmax experiences increases, corresponding rises in Tmin are observed, and conversely. However, rainfall shows non-significant relationships with the temperatures of the region.

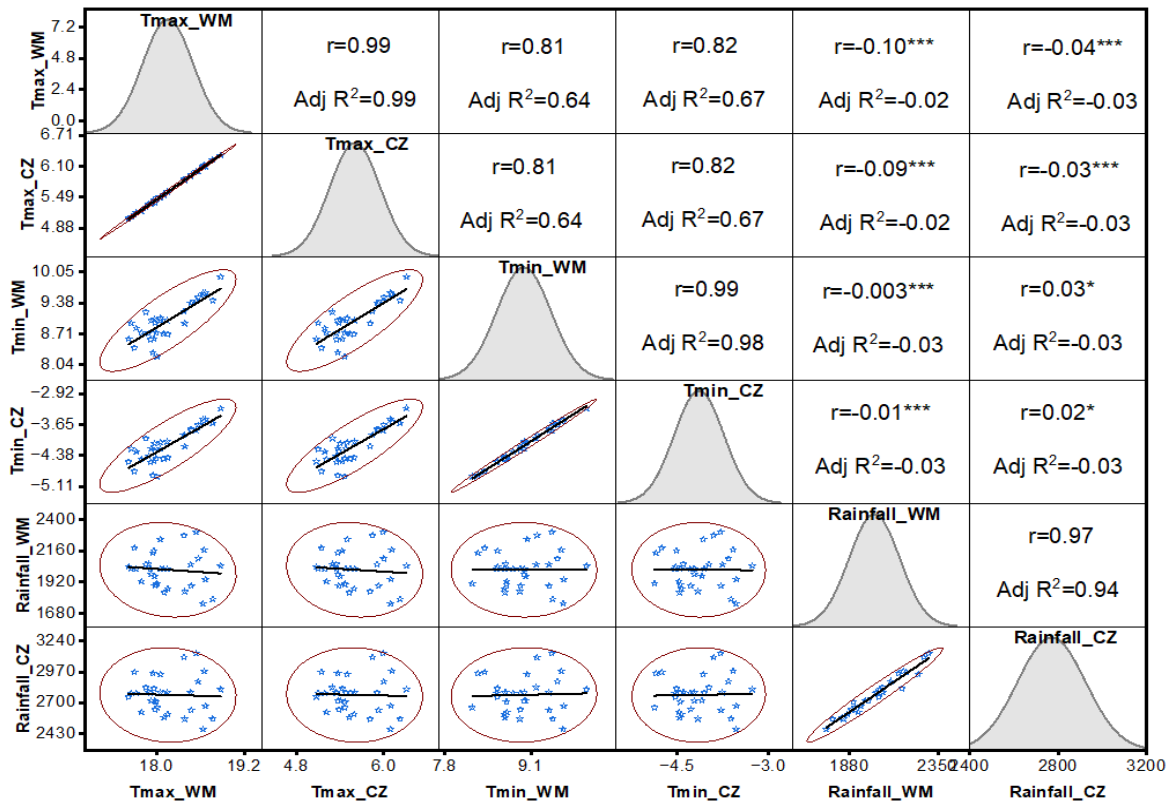


Figure 14. Scatter plot matrix of interactions between maximum temperature (Tmax), minimum temperature (Tmin), and rainfall over the 1991-2020 period. Adjusted Coefficient of determination ($Adj R^2$), Coefficient of correlation (r), Whole mountain (WM), Central zone (CZ).

4.1.1.2. Projected climate on Rwenzori mountains

4.1.1.2a. Spatial difference from projected and historical climate

Under the SSP245 scenario (Figure 15), significant temperature increases are anticipated in the northwest region of the Rwenzori Mountains, with projected increases of up to 3.2°C and 3.4°C in Tmax and Tmin, respectively, during the far future. Conversely, slight decreases in temperatures are expected in the southeast region, except for Tmin in the far future, which is also projected to increase. The central region is expected to undergo moderate temperature increases compared to historical values. Spatially, rainfall distribution appears inversely proportional to temperature changes, with the northwest region characterized by dominant areas of decreases in precipitation, potentially reaching 6.1 mm monthly in the far future. In contrast, the southeast and east parts are projected to experience more significant rainfall increases, up to 11.3 mm in the far future. The central zone, comprising the peaks, will be characterized by moderate increases in precipitation.

Under the SSP585 scenario, (Figure 16), pronounced fluctuations are spatially projected across the Rwenzori Mountains compared to historical climate conditions. The highest increases in Tmax and Tmin are expected to reach values of 5.2°C and 6°C, respectively, during the far future, while corresponding decreases are projected to have peaks of -3.6°C and -2.8°C, respectively. The central region of the mountain is characterized by both areas of decreases and increases in Tmax and Tmin. Concerning rainfall, the trend shows decreases in precipitation as one moves away from the center towards the north and northeast regions, with the opposite projected when moving towards the south and southwest directions. Anticipated increases could reach 10.6 mm and 20.6 mm, respectively, during the near and far future, while decreases could amount to 38.7 mm and 28.7 mm, respectively. Once again, the central zone is projected to have both areas of increases and moderate decreases in precipitation.

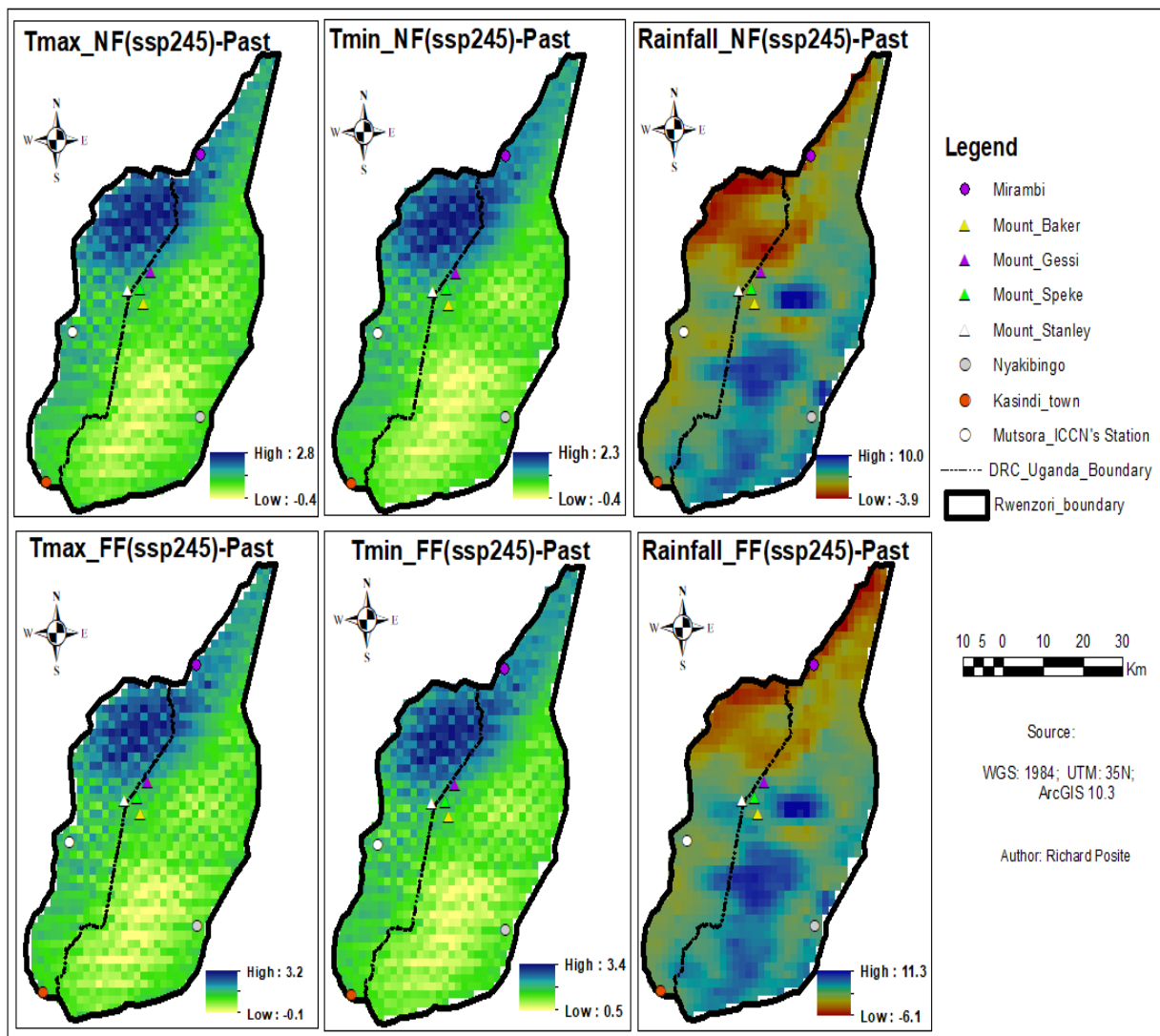


Figure 15. Spatial difference of climate between Past (1991-2020), near future (2021-2060) and far future (2061-2100) time periods under ssp245 scenario. Maximum temperature (Tmax), Minimum temperature (Tmin), Near future (NF), Far future (FF)

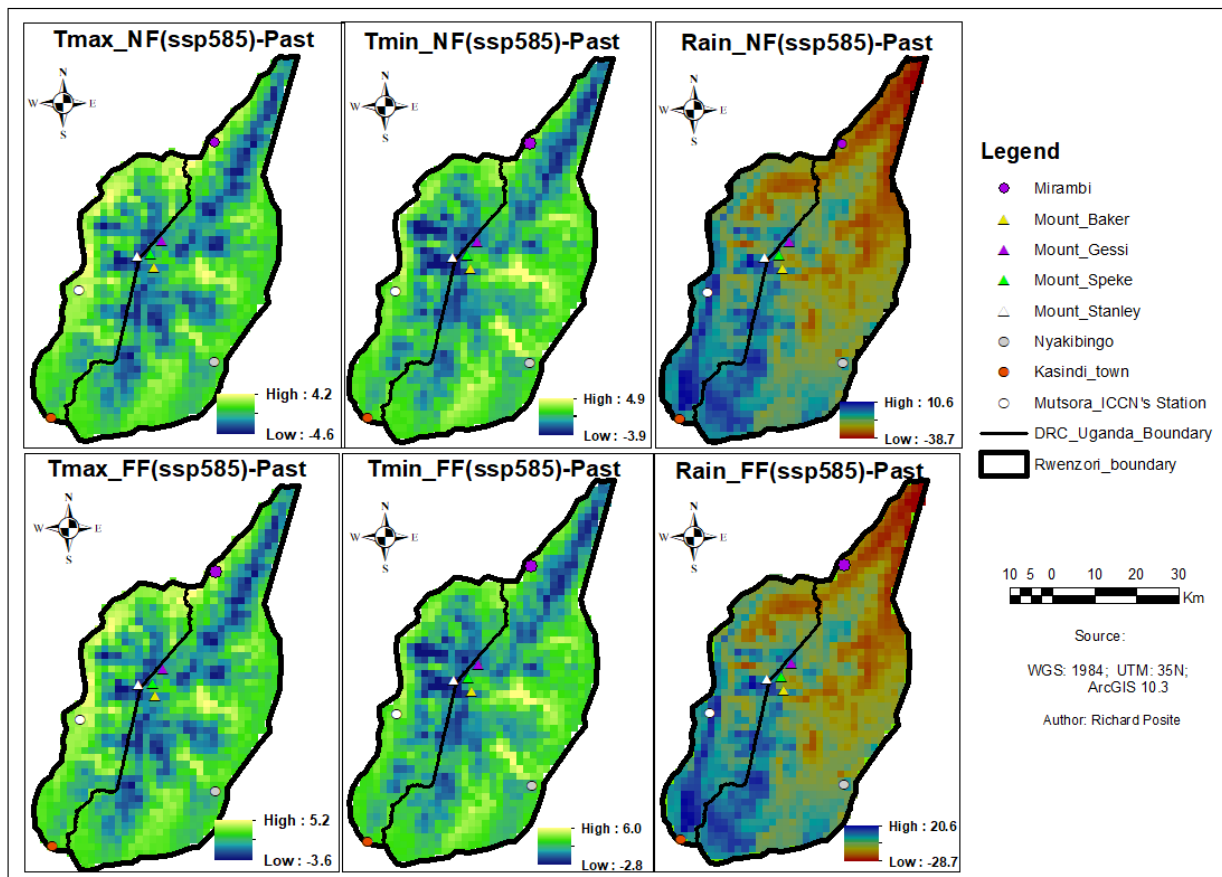


Figure 16. Spatial difference of climate between Past (1991-2020), near future (2021-2060) and far future (2061-2100) time periods under ssp585 scenario. Maximum temperature (Tmax), Minimum temperature (Tmin), Near future (NF), Far future (FF)

4.1.1.2b. Trend in projected climate under different scenarios

In the near future period (Appendix 2), under the SSP245 scenario, positive significant trends are projected for Tmax in all months, seasons, and on an annual scale, both for the entire mountain and when focusing solely on the central zone. Similarly, positive trends are expected for Tmin, except during March when considering the entire mountain. However, no significant trend is anticipated in rainfall under the same scenario. Conversely, under the SSP585 scenario, positive trends are also expected in both Tmax and Tmin for the entire mountain and central zone. However, a negative trend is projected for rainfall in November when analyzing the entire mountain.

Looking ahead to the far future period (Appendix 3), a diverse range of significant trends is expected. Under the SSP245 scenario, a predominantly positive annual trend is anticipated for both Tmax and Tmin across various months and seasons, with exceptions noted for March, May, and November. Focusing on the central zone, positive trends are expected in both Tmax and Tmin annually, monthly, and seasonally, with few exceptions such as March and April showing negative

trends for both Tmax and Tmin. Regarding rainfall, alternating stable months and positive or negative trends are expected for both the entire mountain and the central zone. Similarly, under the SSP585 scenario, seasonal, monthly, and annual positive trends are anticipated for Tmax and Tmin, with exceptions in May and April. Positive trends are also expected in the central zone, although March and April may witness a decrease in Tmax and stability in Tmin. For rainfall, a mixture of stable months and positive or negative trends is expected across both the entire mountain and the central zone.

4.1.2. Snow cover dynamics on Rwenzori mountains

4.1.2.1. Historical snow cover dynamics

4.1.2.1a. Spatial and temporal patterns in snow cover dynamics across Rwenzori mountains

During 2000-2022 period, variations in snow cover dynamics reveal distinct patterns across mounts (Figure 17). For Mount Baker, snow cover reached its lowest value in 2008 ($0.427 \pm 0.124 \text{ km}^2$) before peaking in 2015 ($1.951 \pm 0.41 \text{ km}^2$). Similarly, Mount Gessi exhibited minimal snow cover in 2008 ($0.332 \pm 0.131 \text{ km}^2$) and maximal cover in 2011 ($1.601 \pm 0.424 \text{ km}^2$). Mount Speke displayed its lowest snow cover in 2022 (0.641 km^2) and its highest extent in 2021 ($2.027 \pm 0.512 \text{ km}^2$), while Mount Stanley recorded its lowest cover in 2017 ($1.500 \pm 0.781 \text{ km}^2$) and its peak coverage in 2011 ($3.817 \pm 1.341 \text{ km}^2$). Examining the combined snow cover values across all peaks reveals noticeable patterns, with the lowest overall snow cover recorded in 2022 at $3.082 \pm 1.021 \text{ km}^2$ and the highest in 2011 at $9.664 \pm 2.872 \text{ km}^2$.

Additionally, the Mount Stanley exhibits higher mean snow cover values compared to other mounts, with a mean of $2.534 \pm 0.524 \text{ km}^2$, indicating potentially greater snow accumulation in this area. Conversely, the Mount Gessi shows lower mean snow cover values compared to the other mounts, with a mean of $0.767 \pm 0.302 \text{ km}^2$, suggesting differences in snow accumulation patterns across the mountain range. This significant difference between the snow cover accumulation on different mounts is verified by the ANOVA analysis ($p = 7.11\text{E-}23$; $\alpha = 0.05$) (Appendix 6). Additionally, the overall snow cover value for the entire mountain provides a holistic assessment of snow cover extent, reflecting the combined snow cover across all mounts. With a mean of $5.821 \pm 1.272 \text{ km}^2$, this overall value underscores the importance of considering the entire mountain range in snow cover assessments. However, the analysis of interannual trends demonstrates the lack of significance in the dynamics of snow cover area (Figure 17).

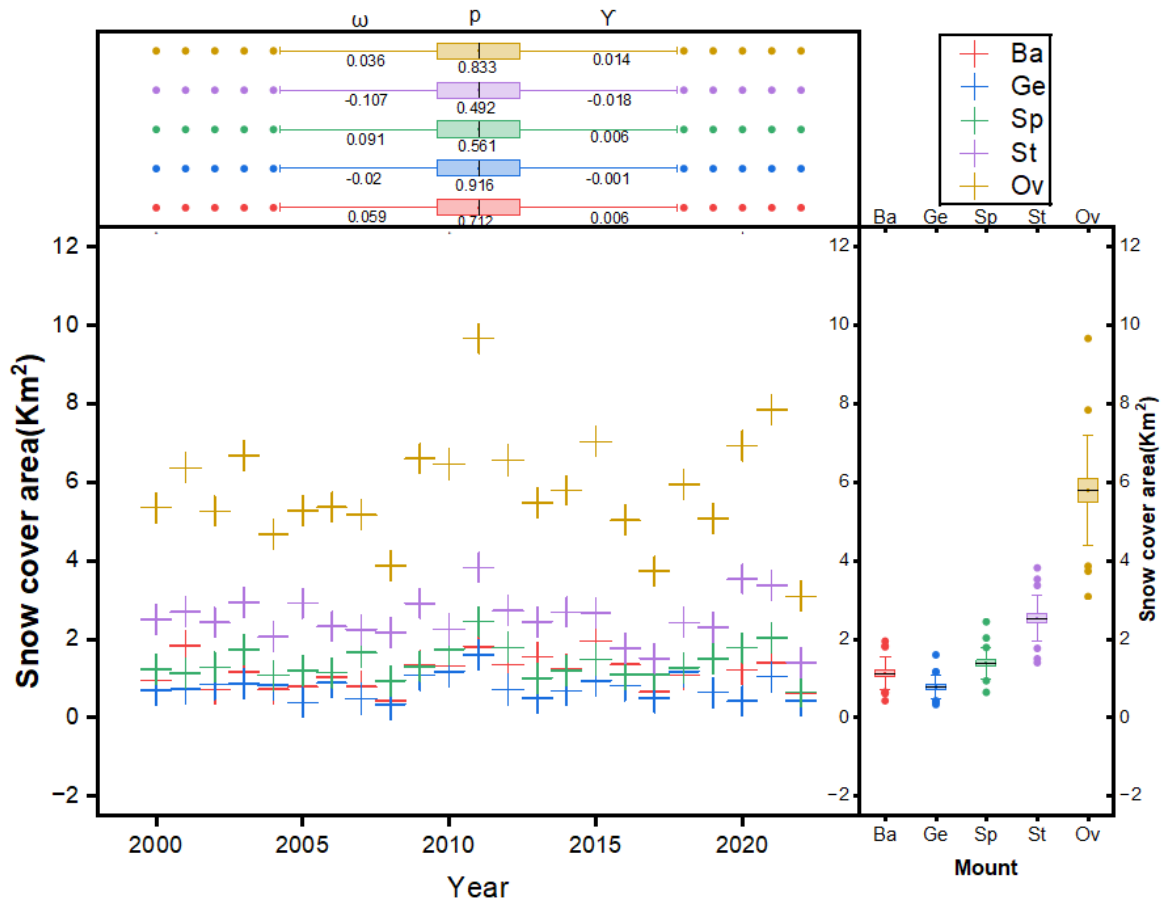


Figure 17. Interannual variations in snow cover dynamics across different mountain peaks. Baker (Ba), Gessi (Ge), Speke (Sp), Stanley (St), Mann-Kendall tau (ω), p value (p), Sen's slope estimator (γ)

Across the seasons, variations in snow cover dynamics are evident for each mount (Figure 18). During the DJF period, snow cover typically peaks across all mounts, with notably higher mean values observed for the Stanley peak compared to others ($1.915 \pm 0.960 \text{ km}^2$ for Stanley in DJF). This trend persists into the MAM season, with Stanley maintaining a higher mean snow cover value. However, as the seasons progress into JJ and ASON, snow cover tends to decrease across all mounts. Stanley consistently exhibits a higher mean snow cover value compared to other mounts during these seasons as well ($3.134 \pm 1.965 \text{ km}^2$ for Stanley in JJ). However, ANOVA analysis did not reveal significant differences in snow cover dynamics between seasons ($p = 0.173$, $\alpha = 0.05$) (Appendix 6). In contrast, the Mann-Kendall test indicates significant seasonal positive trend in JJ on Baker ($\omega=0.448$, $p=0.003$, $\gamma=0.068$), suggesting potential shifts in snow cover dynamics on this mount over time (Figure 18).

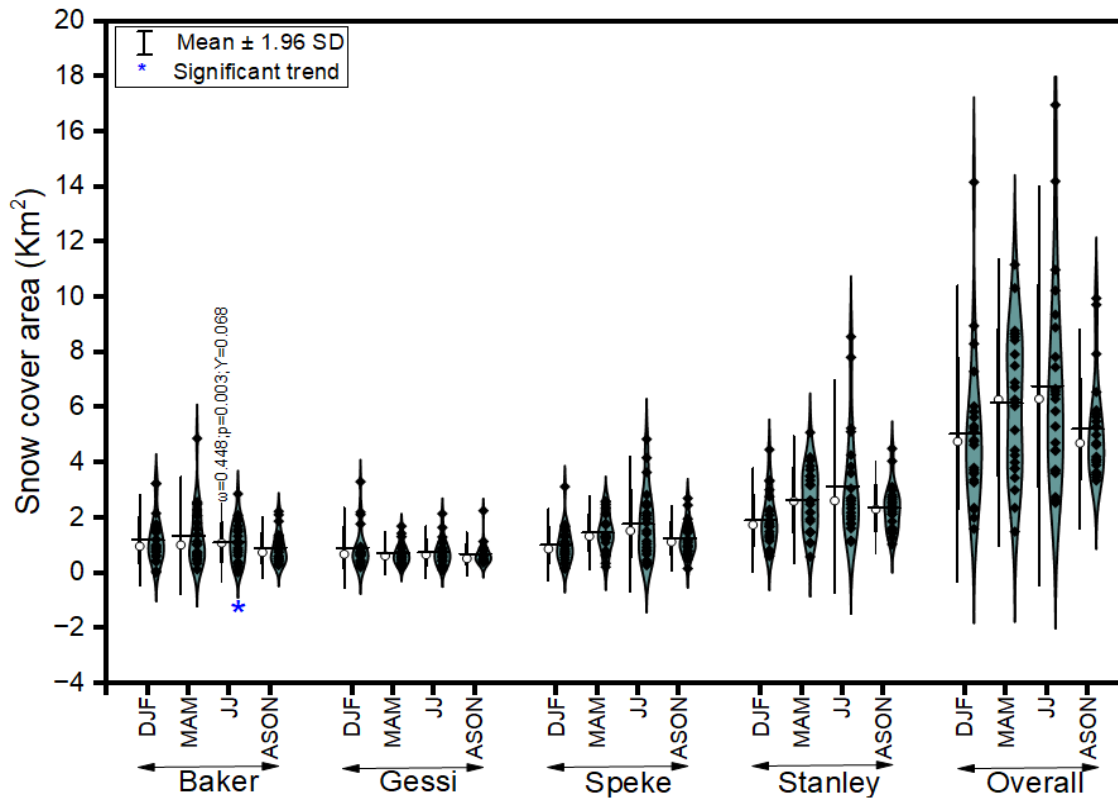


Figure 18. Seasonal snow cover dynamics across Rwenzori mounts during 2000-2022 period. December-January-February (DJF), March-April-May (MAM), June-July (JJ), August-September-October-November (ASON)

Significant variability in snow cover dynamics is observed across different months and peaks in the Rwenzori Mountains. Notably, on Mount Baker, snow cover varies from its lowest point in October ($0.70 \pm 0.47 \text{ km}^2$) to its highest in April ($1.70 \pm 1.16 \text{ km}^2$) (Figure 19a). Conversely, Mount Gessi experiences its lowest snow cover in September ($0.42 \pm 0.37 \text{ km}^2$) and its highest in December ($1.00 \pm 0.41 \text{ km}^2$) (Figure 19b). For Mount Speke, the snow cover fluctuates from its lowest in January ($0.85 \pm 0.64 \text{ km}^2$) to its highest in May ($2.03 \pm 1.51 \text{ km}^2$) (Figure 19c). Similarly, Mount Stanley exhibits its lowest snow cover in February ($1.39 \pm 0.82 \text{ km}^2$) and its highest in Jun ($3.29 \pm 1.964 \text{ km}^2$) (Figure 19d). Overall, snow cover mean values vary across months, ranging from $3.85 \pm 1.90 \text{ km}^2$ in October to $8.22 \pm 4.17 \text{ km}^2$ in May, without a consistent pattern of a single mount consistently having higher or lower snow cover compared to others across all months (Figure 19e). ANOVA analysis demonstrates significant differences between months ($p < 0.05$), indicating varying snow cover dynamics throughout the year (Appendix 6). Additionally, Mann-Kendall test reveals a positive trend over 2000-2022 period in June on Baker and Stanley peaks, but also a negative trend in February on Stanley peak (Figures 19a and 19d). Moreover, considering only the Overall values, negative and positive trends are respectively observed during February and June on the Rwenzori Mountains (Figure 19e).

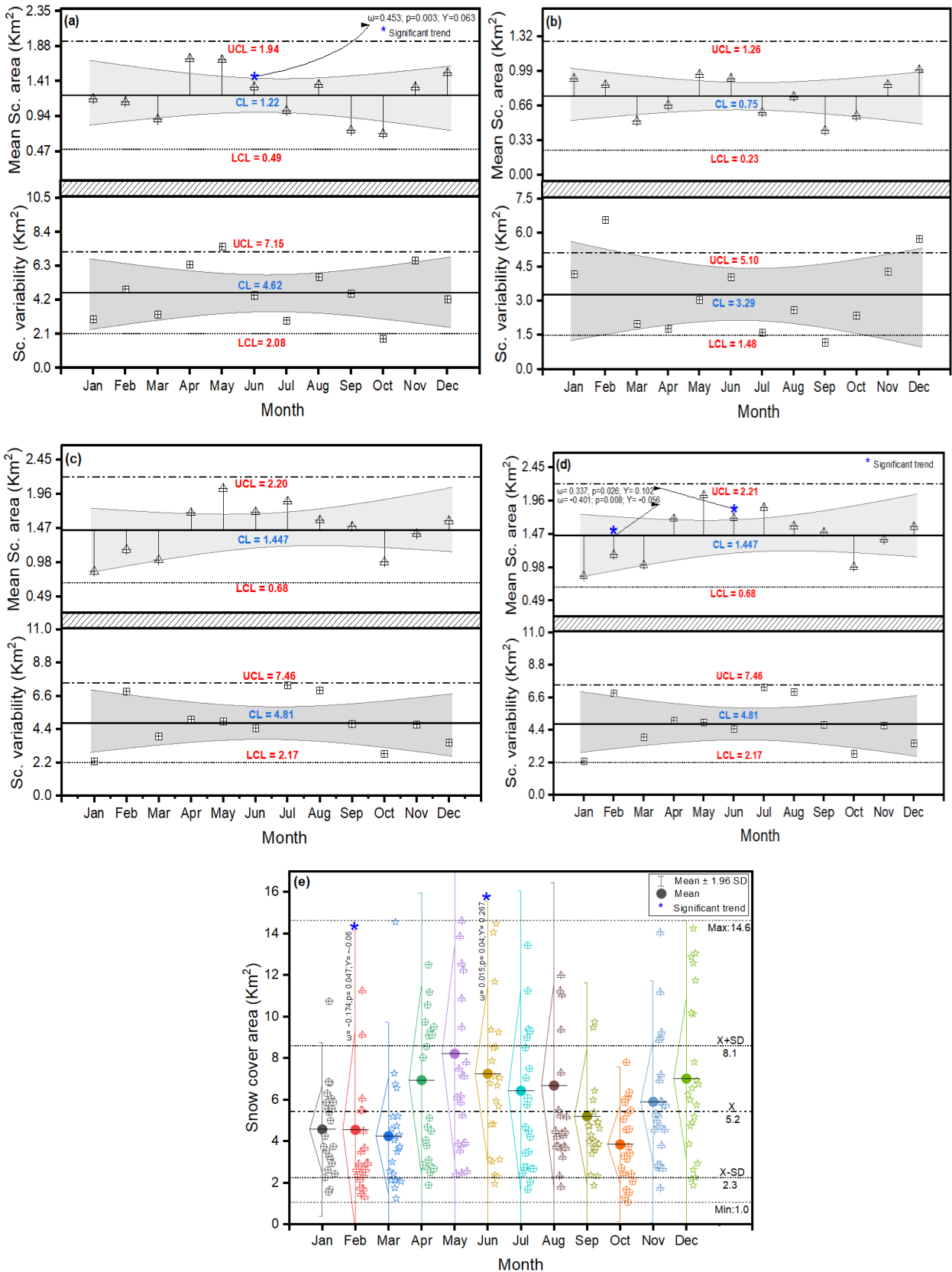


Figure 19. Monthly snow cover dynamic on (a) Baker, (b) Gessi, (c) Speke, (d) Stanley, and (e) Overall scales. Mann-Kendall tau (ω), p value (p), Sen's slope estimator (Y), Upper control limit (UCL), Lower control limit (LCL), Control limit (CL), Mean (X), Standard deviation (SD), Snow cover (Sc)

4.1.2.1b. Snow cover dynamics and climate relationships in Rwenzori mountains range

The investigation into snow cover dynamics across the entire mountain unveils nuanced insights into the climatic factors driving variations on an annual basis (Figure 20). Minimum temperature emerges as a pivotal determinant of snow cover dynamics, exhibiting a discernible negative correlation with snow cover extent on an annual basis ($r = -0.32$, $R^2 = 0.06$). This association suggests that lower T_{min} values are linked to increased snow accumulation across the mountain, while higher T_{min} values coincide with diminished snow cover. However, it's worth noting that this relationship is characterized as weak, implying a noticeable yet not particularly robust trend. In contrast, both rainfall and maximum temperature show negligible correlations with snow cover dynamics, indicating minimal influence on snow cover variability (rainfall: $r = -0.05$, $R^2 = -0.04$; T_{max} : $r = -0.05$, $R^2 = -0.04$), though these relationships lack statistical significance.

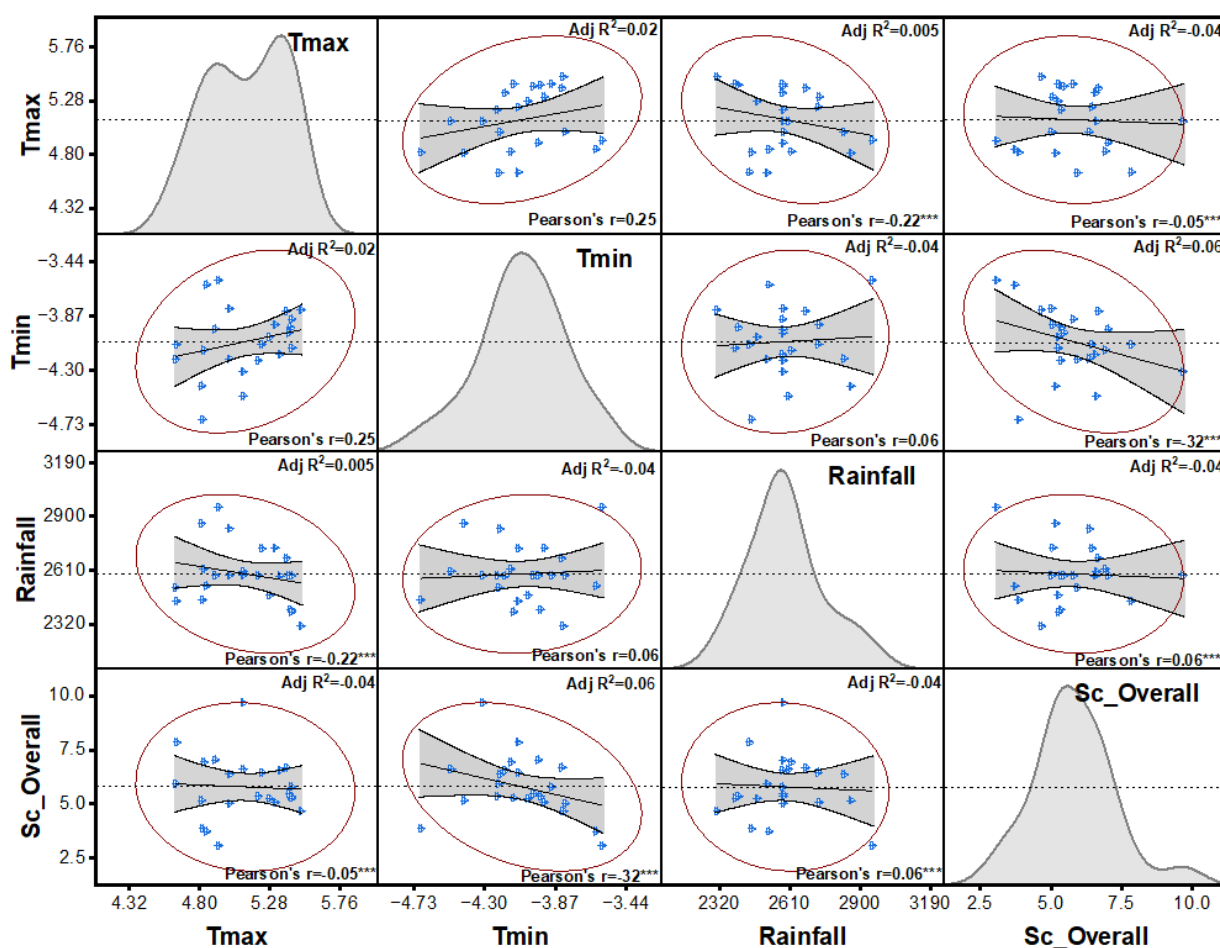


Figure 20. Overall snow cover dynamics scatter plot matrix analysis and climate-snow cover relationships over the 2000-2022 period. Maximum temperature (T_{max}), Minimum temperature (T_{min}), Snow cover (Sc), Adjusted coefficient of determination ($Adj R^2$), Coefficient of correlation (r).

Focusing on specific months that exhibit significant snow cover trends (Figure 19), sheds further light on the interplay between climatic variables and snow cover dynamics. In June, both Mount Baker and Mount Stanley reveal a pronounced negative correlation between snow cover and rainfall, with stronger associations observed on Mount Stanley (Figure 21). The low levels of rainfall correspond to high accumulations of snow during the month of June (rainfall: Mount Baker: $r = -0.65$, $R^2 = 0.40$; Mount Stanley: $r = -0.73$, $R^2 = 0.51$). However, the influence of temperature variables (Tmax and Tmin), appears comparatively subdued. Tmax demonstrates weak negative correlations with snow cover extent on both peaks, indicating limited impact (Tmax: Mount Baker: $r = -0.24$, $R^2 = 0.01$; Mount Stanley: $r = -0.17$, $R^2 = -0.01$). Similarly, while Tmin exhibits slightly stronger negative correlations with snow cover increase, its influence remains modest in comparison (Tmin: Mount Baker: $r = -0.44$, $R^2 = 0.15$; Mount Stanley: $r = -0.55$, $R^2 = 0.27$).

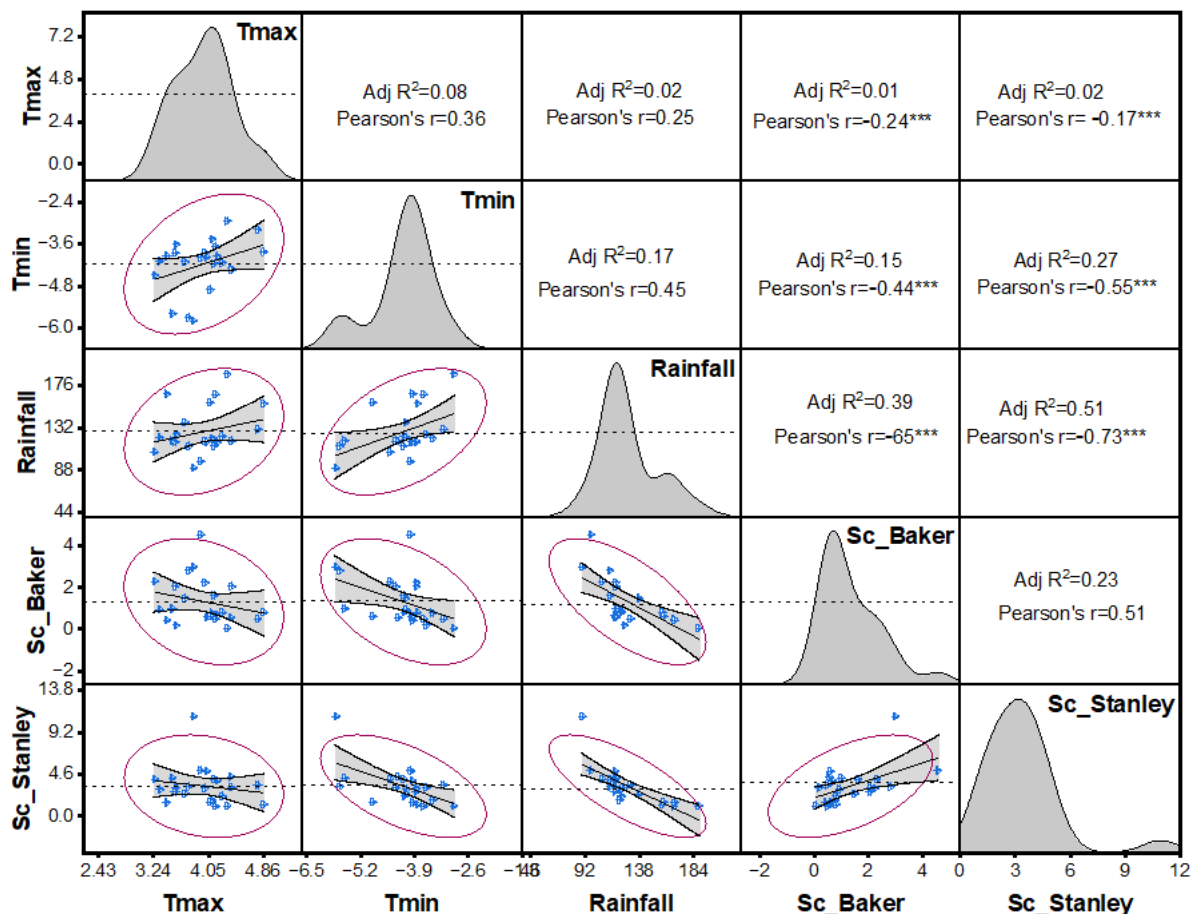


Figure 21. June month-specific scatter plot matrix analysis of snowpack variation across Baker and Stanley peaks and climate-snow cover relationships over the 2000-2022 period. Maximum temperature (Tmax), Minimum temperature (Tmin), Snow cover (Sc), Adjusted coefficient of determination (Adj R²), Coefficient of correlation (r).

Further delving into the February month, specific to Mount Stanley, unveils intriguing insights into temperature-driven snow cover dynamics (Figure 22). Tmin emerges as a significant factor, displaying a strong negative correlation with snow cover extent ($r = -0.76$, $R^2 = 0.56$). This highlights the pivotal role of Tmin in shaping snow cover patterns during February, with higher Tmin values correlating with reduced snow cover. In contrast, rainfall exhibits a weaker negative correlation, suggesting a minor influence on snow cover dynamics ($r = -0.29$, $R^2 = 0.04$). Notably, Tmax showcases a weak positive correlation ($r = 0.07$); however, the negligible R^2 value (-0.04) indicates an absence of a significant relationship. These findings underscore the influential role of Tmin in driving snow cover dynamics on Mount Stanley during February, highlighting the importance of temperature variability in shaping seasonal snow cover patterns.

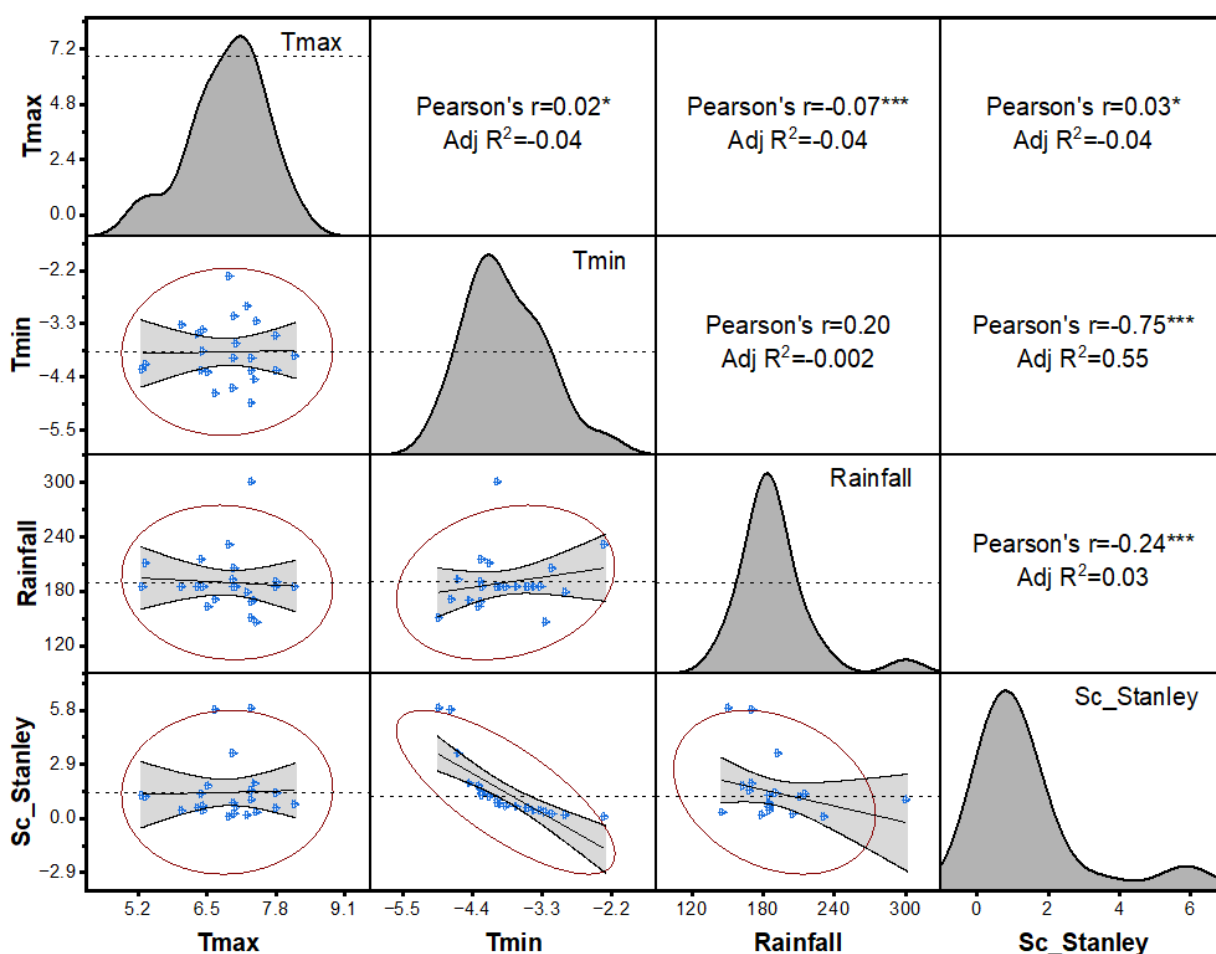


Figure 22. February month-specific snow cover dynamics scatter plot matrix analysis of Mount Stanley and climate-snow cover relationships over the 2000-2022 period. Maximum temperature (Tmax), Minimum temperature (Tmin), Snow cover (Sc), Adjusted coefficient of determination (Adj R^2), Coefficient of correlation (r).

4.1.2.2. Model accuracy and performance in simulating observed snow cover dynamics

Snow cover data from MODIS and the model were compared for calibration (2000-2014) and validation (2015-2022) periods. The model demonstrated strong agreement with MODIS observations, reflected by coefficients of determination (R^2) of 0.89 and 0.93 for calibration and validation, respectively (Figure 23). Assessing the model's accuracy using the entire dataset (2000-2022), the Root Mean Square Error (RMSE) was 0.163, indicating close alignment between predicted and observed values. Additionally, with an R^2 value of 0.9, the model explained approximately 90% of observed data variance, with a low Percent Bias (PBias) of 1.2%, indicating minimal systematic error. These results highlight the model's robust accuracy and performance in characterizing snow cover dynamics.

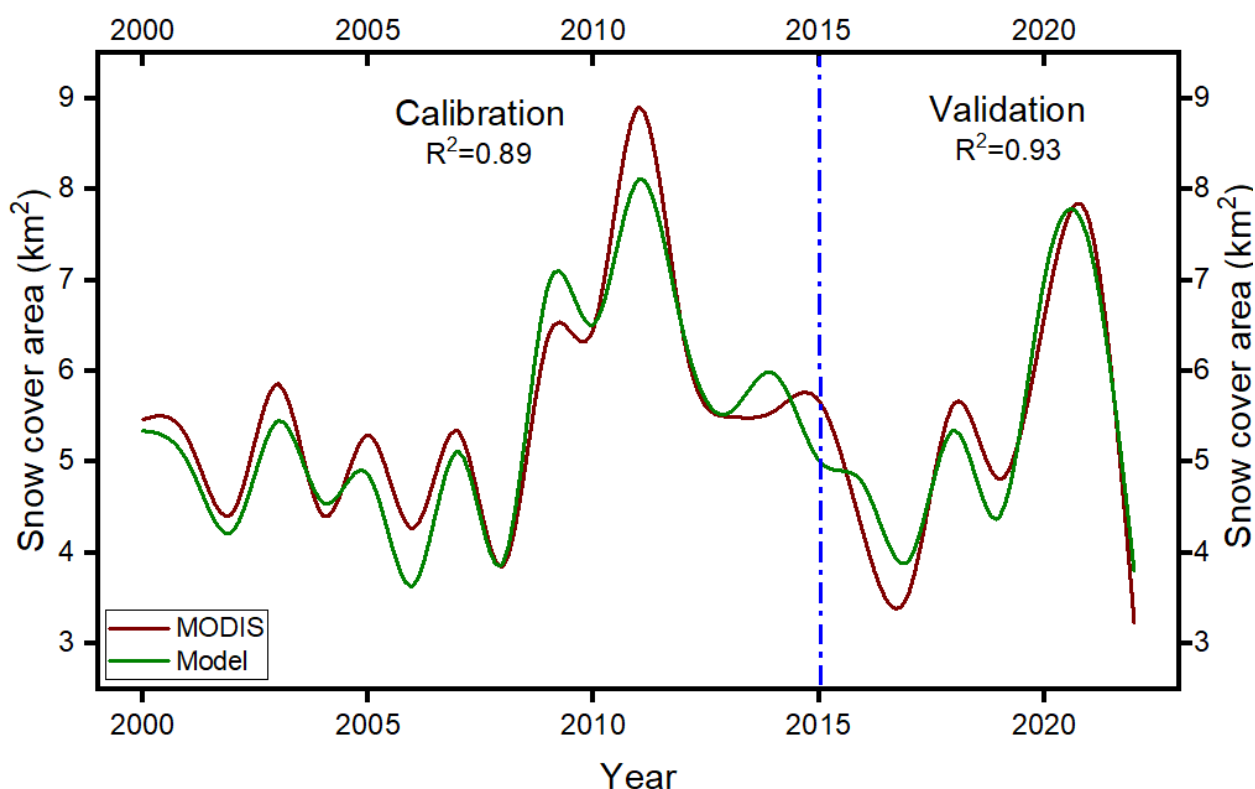


Figure 23. Model agreement with MODIS snow cover data

4.1.2.3. Projected snow cover dynamics

The projected snow cover varies across different peaks in the Rwenzori Mountain. In the near future, under the SSP2-4.5 scenario, Baker mount (Figure 24a) is expected to maintain a snow cover of approximately $1.17 \text{ km}^2 \pm 0.13 \text{ km}^2$, while a similar trend is projected under the SSP5-8.5 scenario, with a cover of around $1.15 \text{ km}^2 \pm 0.12 \text{ km}^2$. Looking further ahead, a decrease in snow cover is anticipated under both scenarios, with projections dropping to approximately $1.04 \text{ km}^2 \pm 0.18 \text{ km}^2$ under SSP2-4.5 and $0.87 \text{ km}^2 \pm 0.16 \text{ km}^2$ under SSP5-8.5. Mount Gessi (Figure 24b) also follows a similar pattern, with near-future projections indicating a snow cover of approximately $0.76 \text{ km}^2 \pm 0.07 \text{ km}^2$ under SSP2-4.5 and $0.75 \text{ km}^2 \pm 0.06 \text{ km}^2$ under SSP5-8.5, and further decreasing in the far future. Mount Speke (Figure 24c) exhibits a near-future snow cover of approximately $1.13 \text{ km}^2 \pm 0.13 \text{ km}^2$ under SSP2-4.5 and $1.15 \text{ km}^2 \pm 0.10 \text{ km}^2$ under SSP5-8.5, with a projected decrease in snow cover under SSP2-4.5 to approximately $0.77 \text{ km}^2 \pm 0.13 \text{ km}^2$ and an increase under SSP5-8.5 to approximately $1.09 \text{ km}^2 \pm 0.10 \text{ km}^2$ in the far future. Similarly, Mount Stanley (Figure 24d) shows a decline in snow cover over time, with near-future projections indicating a cover of approximately $1.62 \text{ km}^2 \pm 0.47 \text{ km}^2$ under SSP2-4.5 and $1.58 \text{ km}^2 \pm 0.51 \text{ km}^2$ under SSP5-8.5, and a significant decrease in the far future under both scenarios to approximately $1.38 \text{ km}^2 \pm 0.35 \text{ km}^2$ and $0.43 \text{ km}^2 \pm 0.31 \text{ km}^2$ respectively. Considering the cumulative snow cover values for the entire mountain range (Figure 24e), a consistent trend towards decreased snow cover is observed over time, with both scenarios showing a decrease in overall snow cover to approximately $5.25 \text{ km}^2 \pm 0.40 \text{ km}^2$ under SSP2-4.5 and $5.10 \text{ km}^2 \pm 0.37 \text{ km}^2$ under SSP5-8.5 in the near future, and further decreasing to approximately $4.59 \text{ km}^2 \pm 0.65 \text{ km}^2$ and $3.45 \text{ km}^2 \pm 0.66 \text{ km}^2$ respectively in the far future.

Statistically, a significant negative trend in projected snow dynamics is anticipated. Mount Baker and Mount Gessi are expected to exhibit this trend under both SSP2-4.5 and SSP5-8.5 scenarios in the far future (Figure 24a, Figure 24b, and Appendix 5). Similarly, Mount Stanley is projected to demonstrate such a trend under the SSP2-4.5 scenario in the far future (Figure 24d and Appendix 5). Additionally, a negative significant trend is expected for all SSP5-8.5 periods when considering the cumulative snow cover values for the entire mountain range, along with the SSP2-4.5 scenario in the far future (Figure 24e and Appendix 5).

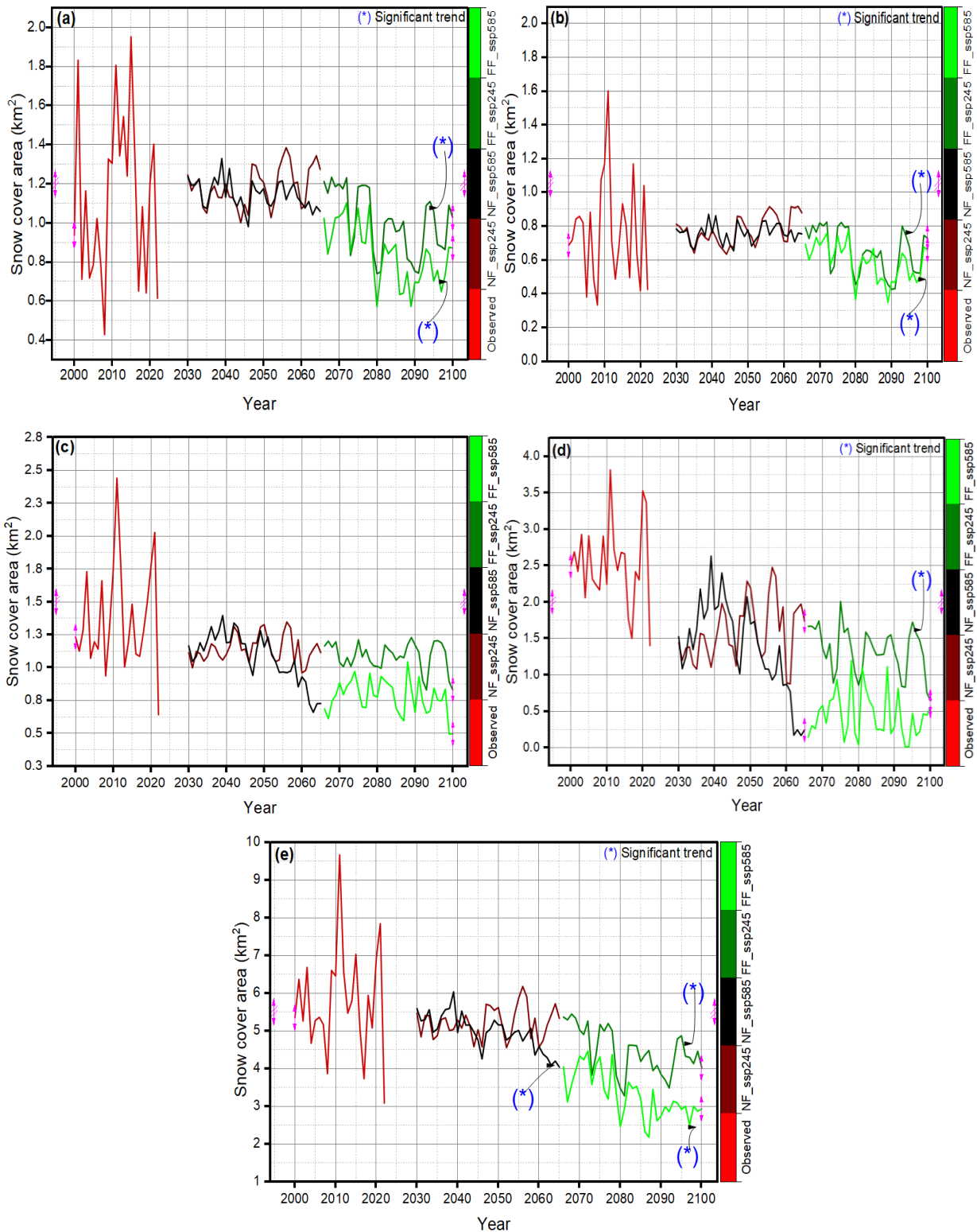


Figure 24. Projected annual snow cover dynamic on (a) Baker, (b) Gessi, (c) Speke, (d) Stanley, and (e) Overall scales. Near future (2030-2065 period: NF), Far future (2066-2100 period: FF)

Comparing projected and observed snow cover areas reveals significant differences across all mounts (Figure 25). Mount Stanley exhibits the most substantial disparities, with differences ranging from -0.912 to -1.158 km² under SSP2-4.5 and from -0.951 to -2.103 km² under SSP5-8.5.

Mount Gessi and Baker are expected to experience relatively lower reductions in snow cover. When considering the cumulative snow cover values for the entire mountain range, discrepancies persist across all scenarios, with differences ranging from -0.559 to -1.247 km² under SSP2-4.5 and from -0.699 to -2.4 km² under SSP5-8.5.

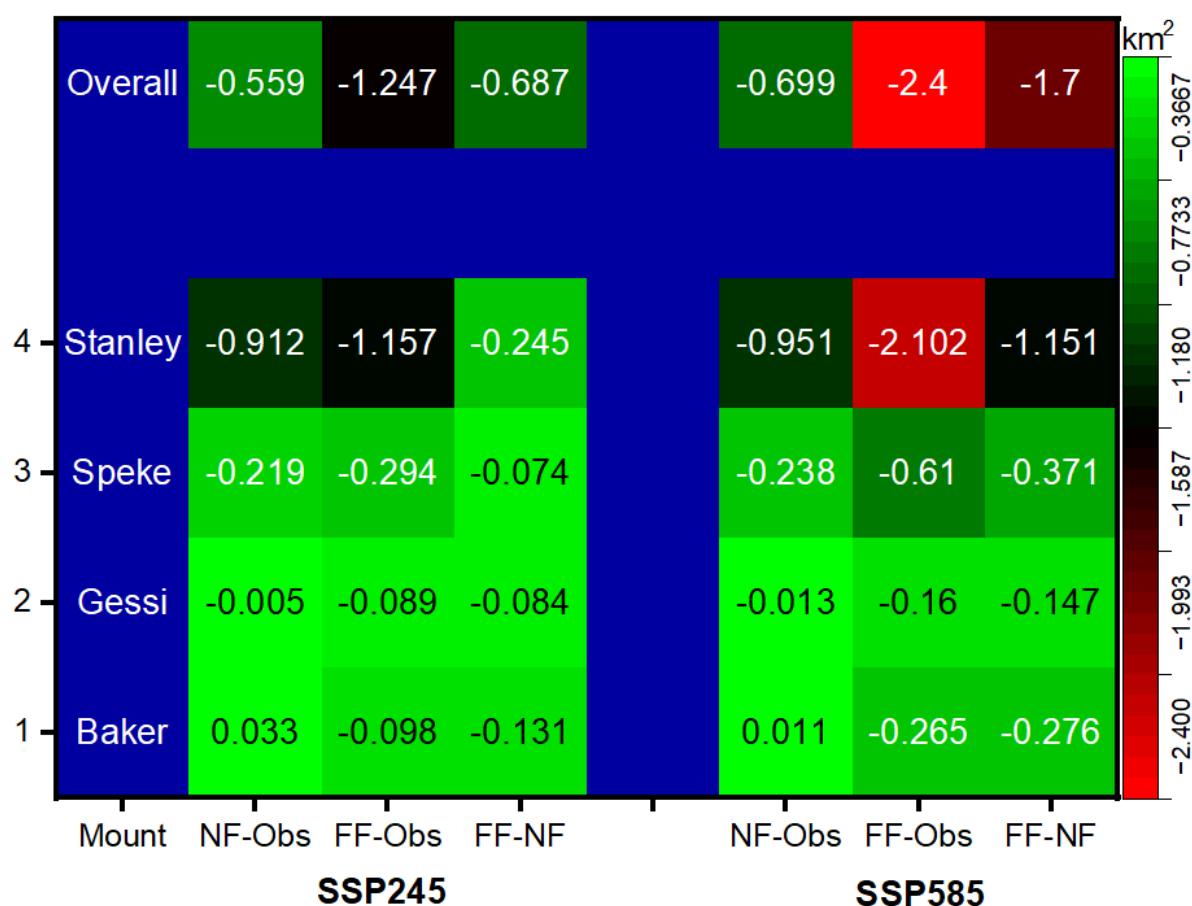


Figure 25. Differences in snow cover area between projected and observed (Obs) data. Near future (2030-2065 period: NF), Far future (2066-2100 period: FF)

In the NF_ssp245 scenario (Figure 26a), February emerges as the month with the lowest expected snow cover across all peaks, with Mount Baker, Mount Gessi, Mount Speke, and Mount Stanley exhibiting their lowest snow cover values during this month, measuring 1.009 km², 0.705 km², 1.004 km², and 1.28 km², respectively. Conversely, the peak snow cover month varies among the peaks, with Mount Baker and Mount Gessi peaking in June at 1.177 km² and 0.733 km², respectively, while Mount Speke and Mount Stanley reach their peaks in July, measuring 1.229 km² and 1.695 km², respectively. Similarly, under the NF_ssp585 scenario (Figure 26b), February also stands out as the month with the lowest expected snow cover for Mount Baker and Mount Gessi, with measurements of 0.998 km² and 0.717 km², respectively, while Mount Speke and Mount Stanley exhibit their lowest snow cover values during March, measuring 0.942 km² and

1.15 km², respectively. Conversely, June emerges as the month with the highest expected snow cover across all peaks, with Mount Baker, Mount Gessi, Mount Speke, and Mount Stanley reaching peak values of 1.227 km², 0.76 km², 1.215 km², and 1.715 km², respectively. Under the FF_ssp245 scenario (Figure 26c), December consistently portrays the month with the lowest projected snow cover across all Mounts, with Mount Baker, Mount Gessi, Mount Speke, and Mount Stanley each displaying their lowest snow cover values during this period, measuring 0.956 km², 0.669 km², 0.947 km², and 1.044 km², respectively. Conversely, Mount Baker reaches its highest snow cover in July at 1.096 km², while Mount Gessi, Mount Speke, and Mount Stanley are expected to attain their highest snow cover in August, recording values of 0.688 km², 1.187 km², and 1.590 km², respectively. Finally, under the FF_ssp585 scenario (Figure 26d), January emerges as the month with the lowest projected snow cover across all peaks, with Mount Baker, Mount Gessi, Mount Speke, and Mount Stanley showing their lowest snow cover values during this month, measuring 0.766 km², 0.579 km², 0.644 km², and 0.003 km², respectively. In contrast, July stands out as the month with the highest expected snow cover across all peaks, with Mount Baker, Mount Gessi, Mount Speke, and Mount Stanley reaching peak values of 0.964 km², 0.635 km², 0.877 km², and 0.518 km², respectively.

The cumulative projected snow cover values for the entire mountain range show distinct patterns across various months and scenarios (Figure 26e). In the near future under both the SSP245 and SSP585 scenarios, June emerges with the highest cumulative snow cover values, measuring 5.961 km² and 5.738 km², respectively. Conversely, February consistently records the lowest cumulative snow cover values across all scenarios, with 4.251 km² and 3.992 km² under SSP245 and SSP585, respectively. Looking into the far future, December is projected to have the lowest cumulative snow cover value under the SSP245 scenario, at 3.920 km², while February is anticipated to have the lowest value under the ssp585 scenario, with 2.827 km². Conversely, July is forecasted to have the highest cumulative snow cover values during this period, reaching 5.135 km² and 4.170 km² for SSP245 and SSP585, respectively.

In the monthly trend analysis over time, distinct patterns emerge across various mounts, periods, and scenarios (Appendix 5). Additionally, significant negative trends are projected when considering the cumulative snow cover values for the entire mountain range (Appendix 5). For the near future, under the SSP245 scenario, this trend is expected in April, while under SSP585, it is anticipated in March, April, May, July, and November. Looking further ahead into the far future, under the SSP245 scenario, the negative trend is expected in 10 months of the year, except for February and April. Likewise, under SSP585, the trend is projected in 10 months, excluding March and April.

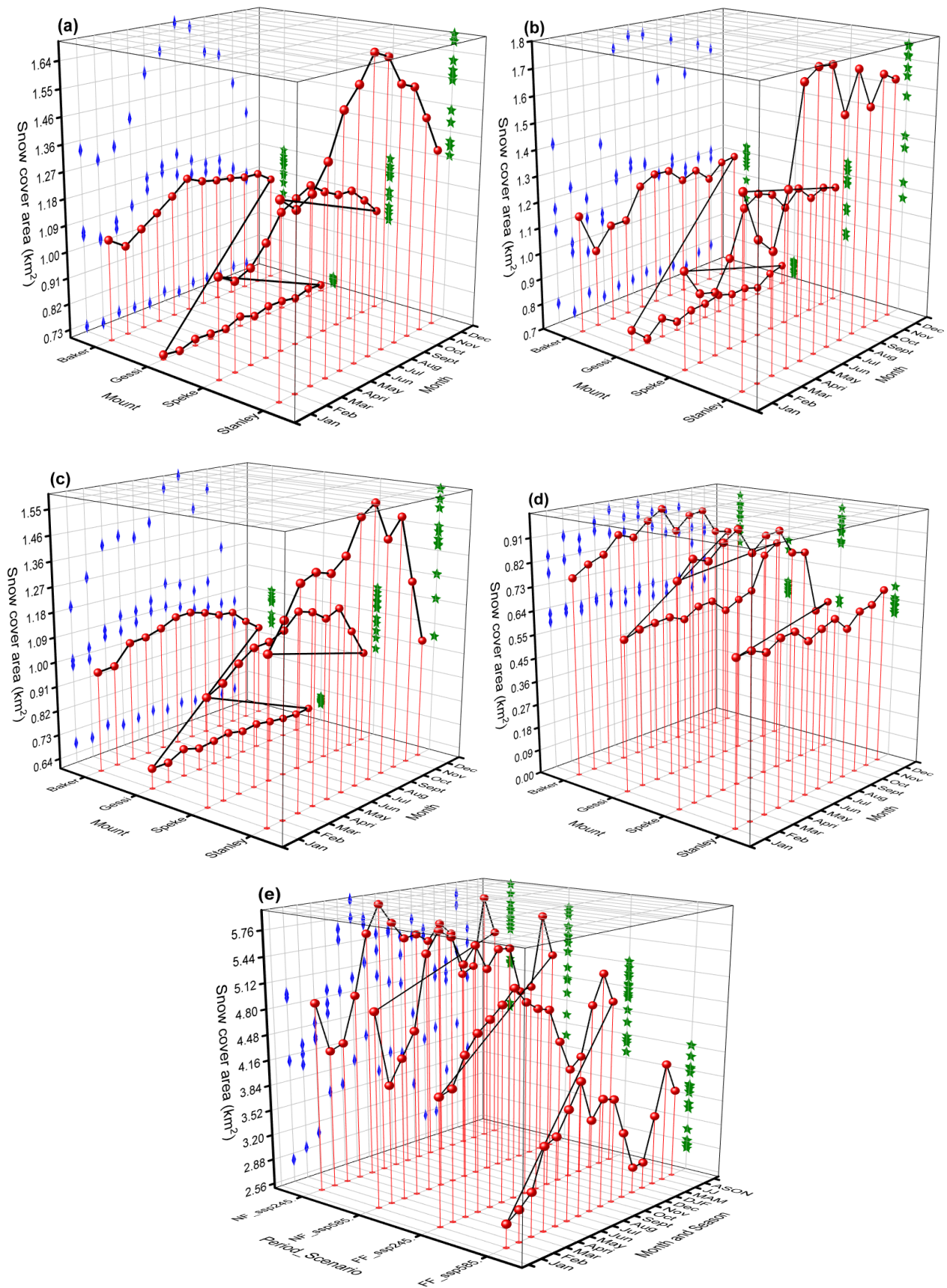


Figure 26. Projected monthly snow cover under different period and scenarios. NF_ssp245(a), NF_ssp585(b), FF_ssp245(c), FF_ssp585(d), Overall(e), Near future (NF), Far future (FF)

4.2. Discussion

4.2.1. Climate dynamics and future trends in the Rwenzori mountains

4.2.1.1. Climate dynamics in the Rwenzori mountains: Insights from historical temperature and rainfall

The analysis of temperature and rainfall patterns over the past three decades on the Rwenzori mountains underscores the region's dynamic climate. Mann-Kendall and Sen's slope analysis reveals a discernible warming trend in both interannual minimum temperatures across the entire mountain range and in minimum and maximum temperatures when considering only the central zone, aligning with global climate change projections (Jones et al., 2019). This warming trend holds profound implications for the region's ecosystems, affecting vegetation, glacier/snow/ice dynamics, and water resources (Smith et al., 2020).

On a monthly basis, trends in Tmax and Tmin exhibit variability across the entire mountain range and the central zone. Significant positive trends in Tmax during June and in Tmin during January, July, September, October, and December, as well as in Tmax during April, May, and July in the central zone, are consistent with previous studies highlighting regional warming (Onyutha, 2021; Smith et al., 2020). However, divergent trends in specific months underscore the complex interplay between regional climate dynamics and local environmental factors (Ougahi et al., 2022). Concerns arise from the observed decrease in rainfall during March in the central zone, prompting further investigation into its potential impacts on water resources and ecosystem dynamics (Worku et al., 2022; Dai et al., 2006). In addition, the significant increase in Tmin during DJF, JJ, and ASON suggests implications for ecosystem processes and species distributions, especially in high-altitude regions (Hannah et al., 2013).

The spatial distribution of temperatures and rainfall, influenced by altitude, underscores the intricate relationship between topography and climate on the Rwenzori mountains. Studies in analogous settings, such as the Himalayas, have demonstrated variations in temperature and precipitation across different elevations, emphasizing the need for validation of climatic linkages between stations in distinct topographic conditions (Chauhan et al., 2023; Diksha et al., 2022). The observed increase in rainfall with altitude aligns with the orographic effect, where moist air is compelled to ascend over mountainous terrain, resulting in increased rainfall (Dai et al., 2006; Shrestha et al., 2021; Nakulopa et al., 2022). However, localized disparities in rainfall distribution, particularly in the central zone of the mountain, imply the influence of additional factors such as microclimate dynamics (Stefanidis & Stathis, 2018). These findings are consistent with those of Nakulopa et al. (2022), who recorded that rainfall in the complex terrain of the

Rwenzori mountains exhibits high variability both spatially and temporally. These temporal variations are mainly shaped by the Intertropical Convergence Zone (ITCZ)'s bimodal influence, engendering significant wet and dry seasonal shifts (Taylor et al., 2020; Kizonde, 2012). Situated in East Africa, the interannual variability of rainfall over the Rwenzori mountains is also subject to the influence of teleconnections such as the El Niño-Southern Oscillation (ENSO) and the Indian Ocean Dipole (IOD) (Nicholson, 2019; Mbigi et al., 2022). These teleconnections exert significant impacts on the timing and intensity of rainfall, with ENSO particularly influential across all seasons (Vaidya, 2005; Preethi et al., 2015).

The observed robust correlations between maximum (Tmax) and minimum (Tmin) temperatures throughout the Rwenzori mountains range and its central region underscore the intricate nature of temperature dynamics within mountainous environments (Karki et al., 2020). These findings align with global observations, highlighting the influence of broader climatic processes on local temperature patterns (Zhang et al., 2022a). The reciprocal relationship between Tmax and Tmin suggests common drivers shaping temperature variability on the Rwenzori mountains, including atmospheric circulation patterns and elevation gradients (Kaufmann et al., 2016; Guo et al., 2016). In contrast, the lack of significant relationships between rainfall and temperatures underscores the intricate interplay between precipitation dynamics and local climate processes (Kaufmann et al., 2016). While temperature variations are closely linked to broader climatic factors, such as atmospheric circulation and topographic features, rainfall patterns are influenced by a multitude of factors, including regional weather systems and land surface characteristics (Beniston et al., 2018). Catchment-scale studies in the Rwenzori mountains indicate that rainfall dynamics are primarily influenced by land use/cover change, while temperature variations are predominantly affected by elevation differences (Kaufmann et al., 2016). The absence of significant correlations between rainfall and temperatures suggests that precipitation variability on the Rwenzori mountains may be governed by factors independent of temperature dynamics, such as local moisture sources and atmospheric moisture transport (Kirtman et al., 2013).

4.2.1.2. Future climate trends and implications for the Rwenzori mountains

The projected climate trends on the Rwenzori mountains, as outlined in the SSP245 and SSP585 scenarios, provide valuable insights into the potential future climate dynamics of the region. The significant temperature increases projected under both scenarios, particularly in the far future, align with broader global climate change projections and highlight the vulnerability of mountainous regions to anthropogenic greenhouse gas emissions. These findings are consistent with previous studies examining climate trends in high-elevation environments (Kolby et al.,

2016; Knight, 2022, Chimborazo et al. 2022). The spatial differences in temperature changes across the mountain range underscore the complex interplay between local topography, elevation, and atmospheric circulation patterns, which can modulate the regional climate response to global warming (Immerzeel et al., 2021).

Comparing the projected climate changes under the SSP245 and SSP585 scenarios, notable differences emerge in the magnitude and spatial distribution of temperature and rainfall changes. While both scenarios project overall warming trends, the SSP585 scenario indicates more pronounced temperature increases, particularly in the far future, which is consistent with higher greenhouse gas emissions trajectories (Pachauri et al., 2014). This highlights the critical importance of emission mitigation efforts in shaping the future climate trajectory of the Rwenzori mountains and underscores the urgent need for ambitious climate action at the global scale (Bedair et al. 2023; Opiyo et al. 2023).

The projected changes in rainfall patterns exhibit spatial variability across the mountain range, with implications for regional hydrology, water resources, and ecosystem dynamics. While some regions may experience increases in precipitation, others may face drier conditions, exacerbating water stress and environmental degradation (Hock et al., 2019).

Both historical and projected climate findings underscore the complex nature of climate change impacts in mountainous regions and emphasize the need for locally relevant adaptation strategies tailored to the unique socio-environmental context of the Rwenzori mountains (Immerzeel et al., 2021).

4.2.2. Snow cover dynamics in the Rwenzori mountains

4.2.2.1. Complexities of Snow cover dynamics in the Rwenzori Mountains: Insights from historical analysis

The analysis of historical snow cover dynamics spanning from 2000 to 2022 across the Rwenzori Mountains underscores the intricate interplay of climate variability and change within mountain ecosystems (Beniston, 2003). Observations indicate notable spatial and temporal variations in snow cover extent, with Mount Stanley consistently exhibiting higher values compared to other peaks. This observation aligns with Taylor et al. (2006), who demonstrated using Normalized Difference Snow Index (NDSI) analysis that Mount Stanley boasts the largest portion of glacier extent among the peaks. Conversely, Mount Gessi presents lower snow cover values, suggesting potential microclimatic or topographic influences shaping snow accumulation dynamics. Similar studies in various mountain regions emphasize the significance of elevation gradients, aspect, and proximity to moisture sources in determining snow distribution patterns (Keyser et al., 2023;

Misra, 2022; Pimentel et al., 2022), which may also apply to the Rwenzori Mountains due to variations in elevation and exposure to prevailing winds.

Temporal analysis indicates fluctuations in snow cover extent over time, emphasizing the necessity of understanding the underlying mechanisms driving seasonal variations (Mukasa et al., 2020). While February shows a significant seasonal decrease and June exhibits a slight increase in snow cover extent, suggesting potential shifts in snow cover dynamics, further comprehensive research is warranted to elucidate the complexities of seasonal snow dynamics (Klein et al., 2019). The no pronounced negative trends observed during several months of the year, implying a reduced contribution of snowmelt runoff to streamflow in the Rwenzori Mountains region and consequently to the recurrent floods recorded in the foothill areas. This observation aligns with the findings of Taylor et al. (2009), who noted the nonsignificant contribution of snowmelt to the flow of the Nyamwamba River, a basin prone to repetitive flooding (Jacobs et al., 2016b). However, evidence suggests that the floods observed in the foothill areas of the Rwenzori Mountains are more likely attributed to intense and regular rainfall events occurring in the central zone of the mountain (Figures 4-11). Given that the slopes of the Rwenzori Mountains are characterized by very steep slopes (Figure 3), this amplifies rainfall runoff, leading to perpetual flooding in the foothill areas of the mountains.

Investigating the correlation between snow cover dynamics and climatic variables elucidates the influence of minimum temperature on snow cover extent, while rainfall and maximum temperature exhibit minimal correlations, suggesting limited influence on snow cover variability (Frei et al., 2019). Focusing on specific months reveals the interplay between climatic variables and snow cover dynamics, with rainfall intensity playing a crucial role in determining snow accumulation during June on Mount Baker and Mount Stanley, while temperature variability drives the snow pack reduction in February specific to Mount Stanley. These findings underscore the multifaceted nature of snow-climate relationships in mountainous regions and emphasize the importance of considering diverse factors in assessing snow cover dynamics and its implications for ecosystem management and conservation efforts (Monteiro & Morin, 2023).

In comparison to other mountain ranges worldwide, the Rwenzori Mountains demonstrate distinct snow cover dynamics influenced by their equatorial location and unique climatic and topographic characteristics. While temperate and polar mountain ranges typically experience snow cover variability driven by seasonal temperature and precipitation changes, the Rwenzori Mountains undergo complex interactions between equatorial climate systems, local topography, and regional atmospheric circulation patterns (Mukasa et al., 2020). Comparisons with other equatorial mountain ranges, such as the Andes or the East African Mountains, further highlight similarities

and differences in snow cover dynamics driven by regional climate patterns and geographical features. Despite experiencing less snow cover compared to higher latitudes, variations in elevation, latitude, and local climate regimes contribute to diverse snow cover patterns within and among equatorial mountain systems (Huggel et al., 2010; Vuille et al., 2018).

4.2.2.2. Projected snow cover dynamics in the Rwenzori mountains: Insights into climate change impacts and modeling approach

The analysis of projected snow cover dynamics in the Rwenzori Mountains reveals a worrisome trend of diminishing snow cover across various peaks and emission scenarios. While a moderate increase is anticipated in the near future under both SSP245 and SSP585 on Mount Baker (Figure 22), all other peaks are expected to undergo reductions in snow cover over time, with particularly notable negative trends observed, especially in the far future period. The statistical analysis underscores the reliability of these projections, not only highlighting anticipated reductions in snow cover but also emphasizing the necessity of incorporating additional scenarios into current modeling approaches for a more comprehensive assessment. Thus, it is recommended that the modeling approach considers projections under scenarios characterized by lower and moderate greenhouse gas emissions and environmental impacts, such as SSP1-1.9, SSP1-2.6, and SSP5-3.4OS (Riahi et al., 2017; O'Neill et al., 2017), given the significant environmental impacts associated with both SSP2-4.5 and SSP5-8.5 scenarios.

Comparisons with research conducted worldwide further validate the projections of decreasing snow cover in the Rwenzori Mountains. Studies by Wypych et al. 2023, Zhang et al. (2020) and Rangwala et al. (2019) demonstrate similar trends of declining snow cover over mountainous regions under different emission scenarios, providing additional context for the observed changes in the Rwenzori Mountains. Additionally, local studies on neighboring mountain ranges, such as Kilimanjaro, support these findings, further strengthening the scientific consensus on the impacts of climate change on snow cover dynamics in East Africa (Mölg & Hardy, 2010). Moreover, analyses of optical spaceborne images (LandSat5, LandSat7) conducted on the Rwenzori Mountains by Taylor et al. (2006) reported a decline in the areal extent of glaciers from $2.01 \pm 0.56 \text{ km}^2$ in 1987 to $0.96 \pm 0.34 \text{ km}^2$ in 2003. According to these authors, extrapolation of trends in glacial recession since 1906 suggested that glaciers in the Rwenzori Mountains could disappear within the next two decades (from 2004). The alignment of projections with both global and local research underscores the urgency of addressing climate change impacts in the region to mitigate adverse effects on mountain ecosystems and associated socio-economic systems.

In comparing the findings of Taylor et al. (2006) with the present study's analysis using MODIS daily dataset, disparities arise regarding the estimation of snow cover dynamics in the Rwenzori

Mountains. While Taylor et al. projected a decline in glacier extent with potential disappearance within the 2004-2024 period, the current study's analysis reveals significant snow cover presence on the mountains up to 2022, contradicting their projection. These disparities may result from variations in data sources, methodologies, and the chosen time periods for analysis. Further investigation and validation, integrating diverse datasets and methodologies, is essential to reconcile these differences and advance our understanding of snow cover dynamics in the region.

5. CONCLUSIONS AND RECOMMENDATIONS

5.1. Conclusions

Through an extensive examination of historical climate data and future projections, the current study has assessed the impacts of climate change on snow cover dynamics within the Rwenzori Mountains. By employing a combination of reanalysis climate data and MODIS snow observations, alongside the use of the J2000 hydrological model, a nuanced understanding of past trends and future scenarios has been achieved. The findings reveal significant climatic shifts over the last three decades, characterized by a significant warming trend and pronounced variability in rainfall patterns. These shifts have had effects on the dynamics of snow cover in the region, underscoring the delicate balance between climatic factors and snow cover sustainability. The projected future scenarios paint a concerning picture of continued warming and decreased snow cover across the Rwenzori Mountains, which is anticipated to persist under both SSP245 and SSP585 scenarios. Notably, a modest increase in snow cover is expected on Mount Baker in the near term (2030-2065), offering a sliver of variability amidst the broader trend of decline. This trend of diminishing snow cover bears critical implications for the region's water resources, biodiversity, and the communities that rely on these ecosystems. The urgency for integrated strategies to manage these resources and conserve biodiversity in light of decreasing snow cover is starkly highlighted by the study's findings. This study not only enriches our understanding of the complex interplay between climate change and snow cover dynamics but also calls for immediate action to mitigate the adverse effects of these changes on the Rwenzori Mountains and similar ecosystems worldwide.

5.2. Recommendations

To address the gaps in weather and snow/glacier data collection in the Rwenzori Mountains, establishing a comprehensive climate monitoring network is imperative. This network should include traditional weather stations alongside advanced remote sensing technologies to enhance the accuracy, reliability, and spatial coverage of climate data. The integration of ground-truth data from weather stations with remote sensing observations will facilitate the validation of remote data and the development of specific climate change adaptation strategies. Engaging local communities through awareness programs is also essential for promoting conservation efforts and adapting to climate changes. Empowering these communities with knowledge and resources will foster the adoption of sustainable practices and enhance resilience to climate impacts.

Further research into the relationship between climate change and snow cover dynamics is vital. This should include a focused study on Mount Baker to uncover the mechanisms driving the

observed trends in snow cover extent. Expanding research to incorporate parameters such as snowmelt and snow water equivalent will deepen our understanding of snow cover dynamics. Additionally, projecting snow cover under a broader range of CMIP6 scenarios, including SSP1-1.9, SSP1-2.6, and SSP5-3.4OS, will provide insights into the potential future changes in snow cover under various mitigation efforts and environmental impacts.

Policy development, informed by this study, should aim to protect mountain ecosystems, manage water resources sustainably, and conserve biodiversity in the face of climate change. Implementing sustainable land and water management practices, such as water harvesting, efficient irrigation, and soil conservation, is crucial for mitigating the impact of decreased snow cover on water availability. Advancements in satellite imagery and GIS tools should be leveraged for monitoring climate change impacts and guiding conservation efforts, enabling effective mapping of vulnerable areas, prediction of future changes, and planning of conservation initiatives.

By embracing these recommendations, stakeholders can address the challenges posed by climate change in the Rwenzori Mountains, ensuring the sustainability of the region's water resources, biodiversity, and the livelihoods of communities dependent on these ecosystems. This multi-faceted approach, combining technological advancements, community engagement, and further research, offers a path toward understanding and mitigating the impacts of climate change on mountainous ecosystems.

6. REFERENCES

- Ahmadalipour, A.; Rana, A.; Moradkhani, H.; Sharma, A. 2017. Multicriteria evaluation of CMIP5 GCMs for climate change impact analysis. *Theor. Appl. Climatol.*, 128, 71–87.
- Alaminie, A. A., Tilahun, S. A., Legesse, S. A., Zimale, F. A., Tarkegn, G. B., & Jury, M. R. (2021). Evaluation of past and future climate trends under CMIP6 scenarios for the UBNB (Abay), Ethiopia. *Water*, 13, 2110.
- Almazroui, M., Saeed, F., Saeed, S., Nazrul Islam, M., Ismail, M., Klutse, N. A. B., & Siddiqui, M. H. (2020). Projected change in temperature and precipitation over Africa from CMIP6. *Earth Systems and Environment*, 4, 455-475.
- Bahati, G., Pang, Z., Armannsson, H., Isabirye, E. M., & Kato, V. (2005). Hydrology and reservoir characteristics of three geothermal systems in western Uganda. *Geothermics*, 34, 568-591.
- Banholzer, S.; Kossin, J.; Donner, S., 2014 The impact of climate change on natural disasters. In reducing disaster: Early warning systems for climate change; Singh, A., Zommers, Z., Eds.; Springer: Dordrecht, The Netherlands.
- Barnett, T. P., Adam, J. C., & Lettenmaier, D. P. (2005). Potential impacts of a warming climate on water availability in snow-dominated regions. *Nature*, 438, 303–309.
- Barnett, T. P., et al. (2008). Human-induced changes in the distribution of precipitation. *Nature Geoscience*, 1, 627–631.
- Bauer, M. W. (2011). Public attention to science 1820–2010—A ‘longue durée’ picture. In The sciences’ media connection. Public communication and its repercussions. *Dordrecht: Springer; Netherlands*.
- Bedair, H., Alghariani, M. S., Omar, E., Anibaba, Q. A., Remon, M., Bornman, C. & Alzain, H. M. (2023). Global warming status in the African continent: sources, challenges, policies, and future direction. *International Journal of Environmental Research*, 17, 45.
- Bell, B. A., Hughes, P. D., Fletcher, W. J., Cornelissen, H. L., Rhoujjati, A., Hanich, L., & Braithwaite, R. J. (2022). Climate of the Marrakech High Atlas, Morocco: Temperature lapse rates and precipitation gradient from piedmont to summits. *Arctic, Antarctic, and Alpine Research*, 54, 78-95.
- Beniston, M. (2003). Climatic change in mountain regions: a review of possible impacts. *Climatic Change*, 59, 5-31.
- Beniston, M., Farinotti, D., Stoffel, M., Andreassen, L. M., Coppola, E., Eckert, N., ... & Urrutia, R. (2018). The European mountain cryosphere: a review of its current state, trends, and future challenges. *The Cryosphere*, 12, 759-794.
- Beniston, M., Stoffel, M., & Hill, M. (2011). Impacts of climatic change on water and natural

- hazards in the Alps: can current water governance cope with future challenges? Examples from the European “ACQWA” project. *Environmental Science & Policy*, 14, 734-743.
- Benveniste, H., Oppenheimer, M., & Fleurbaey, M. (2020). Effect of border policy on exposure and vulnerability to climate change. *Proceedings of the National Academy of Sciences*, 117, 26692-26702.
- Bharath, A. L., & Venkatesh, B. (2022). Precipitation concentration index and rainfall trend analysis for south western districts of Karnataka, India. *Indian Journal of Ecology*, 49, 462-469.
- Bhatta, B., Shrestha, S., Shrestha, P. K., & Talchabhadel, R. (2020). Modelling the impact of past and future climate scenarios on streamflow in a highly mountainous watershed: A case study in the West Seti River Basin, Nepal. *Science of the Total Environment*, 740, 140156.
- Bibi, S., Wang, L., Li, X., Zhou, J., Chen, D., & Yao, T. (2018). Climatic and associated cryospheric, biospheric, and hydrological changes on the Tibetan Plateau: A review. *International Journal of Climatology*, 38, e1-e17.
- Bitner, D., Carroll, T., Cline, D., & Romanov, P. (2002). An assessment of the differences between three satellite snow cover mapping techniques. *Journal of Hydrometeorology*, 3, 410-425.
- Bouramdane, A. A. (2022). Assessment of CMIP6 multi-model projections worldwide: Which regions are getting warmer and are going through a drought in Africa and Morocco? What changes from CMIP5 to CMIP6? *Sustainability*, 15, 690.
- Braun, A., & Fotopoulos, G. (2007). Assessment of SRTM, ICESat, and survey control monument elevations in Canada. *Photogrammetric Engineering & Remote Sensing*, 73, 1333-1342.
- Brühl, C. (1997). Flightless insects: a test case for historical relationships of African mountains. *Journal of Biogeography*, 24, 233-250.
- Cervera, Á. G., & Durán, L. (2023). Multi-year hyper-high resolution snow cover simulation in a mountainous region in central Spain (Peñalara Massif) (No. EGU23-755). *Copernicus Meetings*.
- Chauhan, H. K., Gallacher, D., Bhatt, A., & Bisht, A. K. (2023). The Himalayas: A climate change laboratory. *Environmental Development*, 45, 100814.
- Chimborazo, O., Minder, J. R., & Vuille, M. (2022). Observations and simulated mechanisms of elevation-dependent warming over the Tropical Andes. *Journal of Climate*, 35, 1021-1044.
- Chu, D., Liu, L., & Wang, Z. (2023). Snow cover on the Tibetan Plateau and topographic controls. *Remote Sensing*, 15, 4044.
- Dai, A., Qian, T., Trenberth, K. E., and Milliman, J. D. (2006). Changes in continental freshwater discharge from 1948 to 2004. *Journal of Climate*, 22, 2773-2792.

- Daloz, A. S., Schwingshackl, C., Mooney, P., Strada, S., Rechid, D., Davin, E. L. & Lund, M. T. (2022). Land-atmosphere interactions in sub-polar and alpine climates in the CORDEX flagship pilot study Land Use and Climate Across Scales (LUCAS) models-Part 1: Evaluation of the snow-albedo effect. *The Cryosphere*, 16, 2403-2419.
- Das, S., Kamruzzaman, M., & Islam, A. R. M. T. (2022). Assessment of characteristic changes of regional estimation of extreme rainfall under climate change: A case study in a tropical monsoon region with the climate projections from CMIP6 model. *Journal of Hydrology*, 610, 128002.
- DeBeer, C. M., & Pomeroy, J. W. (2010). Spatial and temporal variations in snow accumulation and ablation sensitivity in the Canadian Rocky Mountains. *Hydrological Processes*, 24, 2173-2185.
- DeBeer, C. M., Wheeler, H. S., Carey, S. K., & Chun, K. P. (2016). Recent climatic, cryospheric, and hydrological changes over the interior of western Canada: A review and synthesis. *Hydrology and Earth System Sciences*, 20, 1573-1598.
- Deepa, R., Kumar, V., & Sundaram, S. (2024). A systematic review of regional and global climate extremes in CMIP6 models under shared socio-economic pathways. *Theoretical and Applied Climatology*, 1-21.
- Deng, G., Tang, Z., Hu, G., Wang, J., Sang, G., & Li, J. (2021). Spatiotemporal dynamics of snowline altitude and their responses to climate change in the Tianshan mountains, Central Asia, During 2001–2019. *Sustainability*, 13, 3992.
- Derksen, C., & Brown, R. (2012). Spring snow cover extent reductions in the 2008–2012 period exceeding climate model projections. *Geophysical Research Letters*, 39, 19504.
- Di Marco, N., Avesani, D., Righetti, M., Zaramella, M., Majone, B., & Borga, M. (2021). Reducing hydrological modelling uncertainty by using MODIS snow cover data and a topography-based distribution function snowmelt model. *Journal of Hydrology*, 599, 126020.
- Diksha, Kumar, A., & Lal, P. (2022). Analysing climatic variability and extremes events in the Himalayan regions focusing on mountainous urban agglomerations. *Geocarto International*, 37, 14148-14170.
- Doughty, A. M., Kelly, M. A., Russell, J. M., Jackson, M. S., Anderson, B. M., Chipman, J. & Dee, S. G. (2021). Modeling glacier extents and equilibrium line altitudes in the Rwenzori Mountains, Uganda, over the last 31,000 yr.
- Doughty, A. M., Kelly, M. A., Russell, J. M., Jackson, M. S., Anderson, B. M., Chipman, J., & Nakileza, B. R. (2023). Last glacial maximum reconstructions of Rwenzori mountain

- glaciers. *Paleoceanography and Paleoclimatology*, 38, e2022PA004527.
- Dutta, R., Chanda, K., & Maity, R. (2022). Future of solar energy potential in a changing climate across the world: A CMIP6 multi-model ensemble analysis. *Renewable Energy*, 188, 819-829.
- Easterling, D. R., Arnold, J. R., Knutson, T., Kunkel, K. E., LeGrande, A. N., Leung, L. R. & Wehner, M. F. (2017). Precipitation change in the United States. In: *Climate Science Special Report: Fourth National Climate Assessment, Volume I*. U.S. Global Change Research Program.
- Eeckman, J., Nepal, S., Chevallier, P., Camensuli, G., Delclaux, F., Boone, A., & De Rouw, A. (2019). Comparing the ISBA and J2000 approaches for surface flows modelling at the local scale in the Everest region. *Journal of Hydrology*, 569, 705-719.
- Eggermont, H., Russell, J. M., Schettler, G., Van Damme, K., Bessems, I., & Verschuren, D. (2007). Physical and chemical limnology of alpine lakes and pools in the Rwenzori Mountains (Uganda–DR Congo). *Hydrobiologia*, 592, 151-173.
- Eggermont, H., Verschuren, D., Audenaert, L., Lens, L., Russell, J., Klaassen, G., & Heiri, O. (2010). Limnological and ecological sensitivity of Rwenzori mountain lakes to climate warming. *Hydrobiologia*, 648, 123-142.
- Elmar, Kriegler., Nico, Bauer., Alexander, Popp., Florian, Humpenöder., Marian, Leimbach., Jessica, Strefler., Lavinia, Baumstark., Benjamin, Leon, Bodirsky., Jérôme, Hilaire., David, Klein., Ioanna, Mouratiadou., Isabelle, Weindl., Christoph, Bertram., Jan, Philipp, Dietrich., Gunnar, Luderer., Michaja, Pehl., Robert, C., Pietzcker., Franziska, Piontek., Hermann, Lotze-Campen., Hermann, Lotze-Campen., Anne, Biewald., Markus, Bonsch., Anastasis, Giannousakis., Ulrich, Kreidenweis., Christoph, Müller., Susanne, Rolinski., Anselm, Schultes., Jana, Schwanitz., Miodrag, Stevanovic., Katherine, Calvin., Johannes, Emmerling., Shinichiro, Fujimori., Ottmar, Edenhofer., Ottmar, Edenhofer. (2017). Fossil-fueled development (SSP5): An energy and resource intensive scenario for the 21st century. *Global Environmental Change*, 42, 297-315.
- Forte, A. M., & Rossi, M. W. (2023). Stochastic in space and time: Part 1, characterizing orographic gradients in mean runoff and daily runoff variability. *Authorea Preprints*.
- Frei, A., Tedesco, M., Lee, S., Foster, J., Hall, D. K., Kelly, R., & Robinson, D. A. (2012). A review of global satellite-derived snow products. *Advances in Space Research*, 50, 1007-1029.
- Frei, P., Kotlarski, S., Liniger, M. A., & Schär, C. (2018). Future snowfall in the Alps: projections based on the EURO-CORDEX regional climate models. *The Cryosphere*, 12, 1-24.

- Funk, C., Peterson, P., Landsfeld, M., Pedreros, D., Verdin, J., Shukla, S. & Michaelsen, J. (2015). The climate hazards infrared precipitation with stations a new environmental record for monitoring extremes. *Scientific Data*, 2, 1-21.
- Funk, C., Verdin, A., Michaelsen, J., Peterson, P., Pedreros, D., & Husak, G. (2015). A global satellite-assisted precipitation climatology. *Earth System Science Data*, 7, 275-287.
- Gao, T., Kang, S., Krause, P., Cuo, L., & Nepal, S. (2012). A test of J2000 model in a glacierized catchment in the central Tibetan Plateau. *Environmental Earth Sciences*, 65, 1651-1659.
- Garellick, S., Russell, J., Richards, A., Smith, J., Kelly, M., Anderson, N. & Marshall, C. (2022). The dynamics of warming during the last deglaciation in high-elevation regions of Eastern Equatorial Africa. *Quaternary Science Reviews*, 281, 107416.
- Getachew, B., & Manjunatha, B. R. (2022). Potential climate change impact assessment on the hydrology of the Lake Tana Basin, Upper Blue Nile River Basin, Ethiopia. *Physics and Chemistry of the Earth, Parts A/B/C*, 127, 103162.
- Ghimire, U., Srinivasan, G., & Agarwal, A. (2019). Assessment of rainfall bias correction techniques for improved hydrological simulation. *International Journal of Climatology*, 39, 2386-2399.
- Grekousis, G., Mountrakis, G., & Kavouras, M. (2015). An overview of 21 global and 43 regional land-cover mapping products. *International Journal of Remote Sensing*, 36, 5309-5335.
- Grimmond, S. U. E. (2007). Urbanization and global environmental change: local effects of urban warming. *The Geographical Journal*, 173, 83-88.
- Gummert, M., Lindenfeld, M., Wölbern, I., Rümpler, G., Celestin, K., & Batte, A. (2016). Crustal structure and high-resolution Moho topography across the Rwenzori region (Albertine rift) from P-receiver functions. *Geological Society, London, Special Publications*, 420, 69-82.
- Guo, H., Wang, X., Guo, Z., Zhu, G., Che, T., Wang, J. & OuYang, Z. (2022). Review of snow phenology variation in the Northern Hemisphere and its relationship with climate and vegetation. *The Cryosphere Discussions*, 1-24.
- Guo, X., Wang, L., & Tian, L. (2016). Spatio-temporal variability of vertical gradients of major meteorological observations around the Tibetan Plateau. *International Journal of Climatology*, 36, 1901-1916.
- Onyutha, C. (2021). Trends and variability of temperature and evaporation over the African continent: Relationships with precipitation. *Atmósfera*, 34, 267-287.
- Gütschow, J., Jeffery, M. L., Günther, A., & Meinshausen, M. (2021). Country-resolved combined emission and socio-economic pathways based on the Representative Concentration Pathway (RCP) and Shared Socio-Economic Pathway (SSP) scenarios. *Earth System Science Data*,

13, 1005-1040.

- Hall, D. K., Riggs, G. A., & Salomonson, V. V. (2002). MODIS snow-cover products. *Remote Sensing of Environment*, 83, 181-194.
- Hannah, L., Roehrdanz, P. R., Ikegami, M., Shepard, A. V., Shaw, M. R., Tabor, G., et al. (2013). Climate change, wine, and conservation. *National Academy of Sciences of the United States of America*, 110, 6907-6912.
- Hasan, R. H. (2019). Evaluation of the accuracy of digital elevation model produced from different open source data. *Journal of Engineering*, 25, 100-112.
- Hayhoe, K., VanDorn, J., Croley II, T., Schlegal, N., & Wuebbles, D. (2010). Regional climate change projections for Chicago and the US Great Lakes. *Journal of Great Lakes Research*, 36, 7-21.
- Hayhoe, K., Wake, C. P., Huntington, T. G., Luo, L., Schwartz, M. D., Sheffield, J. & Wolfe, D. (2007). Past and future changes in climate and hydrological indicators in the US Northeast. *Climate Dynamics*, 28, 381-407.
- He, Z., Duethmann, D., & Tian, F. (2021). A meta-analysis based review of quantifying the contributions of runoff components to streamflow in glacierized basins. *Journal of Hydrology*, 603, 126890.
- Hock, R., Rasul, G., Adler, C., Cáceres, B., Gruber, S., Hirabayashi, Y. & Zhang, Y. (2019). High mountain areas. In *IPCC special report on the ocean and cryosphere in a changing climate*. H.O. Pörtner, DC Roberts, V. Masson-Delmotte, P. Zhai, M. Tignor, E. Poloczanska, K. Mintenbeck, A. Alegría, M. Nicolai, A. Okem, J. Petzold, B. Rama, NM Weyer (eds.).
- Hofer, S., Lang, C., Amory, C., Kittel, C., Delhasse, A., Tedstone, A., & Fettweis, X. (2020). Greater greenland Ice Sheet contribution to global sea level rise in CMIP6. *Nature Communications*, 11, 6289.
- Huang, H., Patricola, C. M., & Collins, W. D. (2021). The influence of ocean coupling on simulated and projected tropical cyclone precipitation in the HighResMIP-PRIMAVERA simulations. *Geophysical Research Letters*, 48, e2021GL094801.
- Huggel, C., Kääb, A., Haeberli, W., Teysseire, P., & Paul, F. (2002). Remote sensing based assessment of hazards from glacier lake outbursts: a case study in the Swiss Alps. *Canadian Geotechnical Journal*, 39, 316-330.
- Huggel, C., Salzmann, N., Allen, S., Caplan-Auerbach, J., Fischer, L., Haeberli, W. & Schneider, D. (2010). Recent and future warm extreme events and high-mountain slope stability. *Philosophical transactions of the royal society A: Mathematical, Physical and Engineering*
- Huss, M., Bookhagen, B., Huggel, C., Jacobsen, D., Bradley, R. S., Clague, J. J., ... & Schneider,

- J. (2017). Toward mountains without permanent snow and ice. *Earth's Future*, 5, 418-435.
- Immerzeel, W. W., Lutz, A. F., Andrade, M., Bahl, A., Biemans, H., Bolch, T. & Baillie, J. E. M. (2020). Importance and vulnerability of the world's water towers. *Nature*, 577, 364-369.
- Irannezhad, M., Ronkanen, A. K., & Kløve, B. (2015). Effects of climate variability and change on snowpack hydrological processes in Finland. *Cold Regions Science and Technology*, 118, 14-29.
- Isinkaralar, O. (2023). Bioclimatic comfort in urban planning and modeling spatial change during 2020–2100 according to climate change scenarios in Kocaeli, Türkiye. *International Journal of Environmental Science and Technology*, 20, 7775-7786.
- Jacobs, L., Dewitte, O., Poesen, J., Delvaux, D., Thiery, W., & Kervyn, M. (2016a). The Rwenzori Mountains, a landslide-prone region?. *Landslides*, 13, 519-536.
- Jacobs, L., Maes, J., Mertens, K., Sekajugo, J., Thiery, W., Van Lipzig, N. & Dewitte, O. (2016b). Reconstruction of a flash flood event through a multi-hazard approach: focus on the Rwenzori mountains, Uganda. *Natural Hazards*, 84, 851-876.
- Javadinejad, S., Dara, R., & Jafary, F. (2021). Analysis and prioritization the effective factors on increasing farmers resilience under climate change and drought. *Agricultural Research*, 10, 497-513.
- Jones, P. D., Lister, D. H., Osborn, T. J., Harpham, C., Salmon, M., and Morice, C. P. (2019). Hemispheric and large-scale land-surface air temperature variations: An extensive revision and an update to 2010. *Journal of Geophysical Research: Atmospheres*, 117(D5).
- Joshi, G. S., & Makhasana, P. (2020). Assessment of seasonal climate transference and regional influential linkages to land cover–investigation in a river basin. *Journal of Atmospheric and Solar-Terrestrial Physics*, 199, 105209.
- Kad, P., Ha, K. J., Lee, S. S., & Chu, J. E. (2023). Projected changes in mountain precipitation under CO2-induced warmer climate. *Earth's Future*, 11, e2023EF003886.
- Kamruzzaman, M., Shahid, S., Islam, A. T., Hwang, S., Cho, J., Zaman, M. A. U., ... & Hossain, M. B. (2021). Comparison of CMIP6 and CMIP5 model performance in simulating historical precipitation and temperature in Bangladesh: a preliminary study. *Theoretical and Applied Climatology*, 145, 1385-1406.
- Kapnick, S., & Hall, A. (2012). Causes of recent changes in western North American snowpack. *Climate Dynamics*, 38, 1885-1899.
- Karki, R., Hasson, S. U., Schickhoff, U., Scholten, T., Böhner, J., & Gerlitz, L. (2020). Near surface air temperature lapse rates over complex terrain: a WRF based analysis of controlling factors and processes for the central Himalayas. *Climate Dynamics*, 54, 329-349.

- Kaser, G., & Noggler, B. (1991). Observations on Speke glacier, Rwenzori range, Uganda. *Journal of Glaciology*, 37, 313-318.
- Kaser, G., & Osmaston, H. (2002). *Tropical glaciers*. Cambridge University Press, Cambridge.207
- Katumwehe, A. B., Abdelsalam, M. G., & Atekwana, E. A. (2015). The role of pre-existing precambrian structures in rift evolution: The Albertine and Rhino grabens, Uganda. *Tectonophysics*, 646, 117-129.
- Kaufmann, G., & Romanov, D. (2012). Landscape evolution and glaciation of the Rwenzori mountains, Uganda: Insights from numerical modeling. *Geomorphology*, 138, 263-275.
- Kaufmann, G., Hinderer, M., & Romanov, D. (2016). Shaping the Rwenzoris: balancing uplift, erosion, and glaciation. *International Journal of Earth Sciences*, 105, 1761-1778.
- Kervyn, M., Jacobs, P., Thiery, W., & Frankl, A. (2007). Late Miocene to recent tectonics and geomorphology of the Rwenzori Mountains, West-Central Africa. *Journal of African Earth Sciences*, 48, 268-285.
- Keyser, S. R., Fink, D., Gudex-Cross, D., Radeloff, V. C., Pauli, J. N., & Zuckerberg, B. (2023). Snow cover dynamics: an overlooked yet important feature of winter bird occurrence and abundance across the United States. *Ecography*, 1, e06378.
- Khadka, N., Ghimire, S. K., Chen, X., Thakuri, S., Hamal, K., Shrestha, D., & Sharma, S. (2020). Dynamics of maximum snow cover area and snow line altitude across Nepal (2003-2018) using improved MODIS data. *Journal of Institute of Science and Technology*, 25, 17-24.
- Kirtman, B. P., Power, S. B., Adedoyin, J. A., Boer, G. J., Bojariu, R., Camilloni, I., et al. (2013). Near-term climate change: Projections and predictability. In climate change 2013: The physical science basis. Contribution of working group I to the fifth assessment report of the Intergovernmental Panel on Climate Change. *Cambridge University Press*.
- Kis, A., & Pongrácz, R. (2023). Future changes of snow-related variables in different European regions. *Hungarian Geographical Bulletin*, 72, 3-22.
- Kizonde, J. D. (2012). Climate change and the Rwenzori mountains, Uganda. *Environmental Monitoring and Assessment*, 184, 539-553.
- Klein, A. G., & Barnett, A. C. (2003). Validation of daily MODIS snow cover maps of the Upper Rio Grande River Basin for the 2000–2001 snow year. *Remote Sensing of Environment*, 86, 162-176.
- Klein, A. G., Hörnberg, G., & Jansson, P. (2019). Seasonal and altitudinal variations in snow cover, depth, and density in the subarctic Scandinavian mountains. *Arctic, Antarctic, and Alpine Research*, 51, 428-442.

- Knight, J. (2022). Scientists' warning of the impacts of climate change on mountains. *PeerJ*, 10, e14253.
- Knight, J., & Harrison, S. (2023). The sensitivity and evolutionary trajectory of the mountain cryosphere: Implications for mountain geomorphic systems and hazards. *Land Degradation & Development*, 34, 2464-2482.
- Koehn, D., Link, K., Sachau, T., Passchier, C. W., Aanyu, K., Spikings, A., & Harbinson, R. (2016). The Rwenzori mountains, a Palaeoproterozoic crustal shear belt crossing the Albertine rift system. *International Journal of Earth Sciences*, 105, 1693-1705.
- Kolby Smith, W., Reed, S. C., Cleveland, C. C., Ballantyne, A. P., Anderegg, W. R., Wieder, W. R. & Running, S. W. (2016). Large divergence of satellite and Earth system model estimates of global terrestrial CO₂ fertilization. *Nature climate change*, 6(3), 306-310.
- Kumar, N., Poonia, V., Gupta, B. B., & Goyal, M. K. (2021). A novel framework for risk assessment and resilience of critical infrastructure towards climate change. *Technological Forecasting and Social Change*, 165, 120532.
- Kumar, T. L., Durga, G. P., Aravindhavel, A., Barbosa, H., & Rao, D. N. (2022). Analysis of tropospheric warming and stratospheric cooling in the present and future climate from the suite of CMIP6 models. *Theoretical and Applied Climatology*, 149, 1717-1726.
- Landwehr, S., Volpi, M., Haumann, F. A., Robinson, C. M., Thurnherr, I., Ferracci, V. & Schmale, J. (2021). Exploring the coupled ocean and atmosphere system with a data science approach applied to observations from the Antarctic circumnavigation expedition. *Earth System Dynamics*, 12, 1295-1369.
- Lee, J., Lee, O., Choi, J., Seo, J., Won, J., Jang, S., & Kim, S. (2023). Estimation of real-time rainfall fields reflecting the mountain effect of rainfall explained by the WRF rainfall fields. *Water*, 15, 1794.
- Lehmann, I. (2008). Ten new species of Metarbelidae (Lepidoptera: Cossioidea) from the coastal forests and the Eastern Arc Mountains of Kenya and Tanzania, including one species from two upland forests. *Journal of East African Natural History*, 97, 43-82.
- Levizzani, V., & Cattani, E. (2019). Satellite remote sensing of precipitation and the terrestrial water cycle in a changing climate. *Remote sensing*, 11, 2301.
- Li, X., Wang, L., Hu, B., Chen, D., & Liu, R. (2023). Contribution of vanishing mountain glaciers to global and regional terrestrial water storage changes. *Frontiers in Earth Science*, 11, 1134910.
- Li, Y., Zhang, W., & Wei, X. (2021). Changes in alpine grassland ecosystems under climate change in the Qinghai-Tibetan Plateau. *Science of the Total Environment*, 761, 143244.

- Liu, J., Chen, J., Shi, W., Xu, X., & Lu, S. (2019). Changes in snow cover and its impacts on runoff in mountainous regions of China during 2002–2016. *Journal of Hydrology*, 574, 228-238.
- Liu, Y., Hansen, B. U., Elberling, B., & Westergaard-Nielsen, A. (2023). Snow insulation effects on soil surface temperatures in a snow-fence manipulation experiment (No. EGU23-12055). *Copernicus Meetings*.
- Londhe, D. S., Katpatal, Y. B., & Bokde, N. D. (2023). Performance assessment of bias correction methods for precipitation and temperature from CMIP5 model simulation. *Applied Sciences*, 13, 9142.
- Loukas, A., Mylopoulos, N., & Vasiliades, L. (2007). A modeling system for the evaluation of water resources management strategies in Thessaly, Greece. *Water Resources Management*, 21, 1673-1702.
- Lutz, A. F., Immerzeel, W. W., Shrestha, A. B., & Bierkens, M. F. (2020). Consistent increase in High Asia's runoff due to increasing glacier melt and precipitation. *Nature Climate Change*, 10, 687-692.
- Mackay, A. W., Lee, R., & Russell, J. M. (2021). Recent climate-driven ecological changes in tropical montane lakes of Rwenzori Mountains National Park, central Africa. *Journal of Paleolimnology*, 65, 219-234.
- Maggioni, V., & Massari, C. (2018). On the performance of satellite precipitation products in riverine flood modeling: A review. *Journal of Hydrology*, 558, 214-224.
- Magnus, Merkle., Ornella, Dellaccio., Robert, Dunford., Zuzana, V., Harmáčková., Paula, A., Harrison., Jean-Francois, Mercure., Simona, Pedde., Bumsuk, Seo., Yeliz, Simsek., Jon, Stenning., Mark, Rounsevell. (2022). Creating quantitative scenario projections for the UK shared socioeconomic pathways. *Available at SSRN 4006905*.
- Malte, Meinshausen., Malte, Meinshausen., Zebedee, Nicholls., Jared, Lewis., Matthew, Gidden., Elisabeth, Vogel., Mandy, Freund., Mandy, Freund., Urs, Beyerle., Claudia, Gessner., Alexander, Nauels., Nico, Bauer., Josep, G., Canadell., John, S., Daniel., Andrew, John., Paul, B., Krummel., Gunnar, Luderer., Nicolai, Meinshausen., Stephen, A., Montzka., Peter, Rayner., Stefan, Reimann., Steven, J., Smith., Marten, van, den, Berg., Guus, J., M., Velders., Martin, K., Vollmer., Ray, H., J., Wang. (2019). The SSP greenhouse gas concentrations and their extensions to 2500. *Geoscientific Model Development Discussions*, 2019, 1-77.
- Mankin, J. S., Viviroli, D., Singh, D., & Hoekstra, A. Y. (2015). The potential for snow to supply human water demand in the present and future. *Environmental Research Letters*, 10, 114016.

- Masson-Delmotte, V., Zhai, P., Pirani, A., Connors, S. L., Péan, C., Berger, S., ... & Zhou, B. (2021). Climate change 2021: the physical science basis. *Contribution of working group I to the sixth assessment report of the intergovernmental panel on climate change*, 2.
- Maurer, E. P., Rhoads, J. D., Dubayah, R. O., & Lettenmaier, D. P. (2003). Evaluation of the snow-covered area data product from MODIS. *Hydrological Processes*, 17, 59–71.
- Mbigi, D., Onyango, A. O., Mteweke, Z. F., Kiprotich, P., & Xiao, Z. (2022). Coupled model intercomparison project phase 6 simulations of the spatial structure of rainfall variability over East Africa: Evaluation and projection. *International Journal of Climatology*, 42, 9865-9885.
- McBride, L. A., Hope, A. P., Canty, T. P., Bennett, B. F., Tribett, W. R., & Salawitch, R. J. (2021). Comparison of CMIP6 historical climate simulations and future projected warming to an empirical model of global climate. *Earth System Dynamics*, 12, 545-579.
- Meinshausen, M., Nicholls, Z. R., Lewis, J., Gidden, M. J., Vogel, E., Freund, M., ... & Wang, R. H. (2020). The shared socio-economic pathway (SSP) greenhouse gas concentrations and their extensions to 2500. *Geoscientific Model Development*, 13, 3571-3605.
- Melnikova, I., Boucher, O., Cadule, P., Tanaka, K., Gasser, T., Hajima, T., ... & Ciais, P. (2021). Impact of bioenergy crops expansion on climate-carbon cycle feedbacks in overshoot scenarios. *Earth System Dynamics Discussions*, 2021, 1-22.
- Ménégoz, M., Gallée, H., Krinner, G., & Salas-Méllia, D. (2013). Impact of snow cover formulation in a land surface model on Arctic climate simulations. *Journal of Geophysical Research: Atmospheres*, 118, 10892-10910.
- Michel, A., Aschauer, J., Jonas, T., Gubler, S., Kotlarski, S., & Marty, C. (2023). SnowQM 1.0: A fast R Package for bias-correcting spatial fields of snow water equivalent using quantile mapping. *Geoscientific Model Development Discussions*, 2023, 1-28.
- Miska, Luoto., Juha, Aalto., Julia, Kemppinen., Henny, C., van, der, Mei., Jesús, Rogel-Salazar., Victoria, Alcalá. (2023). Variability and drivers of winter near-surface temperatures over boreal and tundra landscapes.
- Misra, A. (2022). Snow Cover variability as climate change indicator: A case study from higher Himalaya in Garhwal, Uttarakhand. In *Environmental Studies and Climate Change* (pp. 485-518). CRC Press.
- Mölg, T., & Hardy, D. R. (2010). Ablation and associated energy balance of a horizontal glacier surface on Kilimanjaro. *Journal of Geophysical Research: Atmospheres*, 115(D11).
- Molotch, N. P., et al. (2010). Estimating the distribution of snow water equivalent using remotely sensed snow cover data and a spatially distributed snowmelt model. *Advances in Water Resources*, 33, 1464–1475.

- Monteiro, D., & Morin, S. (2023). Multi-decadal past winter temperature, precipitation and snow cover information over the European Alps using multiple datasets. *EGUsphere*, 17, 3617–3660.
- Muhammad, S., & Thapa, A. (2021). Daily Terra–Aqua MODIS cloud-free snow and Randolph Glacier Inventory 6.0 combined product (M* D10A1GL06) for high-mountain Asia between 2002 and 2019. *Earth System Science Data*, 13, 767-776.
- Mukasa, N. A., Gachari, M. K., & Wamue, G. G. (2020). Climate change adaptation options in the Rwenzori mountains, western Uganda. *Climate*, 8, 98.
- Nakulopa, F., Vanderkelen, I., Van de Walle, J., van Lipzig, N. P., Tabari, H., Jacobs, L. & Thiery, W. (2022). Evaluation of high-resolution precipitation products over the Rwenzori mountains (Uganda). *Journal of Hydrometeorology*, 23, 747-768.
- Nepal, S., Khatiwada, K. R., Pradhananga, S., Kralisch, S., Samyn, D., Bromand, M. T. & Chevallier, P. (2021). Future snow projections in a small basin of the Western Himalaya. *Science of the Total Environment*, 795, 148587.
- Nicholson, S. E. (2019). A review of climate dynamics and climate variability in Eastern Africa. *Limnology, Climatology and paleoclimatology of the East African lakes*, 25-56.
- Novella, N. S., & Thiaw, W. M. (2013). African rainfall climatology version 2 for famine early warning systems. *Journal of Applied meteorology and Climatology*, 52, 588-606.
- Nyakecho, C., & Hagemann, S. G. (2014). An overview of gold systems in Uganda. *Australian Journal of Earth Sciences*, 61, 59-88.
- Nyikadzino, B., Chitakira, M., Muchuru, S. (2020). Rainfall and runoff trend analysis in the Limpopo river basin using the Mann-Kendall statistic. *Physics and Chemistry of the Earth, Parts A/B/C*, 117, 102870.
- Oleksy, I. A., & Richardson, D. C. (2021). Climate change and teleconnections amplify lake stratification with differential local controls of surface water warming and deep-water cooling. *Geophysical Research Letters*, 48, e2020GL090959.
- Oliver, Fricko., Petr, Havlik., Joeri, Rogelj., Zbigniew, Klimont., Mykola, Gusti., Mykola, Gusti., Nils, Johnson., Peter, Kolp., M., Strubegger., Hugo, Valin., Markus, Amann., Tatiana, Ermolieva., Nicklas, Forsell., Mario, Herrero., Chris, Heyes., Georg, Kindermann., Volker, Krey., David, L., McCollum., Michael, Obersteiner., Shonali, Pachauri., Shilpa, Rao., Erwin, Schmid., Wolfgang, Schoepp., Keywan, Riahi., Keywan, Riahi. (2017). The marker quantification of the Shared Socioeconomic Pathway 2: A middle-of-the-road scenario for the 21st century. *Global Environmental Change*, 42, 251-267.
- O'Neill, B. C., Kriegler, E., Ebi, K. L., Kemp-Benedict, E., Riahi, K., Rothman, D. S., van

- Ruijven, B. J., van Vuuren, D. P., Birkmann, J., Kok, K., Levy, M., & Solecki, W. (2017). The roads ahead: Narratives for shared socioeconomic pathways describing world futures in the 21st century. *Global Environmental Change*, 42, 169-180.
- O'Neill, B. C., Tebaldi, C., Van Vuuren, D. P., Eyring, V., Friedlingstein, P., Hurtt, G., ... & Sanderson, B. M. (2016). The scenario model intercomparison project (ScenarioMIP) for CMIP6. *Geoscientific Model Development*, 9, 3461-3482.
- Opio, R., Mugume, I., Nakatumba-Nabende, J., Nimusiima, A., & Okurut, I. T. (2023). The impact of global changes in near-term climate forcings on East Africa's climate. *Environmental Systems Research*, 12, 16.
- Osmaston, H. (1989). Glaciers, glaciations and equilibrium line altitudes on the Ruwenzori. *Quaternary and environmental research on East African mountains*, 31, 104.
- Osmaston, H. A. (1966). The geology of the Ruwenzori Mountains and surrounding areas. *Memoirs of the Geological Survey of Uganda*, 3.
- Ougahi, J. H., EJ Cutler, M., & J. Cook, S. (2022). Assessment of climate change effects on vegetation and river hydrology in a semi-arid river basin. *Plos One*, 17, e0271991.
- Pachauri, R. K., Allen, M. R., Barros, V. R., Broome, J., Cramer, W., Christ, R., ... & van Ypersele, J. P. (2014). *Climate change 2014: synthesis report. Contribution of Working Groups I, II and III to the fifth assessment report of the Intergovernmental Panel on Climate Change* (p. 151). Ipc.
- Parajka, J., & Blöschl, G. (2006). Validation of MODIS snow cover images over Austria. *Hydrology and Earth System Sciences*, 10, 679-689
- Paredes Trejo, F. J., Alves Barbosa, H., Peñaloza-Murillo, M. A., Moreno, M. A., & Farias, A. (2016). Intercomparison of improved satellite rainfall estimation with CHIRPS gridded product and rain gauge data over Venezuela. *Atmósfera*, 29, 323-342.
- Parmesan, C., Morecroft, M. D., & Trisurat, Y. (2022). *Climate change 2022: Impacts, adaptation and vulnerability* (Doctoral dissertation, GIEC).
- Pepin, N. C., Arnone, E., Gobiet, A., Haslinger, K., Kotlarski, S., Notarnicola, C. & Adler, C. (2022). Climate changes and their elevational patterns in the mountains of the world. *Reviews of Geophysics*, 60, e2020RG000730.
- Pérez-Hoyos, A., Rembold, F., Kerdiles, H., & Gallego, J. (2017). Comparison of global land cover datasets for cropland monitoring. *Remote Sensing*, 9, 1118.
- Pielke Jr, R., & Ritchie, J. (2021). Distorting the view of our climate future: The misuse and abuse of climate pathways and scenarios. *Energy Research & Social Science*, 72, 101890.
- Pimentel, R., Aparicio, J., Torralbo, P., Contreras, E., Moreno-Pérez, F., Aguilar, C., & José Polo,

- M. (2022). Quantifying the role of mixed pixels in snow cover distribution in semiarid regions: A study case in Sierra Mountain (Spain). In *EGU General Assembly Conference Abstracts* (pp. EGU22-12801).
- Plumptre, A. J., Davenport, T. R., Behangana, M., Kityo, R., Eilu, G., Ssegawa, P., ... & Moyer, D. (2007). The biodiversity of the Albertine Rift. *Biological conservation*, *134*, 178-194.
- Poulsen, A. D., Hafashimana, D. A. V. I. D., Eilu, G. E. R. A. L. D., Liengola, I. B., Ewango, C. E., & Hart, T. B. (2005). Composition and species richness of forest plants along the Albertine Rift, Africa. *Biologiske Skrifter*, *55*, 129-143.
- Preethi, B., Sabin, T. P., Adedoyin, J. A., & Ashok, K. (2015). Impacts of the ENSO Modoki and other tropical Indo-Pacific climate-drivers on African rainfall. *Scientific Reports*, *5*, 16653.
- Rangwala, I., Miller, J. R., Xu, M., & Russell, G. L. (2019). Using a weather research and forecasting model to understand impacts of changing snowpack composition on land surface albedo and radiative forcing in mountainous regions. *Journal of Geophysical Research: Atmospheres*, *124*, 6190-6207.
- Riahi, K., van Vuuren, D. P., Kriegler, E., Edmonds, J., O'Neill, B. C., Fujimori, S., Bauer, N., Calvin, K., Dellink, R., Fricko, O., Lutz, W., Popp, A., Cuaresma, J. C., Kc, S., Leimbach, M., Jiang, L., Kram, T., Rao, S., Emmerling, J., Ebi, K., Hasegawa, T., Havlik, P., Humpenöder, F., Da Silva, L. A., Smith, S., Stehfest, E., Bosetti, V., Eom, J., Gernaat, D., Masui, T., Rogelj, J., Strefler, J., Drouet, L., Krey, V., Luderer, G., Harmsen, M., Takahashi, K., Baumstark, L., Doelman, J. C., Kainuma, M., Klimont, Z., Marangoni, G., Lotze-Campen, H., Obersteiner, M., Tabeau, A., & Tavoni, M. (2017). The Shared Socioeconomic Pathways and their energy, land use, and greenhouse gas emissions implications: An overview. *Global Environmental Change*, *42*, 153-168.
- Ribeiro, E. C., Batjes, N. H., Leenaars, J. G., Van Oostrum, A. J. M., & de Jesus, J. M. (2015). *Towards the standardization and harmonization of world soil data: Procedures Manual ISRIC World Soil Information Service (WoSIS version 2.0)* (No. 2015/03). ISRIC.
- Riggs, G. A., Hall, D. K., & Salomonson, V. V. (2006). MODIS snow products user guide for collection 4 data products. NASA Goddard Space Flight Center.
- Roller, S., Speriosu, M., Rallapalli, S., Wing, B., & Baldridge, J. (2012, July). Supervised text-based geolocation using language models on an adaptive grid. In *Proceedings of the 2012 joint conference on empirical methods in natural language processing and computational natural language learning* (pp. 1500-1510).
- Romanov, P., Gutman, G., & Csiszar, I. (2003). Assessment of the utility of the MODIS snow-cover product for hydrologic applications. *Cryosphere Discussions*, *1*, 35–45.

- Rood, S. B., Pan, T., Gill, K. M., Franks, C. G., Samuelson, G. M., Shepherd, A., & Shugart, H. H. (2012). Declining summer flows of Rocky Mountain rivers: changing seasonal hydrology and probable impacts on floodplain forests. *Journal of Hydrology*, 420, 147-159.
- Salarian, M., Larijani, S., Banejad, H., Heydari, M., & Ghadim, H. B. (2022). Trend analysis of water flow on Neka and Tajan rivers using parametric and non-parametric tests. *Időjárás/quarterly Journal of the Hungarian Meteorological Service*, 126, 387-402.
- Salathe Jr, E. P., Steed, R., Mass, C. F., & Zahn, P. H. (2008). A high-resolution climate model for the US Pacific Northwest: Mesoscale feedbacks and local responses to climate change. *Journal of Climate*, 21(21), 5708-5726. <https://doi.org/10.1175/2008JCLI2090.1>
- Schär, C., Vidale, P. L., Lüthi, D., Frei, C., Häberli, C., Liniger, M. A., & Appenzeller, C. (2004). The role of increasing temperature variability in European summer heatwaves. *Nature*, 427, 332-336.
- Sheffield, J., Wood, E. F., Pan, M., Beck, H., Coccia, G., Serrat-Capdevila, A., & Verbist, K. (2018). Satellite remote sensing for water resources management: Potential for supporting sustainable development in data-poor regions. *Water Resources Research*, 54(12), 9724-9758.
- Shen, Y. J., Shen, Y., Fink, M., Kralisch, S., Chen, Y., & Brenning, A. (2018). Trends and variability in streamflow and snowmelt runoff timing in the southern Tianshan Mountains. *Journal of Hydrology*, 557, 173-181.
- Shrestha, D., Sharma, S., Talchabhadel, R., Deshar, R., Hamal, K., Khadka, N., & Nakamura, K. (2021). Detection of Spatial Rainfall Variation over the Andean Region Demonstrated by Satellite-Based Observations. *Atmosphere*, 12, 1204.
- Shrestha, S., & Nepal, S. (2019). Water balance assessment under different glacier coverage scenarios in the Hunza Basin. *Water*, 11, 1124.
- Siirila-Woodburn, E. R., Rhoades, A. M., Hatchett, B. J., Huning, L. S., Szinai, J., Tague, C., ... & Kaatz, L. (2021). A low-to-no snow future and its impacts on water resources in the western United States. *Nature Reviews Earth & Environment*, 2, 800-819.
- Simic, A., Fernandes, R., Brown, R., Romanov, P., & Park, W. (2004). Validation of VEGETATION, MODIS, and GOES+SSM/I snow cover products over Canada based on surface snow depth observations. *Hydrological Processes*, 18, 1089-1104.
- Smith, C., Al Khourdajie, A., Yang, P., & Folini, D. (2023). Climate uncertainty as an integral part of integrated assessment models. In *EGU General Assembly Conference Abstracts* (pp. EGU-8191).
- Smith, S. J., Edmonds, J., Hartin, C. A., Mundra, A., Calvin, K., and Thomson, A. (2020). Near-

- Term Acceleration in the Rate of Temperature Change. *Nature Climate Change*, 2, 153-158.
- Song, Y. H., Chung, E. S., & Shahid, S. (2021). Spatiotemporal differences and uncertainties in projections of precipitation and temperature in South Korea from CMIP6 and CMIP5 general circulation models. *International Journal of Climatology*, 41, 5899-5919.
- Specht, M., Behangana, M., Bobo, K. S., Davenport, T. R. B., Dupuis, J. R., Ganzhorn, J. U., ... & Mulindahabi, F. (2014). The Rwenzori Mountains: A biogeographical and ecological overview. *Journal of Biogeography*, 41, 143-177.
- Stefanidis, S., & Stathis, D. (2018). Spatial and temporal rainfall variability over the Mountainous Central Pindus (Greece). *Climate*, 6, 75.
- Stewart, I. T. (2009). Changes in snowpack and snowmelt runoff for key mountain regions. *Hydrological Processes: An International Journal*, 23, 78-94.
- Tang, Z., Wang, X., Deng, G., Wang, X., Jiang, Z., & Sang, G. (2020). Spatiotemporal variation of snowline altitude at the end of melting season across High Mountain Asia, using MODIS snow cover product. *Advances in Space Research*, 66, 2629-2645.
- Taylor, R. G., Begum, R. A., Kusimba, S. B., Opolot, E., Mkhandi, R., Bitegeko, G., ... & Maeda, N. (2020). Recent climate-driven ecological changes in tropical montane lakes of Rwenzori Mountains National Park, central Africa. *Journal of Paleolimnology*, 63, 287-
- Taylor, R. G., Mileham, L., Tindimugaya, C., & Mwebembezi, L. (2009). Recent glacial recession and its impact on alpine riverflow in the Rwenzori Mountains of Uganda. *Journal of African Earth Sciences*, 55, 205–213.
- Taylor, R. G., Mileham, L., Tindimugaya, C., Majugu, A., Muwanga, A., Nakileza, B., ... & Malugu, I. (2017). Recent glacial recession in the Rwenzori Mountains of East Africa due to rising air temperature. *Geophysical Research Letters*, 44, 9879-9887.
- Taylor, R. G., Mileham, L., Tindimugaya, C., Majugu, A., Muwanga, A., & Nakileza, B. (2006). Recent glacial recession in the Rwenzori Mountains of East Africa due to rising air temperature. *Geophysical Research Letters*, 33, 12-24.
- Taylor, R.G., Howard, K.W.F., (1998). Post-palaeozoic evolution of weathered landsurfaces in Uganda by tectonically controlled cycles of deep weathering and stripping. *Geomorphology* 25, 173–192.
- Tekeli, A. E., Akyurek, Z., Sorman, A. A., Sensoy, A., & Sorman, A. U. (2005). Using MODIS snow cover maps in modeling snowmelt runoff process in the eastern part of Turkey. *Remote Sensing of Environment*, 97, 216–230.
- Thiemeßl, M. J., Gobiet, A., & Heinrich, G. (2012). Empirical-statistical downscaling and error correction of regional climate models and its impact on the climate change signal. *Climatic*

- Change*, 112, 449-468.
- Thom, H. C. (1958). A note on the gamma distribution. *Monthly weather review*, 86, 117-122.
- Teutschbein, C., & Seibert, J. (2010). Regional climate models for hydrological impact studies at the catchment scale: a review of recent modeling strategies. *Geography Compass*, 4, 834-860.
- Tokarska, K. B., Stolpe, M. B., Sippel, S., Fischer, E. M., Smith, C. J., Lehner, F., & Knutti, R. (2020). Past warming trend constrains future warming in CMIP6 models. *Science Advances*, 6, eaaz9549.
- Tong, R., Parajka, J., Salentinig, A., Pfeil, I., Komma, J., Széles, B., ... & Blöschl, G. (2021). The value of ASCAT soil moisture and MODIS snow cover data for calibrating a conceptual hydrologic model. *Hydrology and Earth System Sciences*, 25, 1389-1410.
- Vaidya, V. V. (2005). *East African hydroclimatic variability: 1950-1999*. Louisiana State University and Agricultural & Mechanical College.
- Van Vuuren, D. P., Kriegler, E., O'Neill, B. C., Ebi, K. L., Riahi, K., Carter, T. R., ... & Winkler, H. (2014). A new scenario framework for climate change research: scenario matrix architecture. *Climatic change*, 122, 373-386.
- Van Vuuren, D. P., Riahi, K., Moss, R., Edmonds, J., Thomson, A., Nakicenovic, N., ... & Arnell, N. (2012). A proposal for a new scenario framework to support research and assessment in different climate research communities. *Global Environmental Change*, 22, 21-35.
- Verdin, A., Funk, C., Peterson, P., Landsfeld, M., Tuholske, C., & Grace, K. (2020). Development and validation of the CHIRTS-daily quasi-global high-resolution daily temperature data set. *Scientific Data*, 7, 303.
- Viloria, R., & Tricio, V. (2023). *Analysis of surface air temperature and precipitation trends and climate indices in mountain areas in Spain* (No. EMS2023-512). Copernicus Meetings.
- Vuille, M., Bradley, R. S., Werner, M., & Keimig, F. (2018). 20th century climate change in the tropical Andes: Observations and model results. *Climatic Change*, 59, 75-99.
- Wang, G., Jiang, L., Pan, F., Weng, H., & Zhang, Y. (2022). Sensitivity of Snow NDSI to Simulated Snow Grain Shape Characteristics. *IEEE Geoscience and Remote Sensing Letters*, 20, 1-5.
- Wang, S., & Russell, H. A. (2016). Forecasting snowmelt-induced flooding using GRACE satellite data: A case study for the Red River watershed. *Canadian Journal of Remote Sensing*, 42, 203-213.
- Westerhof, G. J., & Bohlmeijer, E. T. (2014). Celebrating fifty years of research and applications in reminiscence and life review: State of the art and new directions. *Journal of Aging Studies*,

- Wood, A. W., Leung, L. R., Sridhar, V., & Lettenmaier, D. P. (2004). Hydrologic implications of dynamical and statistical approaches to downscaling climate model outputs. *Climatic Change*, *62*, 189-216.
- Worku, M. A., Feyisa, G. L., & Beketie, K. T. (2022). Climate trend analysis for a semi-arid Borana zone in southern Ethiopia during 1981–2018. *Environmental Systems Research*, *11*, 2.
- Wytych, A., Ustrnul, Z., & Sałaja, J. (2023). *Snow cover response to temperature and precipitation variability in Central European mountain ranges* (No. EMS2023-581). Copernicus Meetings.
- Wyser, K., Kjellström, E., Koenig, T., Martins, H., & Döscher, R. (2020). Warmer climate projections in EC-Earth3-Veg: the role of changes in the greenhouse gas concentrations from CMIP5 to CMIP6. *Environmental Research Letters*, *15*, 054020.
- Yoo, C., Kang, B., & Cho, M. (2020, April). SNOW: Subscribing to knowledge via channel pooling for transfer & lifelong learning of convolutional neural networks. In *International Conference on Learning Representations*.
- Zakeri, S., Samkhaniani, A., Adeli, S., Nikraftar, Z. (2019). Evaluation of long-term trend of different drought indices using Mann-Kendall and Sen's slope estimator over Iran. *The International Archives of the Photogrammetry, Remote Sensing and Spatial Information Sciences*, *42*, 1141-1145.
- Zhang, G., Liu, X., Zhang, Y., Zhang, L., Zhang, Y., & Wu, S. (2020). Spatiotemporal changes of snow cover over China's mountainous regions from 2000 to 2018. *Remote Sensing*, *12*, 47.
- Zhang, Q., Sun, J., Zhang, G., Liu, X., Wu, Y., Sun, J., & Hu, B. (2023). Spatiotemporal dynamics of water supply–demand patterns under large-scale paddy expansion: Implications for regional sustainable water resource management. *Agricultural Water Management*, *285*, 108388.
- Zhang, T., Zhou, Y., Zhao, K., Zhu, Z., Chen, G., Hu, J., & Wang, L. (2022a). A global dataset of daily near-surface air temperature at 1-km resolution (2003–2020). *Earth System Science Data Discussions*, *14*, 1-18.
- Zhang, Y., Woodcock, C. E., Arévalo, P., Olofsson, P., Tang, X., Stanimirova, R., ... & Friedl, M. A. (2022b). A global analysis of the spatial and temporal variability of usable Landsat observations at the pixel scale. *Frontiers in Remote Sensing*, *3*, 894618.
- Zhong, X., Zhang, T., Kang, S., & Wang, J. (2021). Spatiotemporal variability of snow cover timing and duration over the Eurasian continent during 1966–2012. *Science of the Total*

Environment, 750, 141670.

Zhou, X., Xie, H., & Hendrickx, J. M. H. (2005). Statistical evaluation of remotely sensed snow-cover products with constraints from streamflow and SNOTEL measurements. *Remote Sensing of Environment*, 94, 214–231.

APPENDICES

Appendix 1. Mann-Kendall test and Sen's slope estimator for temperatures and rainfall over the 1991-2020 period

Timescale	Maximum Temperature			Minimum Temperature			Rainfall		
	ω	p	Υ	ω	p	Υ	ω	p	Υ
Whole Rwenzori Mountains									
Jan	0,129	0,307	0,012	0,347	0,006	0,038	0,036	0,783	0,036
Feb	0,075	0,559	0,006	0,113	0,372	0,012	0,234	0,062	0,964
Mar	-0,020	0,884	-0,001	0,162	0,200	0,016	-0,181	0,149	-0,270
Apr	0,010	0,948	0,001	0,079	0,538	0,007	0,140	0,270	0,435
May	-0,030	0,820	-0,004	0,069	0,592	0,006	0,179	0,157	0,521
Jun	-0,253	0,044	-0,016	0,160	0,205	0,010	-0,075	0,559	-0,138
Jul	0,121	0,339	0,008	0,287	0,022	0,023	0,149	0,242	0,138
Aug	0,004	0,987	0,000	0,087	0,496	0,007	0,040	0,758	0,065
Sept	0,085	0,506	0,005	0,270	0,031	0,024	0,041	0,758	0,065
Oct	0,239	0,058	0,015	0,350	0,005	0,026	-0,071	0,581	-0,102
Nov	-0,030	0,820	-0,003	0,099	0,436	0,009	0,151	0,230	0,366
Dec	0,059	0,650	0,009	0,242	0,054	0,024	-0,038	0,770	-0,030
Ann.	0,052	0,685	0,002	0,266	0,034	0,016	0,077	0,549	0,960
DJF	0,113	0,372	0,010	0,302	0,016	0,028	0,161	0,200	0,998
MAM	0,008	0,961	0,000	0,113	0,372	0,009	0,081	0,527	0,347
JJ	-0,081	0,527	-0,005	0,259	0,039	0,017	-0,040	0,758	-0,213
ASON	0,056	0,661	0,003	0,268	0,032	0,018	0,125	0,323	0,283
Central Region of Rwenzori Mountains									
Jan	0,161	0,200	0,018	-0,056	0,661	-0,007	0,147	0,243	0,885
Feb	0,181	0,149	0,026	-0,310	0,013	-0,038	0,153	0,224	0,925
Mar	0,218	0,083	0,017	-0,181	0,149	-0,019	0,254	0,043	1,156
Apr	0,274	0,029	0,029	0,026	0,846	0,002	-0,129	0,307	-0,780
May	0,460	0,000	0,036	0,302	0,016	0,026	0,129	0,307	0,835
Jun	0,214	0,089	0,020	0,050	0,697	0,003	0,181	0,149	0,770
Jul	0,310	0,013	0,033	-0,081	0,527	-0,005	-0,286	0,022	-1,618
Aug	-0,044	0,733	-0,003	0,008	0,961	0,001	0,060	0,638	0,349
Sept	0,230	0,067	0,018	0,109	0,390	0,007	-0,121	0,339	-0,703
Oct	0,274	0,029	0,023	-0,052	0,685	-0,003	0,093	0,466	0,743
Nov	0,238	0,058	0,018	-0,052	0,685	-0,004	-0,028	0,833	-0,206
Dec	0,177	0,158	0,016	0,048	0,709	0,003	-0,060	0,638	-0,414
Ann.	0,383	0,002	0,019	0,004	0,987	0,000	0,065	0,615	1,401
DJF	0,230	0,067	0,016	-0,181	0,149	-0,010	0,101	0,427	1,140
MAM	0,427	0,001	0,031	0,069	0,593	0,004	0,210	0,095	2,063
JJ	0,355	0,005	0,025	-0,036	0,783	-0,002	-0,044	0,733	-0,217
ASON	0,181	0,149	0,013	-0,028	0,833	-0,002	-0,004	0,987	-0,133

Mann-Kendall tau (ω), p value (p), Sen's slope estimator (Υ), December-January-February (DJF), March-April-May (MAM), June-July (JJ), August-September-October-November (ASON)

Appendix 2. Mann-Kendall test and Sen's slope estimator for temperatures and rainfall in near future (2021-2060 period)

Timescale	Maximum temperature						Minimum temperature						Rainfaill					
	WM			CZ			WM			CZ			WM			CZ		
	ω	p	Y	ω	p	Y	ω	p	Y	ω	p	Y	ω	p	Y	ω	p	Y
SSP245																		
Jan	0,281	0,006	0,021	0,262	0,011	0,020	0,341	0,001	0,017	0,292	0,004	0,013	-0,042	0,691	-0,230	-0,064	0,538	-0,414
Feb	0,219	0,032	0,013	0,202	0,049	0,014	0,237	0,021	0,015	0,204	0,047	0,013	-0,010	0,932	-0,042	-0,024	0,820	-0,194
Mar	0,366	0,000	0,036	0,378	0,000	0,038	0,169	0,099	0,011	0,221	0,031	0,013	-0,067	0,520	-0,365	-0,042	0,691	-0,257
Apr	0,536	<0,0001	0,050	0,542	<0,0001	0,051	0,264	0,010	0,013	0,318	0,002	0,017	-0,198	0,053	-1,852	-0,146	0,156	-1,962
May	0,476	<0,0001	0,037	0,559	<0,0001	0,043	0,550	<0,0001	0,028	0,627	<0,0001	0,033	0,030	0,776	0,245	0,002	0,992	0,016
Jun	0,567	<0,0001	0,033	0,610	<0,0001	0,034	0,540	<0,0001	0,023	0,486	<0,0001	0,024	-0,028	0,790	-0,002	-0,067	0,552	0,000
July	0,426	<0,0001	0,024	0,374	0,000	0,019	0,407	<0,0001	0,023	0,328	0,001	0,022	0,073	0,491	0,004	0,083	0,463	0,000
Aug	0,258	0,012	0,019	0,304	0,003	0,017	0,347	0,001	0,015	0,287	0,005	0,015	-0,044	0,677	-0,174	-0,021	0,849	0,000
Sept	0,370	0,000	0,028	0,376	0,000	0,027	0,571	<0,0001	0,021	0,567	<0,0001	0,026	-0,129	0,211	-0,623	-0,072	0,489	-0,404
Oct	0,351	0,001	0,020	0,293	0,004	0,017	0,384	0,000	0,015	0,324	0,002	0,013	-0,150	0,145	-1,047	-0,123	0,233	-1,215
Nov	0,322	0,002	0,016	0,302	0,003	0,014	0,573	<0,0001	0,017	0,641	<0,0001	0,019	-0,026	0,806	-0,081	-0,020	0,850	-0,218
Dec	0,324	0,002	0,021	0,291	0,005	0,020	0,577	<0,0001	0,029	0,561	<0,0001	0,028	0,185	0,072	1,675	0,171	0,096	2,054
Ann	0,662	<0,0001	0,025	0,627	<0,0001	0,025	0,722	<0,0001	0,016	0,700	<0,0001	0,017	-0,069	0,507	-1,946	-0,059	0,570	-1,533
DJF	0,393	0,000	0,017	0,389	0,000	0,017	0,509	<0,0001	0,017	0,459	<0,0001	0,015	0,130	0,205	1,668	0,113	0,272	1,939
MAM	0,662	<0,0001	0,041	0,671	<0,0001	0,043	0,414	<0,0001	0,018	0,469	<0,0001	0,022	-0,150	0,145	-2,145	-0,127	0,218	-2,327
JJ	0,554	<0,0001	0,029	0,536	<0,0001	0,026	0,540	<0,0001	0,023	0,413	<0,0001	0,021	0,053	0,609	0,165	0,035	0,745	0,000
ASON	0,436	<0,0001	0,022	0,376	0,000	0,020	0,610	<0,0001	0,017	0,540	<0,0001	0,018	-0,100	0,334	-1,100	-0,063	0,545	-1,064
SSP585																		
Jan	0,405	<0,0001	0,025	0,335	0,001	0,021	0,492	<0,0001	0,029	0,472	<0,0001	0,024	0,208	0,061	1,229	0,142	0,167	1,050
Feb	0,271	0,008	0,019	0,221	0,031	0,013	0,316	0,002	0,023	0,328	0,001	0,023	-0,086	0,442	-0,280	0,024	0,820	0,091
Mar	0,411	<0,0001	0,043	0,413	<0,0001	0,043	0,457	<0,0001	0,035	0,463	<0,0001	0,035	0,013	0,916	0,132	-0,023	0,828	-0,105
Apr	0,501	<0,0001	0,059	0,513	<0,0001	0,060	0,498	<0,0001	0,032	0,509	<0,0001	0,034	-0,154	0,166	-1,489	-0,108	0,293	-1,315
May	0,557	<0,0001	0,052	0,557	<0,0001	0,057	0,602	<0,0001	0,037	0,617	<0,0001	0,043	0,059	0,600	0,390	0,031	0,769	0,439
Jun	0,540	<0,0001	0,040	0,546	<0,0001	0,038	0,484	<0,0001	0,034	0,482	<0,0001	0,032	0,115	0,304	0,585	0,040	0,717	0,000
July	0,532	<0,0001	0,038	0,465	<0,0001	0,026	0,465	<0,0001	0,032	0,387	0,000	0,028	-0,123	0,291	0,000	0,007	0,958	0,000

Aug	0,440	<0,0001	0,035	0,378	0,000	0,027	0,519	<0,0001	0,024	0,461	<0,0001	0,024	-0,013	0,916	-0,087	-0,016	0,887	0,000
Sept	0,362	0,000	0,027	0,357	0,000	0,023	0,542	<0,0001	0,025	0,515	<0,0001	0,027	0,144	0,196	0,607	0,077	0,460	0,379
Oct	0,374	0,000	0,024	0,300	0,003	0,021	0,536	<0,0001	0,020	0,456	<0,0001	0,018	-0,013	0,916	-0,101	-0,113	0,272	-1,101
Nov	0,469	<0,0001	0,033	0,449	<0,0001	0,031	0,652	<0,0001	0,021	0,639	<0,0001	0,023	-0,254	0,022	-2,092	-0,194	0,058	-2,157
Dec	0,515	<0,0001	0,036	0,498	<0,0001	0,033	0,679	<0,0001	0,030	0,656	<0,0001	0,028	-0,003	0,991	-0,031	-0,011	0,925	-0,129
Ann	0,617	<0,0001	0,035	0,556	<0,0001	0,032	0,757	<0,0001	0,029	0,708	<0,0001	0,029	-0,003	0,991	-0,150	-0,049	0,636	-1,092
DJF	0,527	<0,0001	0,026	0,457	<0,0001	0,022	0,621	<0,0001	0,027	0,600	<0,0001	0,025	0,123	0,268	1,770	0,100	0,334	1,722
MAM	0,559	<0,0001	0,052	0,559	<0,0001	0,054	0,598	<0,0001	0,033	0,621	<0,0001	0,036	-0,077	0,492	-1,331	-0,059	0,570	-1,318
JJ	0,565	<0,0001	0,040	0,511	<0,0001	0,033	0,517	<0,0001	0,031	0,457	<0,0001	0,030	0,035	0,762	0,160	0,048	0,654	0,000
ASON	0,571	<0,0001	0,029	0,480	<0,0001	0,025	0,656	<0,0001	0,023	0,621	<0,0001	0,024	-0,115	0,300	-1,914	-0,163	0,112	-2,399

Appendix 3. Mann-Kendall test and Sen's slope estimator for temperatures and rainfall in far future (2061-2100 period)

Timescale	Maximum temperature						Minimum temperature						Rainfall					
	WM			CZ			WM			CZ			WM			CZ		
	ω	p	Υ	ω	p	Υ	ω	p	Υ	ω	p	Υ	ω	p	Υ	ω	p	Υ
SSP245																		
Jan	0,382	0,001	0,052	0,397	0,000	0,049	0,418	0,000	0,028	0,467	<0,0001	0,030	0,192	0,083	1,170	0,090	0,421	0,623
Feb	-0,144	0,196	-0,015	-0,249	0,025	-0,031	0,515	<0,0001	0,038	0,367	0,001	0,021	0,381	0,001	2,552	0,304	0,006	2,180
Mar	-0,436	<0,0001	-0,051	-0,400	0,000	-0,076	0,059	0,600	0,004	-0,338	0,002	-0,031	0,136	0,221	1,289	0,120	0,283	1,111
Apr	-0,136	0,221	-0,023	-0,310	0,005	-0,049	-0,197	0,075	-0,011	-0,485	<0,0001	-0,044	-0,286	0,010	-1,796	-0,368	0,001	-2,079
May	0,123	0,268	0,015	0,110	0,322	0,013	-0,382	0,001	-0,027	-0,031	0,789	-0,002	-0,467	<0,0001	-3,433	-0,422	0,000	-3,300
Jun	0,154	0,166	0,015	0,374	0,001	0,043	0,290	0,009	0,013	0,554	<0,0001	0,050	0,108	0,333	0,616	0,105	0,350	0,615
July	0,087	0,435	0,006	0,172	0,121	0,018	0,179	0,105	0,009	0,221	0,046	0,018	0,500	<0,0001	3,187	0,485	<0,0001	3,418
Aug	0,228	0,039	0,018	0,259	0,019	0,022	0,462	<0,0001	0,030	0,449	<0,0001	0,028	0,474	<0,0001	5,032	0,479	<0,0001	6,476
Sept	0,182	0,100	0,016	0,233	0,035	0,021	0,567	<0,0001	0,041	0,513	<0,0001	0,031	0,395	0,000	4,980	0,420	0,000	7,376
Oct	0,169	0,127	0,013	0,226	0,041	0,015	0,038	0,735	0,001	0,031	0,789	0,001	-0,077	0,492	-0,648	-0,005	0,972	-0,053
Nov	0,497	<0,0001	0,068	0,521	<0,0001	0,074	-0,528	<0,0001	-0,035	-0,484	<0,0001	-0,024	-0,554	<0,0001	-6,855	-0,576	<0,0001	-8,797
Dec	0,505	<0,0001	0,095	0,513	<0,0001	0,105	-0,169	0,127	-0,013	0,038	0,735	0,003	-0,536	<0,0001	-5,222	-0,489	<0,0001	-6,638
Ann	0,308	0,005	0,016	0,246	0,026	0,017	0,321	0,004	0,009	0,326	0,003	0,009	-0,023	0,843	-0,631	-0,074	0,507	-2,568
DJF	0,413	0,000	0,040	0,413	0,000	0,038	0,315	0,004	0,018	0,328	0,003	0,017	-0,087	0,435	-1,344	-0,151	0,173	-3,126
MAM	-0,197	0,075	-0,023	-0,267	0,016	-0,040	-0,262	0,018	-0,012	-0,418	0,000	-0,025	-0,223	0,044	-3,711	-0,285	0,010	-6,008
JJ	0,174	0,116	0,008	0,331	0,003	0,031	0,323	0,003	0,015	0,505	<0,0001	0,034	0,464	<0,0001	4,494	0,378	0,001	4,035
ASON	0,372	0,001	0,025	0,379	0,001	0,028	0,331	0,003	0,012	0,285	0,010	0,010	0,138	0,213	2,566	0,210	0,058	4,356
SSP585																		
Jan	0,474	<0,0001	0,084	0,464	<0,0001	0,082	0,700	<0,0001	0,053	0,700	<0,0001	0,054	0,074	0,507	0,463	-0,072	0,522	-0,594
Feb	0,313	0,005	0,027	0,151	0,173	0,015	0,669	<0,0001	0,064	0,618	<0,0001	0,049	0,272	0,014	2,032	0,281	0,011	2,534
Mar	-0,195	0,079	-0,019	-0,287	0,009	-0,039	0,497	<0,0001	0,039	0,026	0,825	0,003	0,126	0,258	0,867	-0,014	0,907	0,000
Apr	0,141	0,204	0,011	-0,226	0,041	-0,027	0,249	0,025	0,016	-0,167	0,133	-0,012	-0,268	0,016	-2,407	-0,202	0,073	-2,225
May	0,336	0,002	0,043	0,282	0,011	0,036	0,144	0,196	0,008	0,472	<0,0001	0,037	-0,426	0,000	-2,348	-0,376	0,001	-2,551
Jun	0,449	<0,0001	0,045	0,469	<0,0001	0,071	0,541	<0,0001	0,031	0,644	<0,0001	0,072	0,126	0,258	0,564	0,305	0,007	1,694
July	0,300	0,007	0,027	0,307	0,006	0,037	0,490	<0,0001	0,026	0,479	<0,0001	0,036	0,382	0,001	2,101	0,381	0,001	3,295

Aug	0,510	<0,0001	0,055	0,441	<0,0001	0,059	0,685	<0,0001	0,057	0,633	<0,0001	0,053	0,403	0,000	2,484	0,379	0,001	3,759
Sept	0,579	<0,0001	0,044	0,559	<0,0001	0,052	0,787	<0,0001	0,070	0,762	<0,0001	0,060	0,533	<0,0001	5,161	0,576	<0,0001	8,893
Oct	0,351	0,001	0,038	0,323	0,003	0,041	0,608	<0,0001	0,033	0,531	<0,0001	0,032	0,172	0,121	1,426	0,187	0,091	2,714
Nov	0,564	<0,0001	0,091	0,564	<0,0001	0,096	0,074	0,507	0,004	0,208	0,061	0,011	-0,417	0,000	-4,833	-0,453	<0,0001	-6,548
Dec	0,721	<0,0001	0,151	0,641	<0,0001	0,155	0,238	0,031	0,015	0,433	<0,0001	0,034	-0,548	<0,0001	-5,145	-0,538	<0,0001	-6,613
Ann	0,621	<0,0001	0,049	0,554	<0,0001	0,045	0,759	<0,0001	0,036	0,708	<0,0001	0,038	-0,090	0,421	-1,831	0,049	0,666	0,753
DJF	0,667	<0,0001	0,088	0,590	<0,0001	0,085	0,636	<0,0001	0,046	0,659	<0,0001	0,048	-0,210	0,058	-3,323	-0,241	0,029	-4,911
MAM	0,144	0,196	0,013	-0,126	0,258	-0,012	0,372	0,001	0,020	0,144	0,196	0,007	-0,246	0,026	-4,564	-0,227	0,040	-5,282
JJ	0,418	0,000	0,040	0,415	0,000	0,053	0,567	<0,0001	0,028	0,618	<0,0001	0,055	0,367	0,001	2,950	0,396	0,000	5,244
ASON	0,633	<0,0001	0,057	0,600	<0,0001	0,057	0,700	<0,0001	0,042	0,674	<0,0001	0,039	0,313	0,005	4,846	0,369	0,001	9,248

Appendix 4. Mann-Kendall test and Sen's slope estimator for historical snow cover data (2000-2022 period)

Timescale	Baker			Gessi			Speke			Stanley			Overall		
	ω	p	Υ	ω	p	Υ	ω	p	Υ	ω	p	Υ	ω	p	Υ
Jan	0.168	0.278	0.01	-0.164	0.29	-0.017	-0.251	0.101	-0.024	-0.052	0.751	-0.01	-0.06	0.711	-0.03
Feb	0.117	0.458	0.01	-0.207	0.178	-0.01	-0.012	0.958	0	-0.401	0.008	-0.06	-0.174	0.04	-0.06
Mar	0.048	0.771	0.007	-0.128	0.412	-0.008	-0.211	0.169	-0.021	-0.231	0.132	-0.07	-0.253	0.096	-0.13
Apr	-0.223	0.146	-0.039	0.048	0.771	0.003	-0.107	0.492	-0.022	-0.206	0.178	-0.08	-0.281	0.06	-0.17
May	-0.012	0.958	0	-0.004	1	0	0.266	0.081	0.094	0.08	0.615	0.038	0.158	0.303	0.173
Jun	0.453	0.003	0.063	0.084	0.596	0.005	0.207	0.178	0.052	0.337	0.026	0.102	0.368	0.015	0.267
Jul	0.148	0.341	0.018	-0.216	0.16	-0.017	0.08	0.615	0.026	0.008	0.979	0.004	0.004	1	0.011
Aug	-0.076	0.633	-0.007	-0.228	0.138	-0.033	-0.076	0.634	-0.013	-0.008	0.979	-0.01	-0.075	0.635	-0.03
Sep	0.208	0.177	0.022	0.077	0.632	0.003	0.198	0.195	0.045	0.091	0.561	0.031	0.198	0.195	0.059
Oct	-0.102	0.523	-0.01	0.056	0.731	0.006	-0.155	0.315	-0.028	-0.23	0.132	-0.06	-0.249	0.102	-0.11
Nov	-0.144	0.354	-0.022	0.152	0.328	0.012	0	1	0	-0.182	0.234	-0.06	-0.238	0.119	-0.12
Dec	-0.06	0.711	-0.01	-0.02	0.916	0	-0.024	0.895	-0.003	0.091	0.561	0.045	0.083	0.597	0.05
DJF	0.115	0.459	0.018	-0.063	0.692	-0.003	-0.13	0.398	-0.024	-0.107	0.492	-0.02	-0.036	0.833	-0.02
MAM	0	0.561	0	-0.087	0.579	-0.006	-0.083	0.597	-0.009	-0.242	0.113	-0.08	-0.202	0.187	-0.15
JJ	0.448	0.003	0.068	-0.012	0.958	-0.001	0.154	0.316	0.037	0.158	0.303	0.06	0.273	0.073	0.201
ASON	-0.119	0.444	-0.01	0.02	0.916	0.001	0.107	0.492	0.014	-0.083	0.597	-0.02	-0.043	0.792	-0.02
Ann.	0.059	0.712	0.006	-0.02	0.916	-0.001	0.091	0.561	0.006	-0.107	0.492	-0.02	0.036	0.833	0.014

Mann-Kendall tau (ω), p value (p), Sen's slope estimator(Υ), December-January-February (DJF), March-April-May (MAM), June-July (JJ), August-September-October-November (ASON)

Appendix 5. Mann-Kendall test and Sen's slope estimator for projected snow cover dynamics

Period_Scenario	Timescale	Baker			Gessi			Speke			Stanley			Overall		
		ω	p	Υ	ω	p	Υ	ω	p	Υ	ω	p	Υ	ω	p	Υ
NF_ssp245.	January	0.169	0.138	0.003	0.164	0.152	0.003	0.115	0.315	0.002	0.189	0.097	0.011	0.112	0.327	0.012
NF_ssp245.	February	0.132	0.247	0.002	0.155	0.175	0.003	0.132	0.247	0.002	0.272	0.017	0.016	0.07	0.546	0.008
NF_ssp245.	March	-0.05	0.651	-0.001	0.038	0.744	0.001	0.004	0.98	0	0.11	0.339	0.009	-0.141	0.218	-0.011
NF_ssp245.	April	-0.17	0.138	-0.003	-0.01	0.94	0	-0.05	0.669	-0.001	0.075	0.513	0.005	-0.306	0.007	-0.02
NF_ssp245.	May	-0.01	0.96	0	0.064	0.58	0.001	0.05	0.669	0.001	0.152	0.183	0.012	-0.098	0.393	-0.009
NF_ssp245.	June	-0.09	0.436	-0.002	0.038	0.744	0	0.001	1	0	0.058	0.615	0.005	-0.192	0.092	-0.015
NF_ssp245.	July	0.181	0.113	0.005	0.272	0.017	0.005	0.01	0.94	0	0.124	0.28	0.009	0.112	0.327	0.01
NF_ssp245.	August	0.152	0.183	0.003	0.223	0.05	0.004	0.016	0.9	0	0.129	0.258	0.01	0.033	0.782	0.003
NF_ssp245.	September	-0.05	0.651	-0.001	0.061	0.597	0.001	-0.044	0.706	-0.001	0.053	0.651	0.005	-0.121	0.291	-0.012
NF_ssp245.	October	-0.13	0.258	-0.002	-0.064	0.58	-0.001	-0.001	1	0	0.073	0.53	0.007	-0.124	0.28	-0.008
NF_ssp245.	November	0.164	0.152	0.003	0.209	0.066	0.003	0.155	0.175	0.004	0.192	0.092	0.015	0.132	0.247	0.01
NF_ssp245.	December	0.144	0.209	0.003	0.218	0.056	0.003	0.03	0.801	0.001	0.115	0.315	0.006	0.041	0.725	0.003
NF_ssp245.	DJF	0.124	0.28	0.003	0.169	0.138	0.003	0.169	0.138	0.002	0.263	0.021	0.013	0.121	0.291	0.007
NF_ssp245.	MAM	-0.16	0.175	-0.002	-0.038	0.744	-0.001	-0.013	0.92	0	0.186	0.102	0.01	-0.178	0.119	-0.011
NF_ssp245.	JJ	0.064	0.58	0.001	0.201	0.078	0.002	0.013	0.92	0	0.169	0.138	0.011	-0.024	0.841	-0.002
NF_ssp245.	ASON	-0.02	0.9	0	0.055	0.633	0.001	0.041	0.725	0.001	0.135	0.237	0.008	-0.11	0.339	-0.008
NF_ssp245.	Ann	0.016	0.9	0	0.095	0.407	0.001	-0.312	0.006	-0.005	0.166	0.145	0.009	-0.058	0.615	-0.003
FF_ssp245.	January	-0.49	<0.0001	-0.015	-0.428	0	-0.011	-0.246	0.031	-0.004	-0.3	0.008	-0.023	-0.479	<0.0001	-0.066
FF_ssp245.	February	-0.25	0.029	-0.007	-0.343	0.003	-0.008	0.238	0.037	0.006	0.016	0.9	0	-0.058	0.615	-0.006
FF_ssp245.	March	-0.14	0.209	-0.004	-0.385	0.001	-0.008	0.411	0	0.01	0.141	0.218	0.008	0.226	0.047	0.021
FF_ssp245.	April	-0.22	0.056	-0.006	-0.371	0.001	-0.009	0.349	0.002	0.01	0.166	0.145	0.011	0.067	0.563	0.009
FF_ssp245.	May	-0.41	0	-0.012	-0.42	0	-0.01	0.067	0.563	0.001	-0.129	0.258	-0.009	-0.309	0.007	-0.034
FF_ssp245.	June	-0.48	<0.0001	-0.014	-0.403	0	-0.01	-0.155	0.175	-0.002	-0.223	0.05	-0.013	-0.528	<0.0001	-0.058
FF_ssp245.	July	-0.32	0.005	-0.009	-0.346	0.002	-0.007	0.067	0.563	0.001	-0.101	0.379	-0.005	-0.269	0.018	-0.03
FF_ssp245.	August	-0.47	<0.0001	-0.01	-0.448	<0.0001	-0.008	-0.067	0.563	-0.001	-0.203	0.074	-0.012	-0.411	0	-0.032
FF_ssp245.	September	-0.38	0.001	-0.011	-0.374	0.001	-0.009	-0.067	0.563	-0.001	-0.183	0.108	-0.012	-0.312	0.006	-0.034
FF_ssp245.	October	-0.37	0.001	-0.011	-0.326	0.004	-0.009	-0.03	0.801	0	-0.232	0.042	-0.012	-0.391	0.001	-0.037

FF_ssp245.	November	-0.52	<0.0001	-0.017	-0.462	<0.0001	-0.01	-0.371	0.001	-0.007	-0.32	0.005	-0.026	-0.519	<0.0001	-0.083
FF_ssp245.	December	-0.52	<0.0001	-0.019	-0.383	0.001	-0.01	-0.388	0.001	-0.01	-0.405	0	-0.024	-0.602	<0.0001	-0.086
FF_ssp245.	DJF	-0.52	<0.0001	-0.014	-0.468	<0.0001	-0.011	-0.206	0.07	-0.003	-0.28	0.014	-0.016	-0.519	<0.0001	-0.056
FF_ssp245.	MAM	-0.3	0.008	-0.007	-0.442	<0.0001	-0.009	0.337	0.003	0.008	0.07	0.546	0.003	0.001	1	0.001
FF_ssp245.	JJ	-0.42	0	-0.012	-0.391	0.001	-0.009	-0.024	0.841	0	-0.149	0.191	-0.008	-0.437	0	-0.046
FF_ssp245.	ASON	-0.45	<0.0001	-0.012	-0.408	0	-0.009	-0.155	0.175	-0.003	-0.277	0.015	-0.015	-0.431	0	-0.034
FF_ssp245.	Ann	-0.49	<0.0001	-0.011	-0.462	<0.0001	-0.009	0.021	0.86	0	-0.263	0.021	-0.01	-0.491	<0.0001	-0.039
NF_ssp585.	January	-0.04	0.763	-0.001	0.055	0.633	0	-0.118	0.303	-0.003	-0.104	0.365	-0.01	-0.149	0.191	-0.01
NF_ssp585.	February	0.024	0.841	0	0.084	0.466	0.001	-0.064	0.58	-0.001	-0.044	0.706	-0.004	-0.084	0.466	-0.006
NF_ssp585.	March	-0.08	0.481	-0.001	0.144	0.209	0.001	-0.314	0.006	-0.008	-0.263	0.021	-0.018	-0.326	0.004	-0.024
NF_ssp585.	April	-0.16	0.167	-0.003	0.189	0.097	0.003	-0.383	0.001	-0.011	-0.238	0.037	-0.021	-0.417	0	-0.038
NF_ssp585.	May	-0.14	0.209	-0.003	0.058	0.615	0.001	-0.277	0.015	-0.007	-0.189	0.097	-0.017	-0.334	0.003	-0.031
NF_ssp585.	June	-0.12	0.291	-0.002	0.004	0.98	0	-0.283	0.013	-0.006	-0.235	0.039	-0.019	-0.286	0.012	-0.026
NF_ssp585.	July	-0.03	0.801	0	0.075	0.513	0.001	-0.263	0.021	-0.006	-0.189	0.097	-0.013	-0.243	0.033	-0.013
NF_ssp585.	August	0.084	0.466	0.001	0.201	0.078	0.003	-0.289	0.011	-0.007	-0.223	0.05	-0.017	-0.132	0.247	-0.01
NF_ssp585.	September	0.004	0.98	0	0.055	0.633	0.001	-0.272	0.017	-0.006	-0.223	0.05	-0.015	-0.121	0.291	-0.011
NF_ssp585.	October	0.118	0.303	0.002	0.198	0.083	0.002	-0.144	0.209	-0.003	-0.061	0.597	-0.005	-0.027	0.821	-0.002
NF_ssp585.	November	-0.03	0.801	0	0.144	0.209	0.002	-0.252	0.027	-0.007	-0.215	0.059	-0.019	-0.246	0.031	-0.018
NF_ssp585.	December	-0.04	0.744	0	0.087	0.451	0.001	-0.215	0.059	-0.005	-0.164	0.152	-0.013	-0.218	0.056	-0.018
NF_ssp585.	DJF	-0.04	0.763	-0.001	0.087	0.451	0.001	-0.169	0.138	-0.003	-0.118	0.303	-0.006	-0.186	0.102	-0.011
NF_ssp585.	MAM	-0.23	0.044	-0.002	0.235	0.039	0.002	-0.368	0.001	-0.008	-0.277	0.015	-0.017	-0.465	<0.0001	-0.031
NF_ssp585.	JJ	-0.06	0.58	-0.001	0.101	0.379	0.001	-0.289	0.011	-0.006	-0.226	0.047	-0.014	-0.32	0.005	-0.019
NF_ssp585.	ASON	0.044	0.706	0.001	0.229	0.044	0.002	-0.314	0.006	-0.006	-0.189	0.097	-0.013	-0.286	0.012	-0.016
NF_ssp585.	Ann	-0.02	0.9	0	0.206	0.07	0.001	0.041	0.725	0.001	-0.22	0.053	-0.013	-0.351	0.002	-0.015
FF_ssp585.	January	-0.58	<0.0001	-0.016	-0.488	<0.0001	-0.009	-0.206	0.07	-0.006	-0.203	0.074	-0.016	-0.556	<0.0001	-0.067
FF_ssp585.	February	-0.4	0	-0.009	-0.405	0	-0.007	0.195	0.087	0.005	0.127	0.269	0.01	-0.249	0.029	-0.021
FF_ssp585.	March	-0.28	0.014	-0.006	-0.445	<0.0001	-0.009	0.366	0.001	0.011	0.229	0.044	0.018	0.081	0.481	0.008
FF_ssp585.	April	-0.2	0.083	-0.005	-0.349	0.002	-0.006	0.36	0.002	0.01	0.249	0.029	0.019	0.073	0.53	0.006
FF_ssp585.	May	-0.5	<0.0001	-0.013	-0.494	<0.0001	-0.01	0.084	0.466	0.003	0.01	0.94	0	-0.414	0	-0.044
FF_ssp585.	June	-0.41	0	-0.01	-0.303	0.008	-0.006	-0.078	0.497	-0.002	-0.004	0.98	0	-0.408	0	-0.051
FF_ssp585.	July	-0.28	0.016	-0.006	-0.3	0.008	-0.004	-0.087	0.451	-0.002	-0.124	0.28	-0.01	-0.277	0.015	-0.033

FF_ssp585.	August	-0.41	0	-0.01	-0.36	0.002	-0.007	0.058	0.615	0.001	0.104	0.365	0.008	-0.323	0.004	-0.039
FF_ssp585.	September	-0.46	<0.0001	-0.012	-0.434	0	-0.009	0.016	0.9	0	-0.01	0.94	-0.001	-0.459	<0.0001	-0.048
FF_ssp585.	October	-0.33	0.004	-0.008	-0.323	0.004	-0.006	0.132	0.247	0.003	0.053	0.651	0.005	-0.314	0.006	-0.034
FF_ssp585.	November	-0.47	<0.0001	-0.016	-0.371	0.001	-0.008	-0.257	0.024	-0.005	-0.152	0.183	-0.012	-0.553	<0.0001	-0.077
FF_ssp585.	December	-0.67	<0.0001	-0.021	-0.508	<0.0001	-0.009	-0.403	0	-0.011	-0.255	0.025	-0.02	-0.701	<0.0001	-0.119
FF_ssp585.	DJF	-0.67	<0.0001	-0.015	-0.565	<0.0001	-0.009	-0.212	0.063	-0.004	-0.129	0.258	-0.009	-0.693	<0.0001	-0.07
FF_ssp585.	MAM	-0.42	0	-0.008	-0.499	<0.0001	-0.009	0.351	0.002	0.008	0.212	0.063	0.013	-0.158	0.167	-0.012
FF_ssp585.	JJ	-0.41	0	-0.009	-0.337	0.003	-0.005	-0.104	0.365	-0.003	-0.092	0.421	-0.009	-0.351	0.002	-0.042
FF_ssp585.	ASON	-0.48	<0.0001	-0.012	-0.465	<0.0001	-0.008	0.018	0.88	0	0.067	0.563	0.003	-0.505	<0.0001	-0.039
FF_ssp585.	Ann	-0.55	<0.0001	-0.011	-0.536	<0.0001	-0.007	0.058	0.615	0.001	-0.007	0.96	0	-0.522	<0.0001	-0.044

Mann-Kendall tau (ω), p value (p), Sen's slope estimator(γ), December-January-February (DJF), March-April-May (MAM), June-July (JJ), August-September-October-November (ASON), Near future (2061-2100 period: NF), Far future (2061-2100 period: FF)

Appendix 6. Variance analysis on historical snow cover dataset

Timescale	Geoscale	SV	SS	df	MS	F	P-value	F crit
Annual	By Mount	Mount	39.70	3	13.23	68.16	7.11E-23	2.71
		Error	17.08	88	0.19			
		Total	56.78	91				
Seasonal	Overall	Season	46.14	3	15.38	1.94	0.128336	2.71
		Error	696.29	88	7.91			
		Total	742.43	91				
Seasonal	By Mount	Mount	6.80	3	2.27	28.16	6.62E-05	3.86
		Season	0.50	3	0.17	2.08	0.17	3.86
		Error	0.72	9	0.08			
		Total	8.03	15				

Source of variation (SV), Sum of Squares (SS), Degrees of Freedom (df), Mean Square (MS), F-statistic (F), Probability value (P-value), Critical F-value (F crit)